TECHNICKÁ UNIVERZITA V LIBERCI
Fakulta textilní

Vývoj technologie koaxiálního elektrostatického zvlákňování

Disertační práce

Studijní program: P3106 – Textilní inženýrství
Studijní obor: 3106V007 – Textilní materiálové inženýrství

Autor práce: **Ing. Lucie Vysloužilová**
Vedoucí práce: prof. RNDr. David Lukáš, CSc.

Liberec 2016

TECHNICAL UNIVERSITY OF LIBEREC
Faculty of Textile Engineering

Development of Coaxial Electrospinning Technology

Dissertation

Study programme: P3106 – Textile Engineering
Study branch: 3106V007 – Textile and material engineering

Author: **Ing. Lucie Vysloužilová**
Supervisor: prof. RNDr. David Lukáš, CSc.

Liberec 2016

Prohlášení

Byla jsem seznámena s tím, že na mou disertační práci se plně vztahuje zákon č. 121/2000 Sb., o právu autorském, zejména § 60 – školní dílo.

Beru na vědomí, že Technická univerzita v Liberci (TUL) nezasahuje do mých autorských práv užitím mé disertační práce pro vnitřní potřebu TUL.

Užiji-li disertační práci nebo poskytnu-li licenci k jejímu využití, jsem si vědoma povinnosti informovat o této skutečnosti TUL; v tomto případě má TUL právo ode mne požadovat úhradu nákladů, které vynaložila na vytvoření díla, až do jejich skutečné výše.

Disertační práci jsem vypracovala samostatně s použitím uvedené literatury a na základě konzultací s vedoucím mé disertační práce a konzultantem.

Současně čestně prohlašuji, že tištěná verze práce se shoduje s elektronickou verzí, vloženou do IS STAG.

Datum:

Podpis:

Acknowledgment

I am very grateful to my supervisor prof. RNDr. David Lukáš, CSc., whose expertise, understanding, generous guidance, support and motivation made it possible for me to work on the coaxial electrospinning topic. I am thankful for his kind and valuable advice and for many suggestions concerning my experimental work, theory of hydrodynamic and writing of this manuscript.

I would like to thank doc. Ing. Pavel Pokorný, Ph.D. for his immense interest in the coaxial electrospinning topic, especially in the design of coaxial electrospinning electrodes. I am also thankful for his support and friendly cooperation. I appreciate the kind help of prof. Ing. Jaroslav Beran, CSc. and his team from the Department of Textile Machine Design at Technical University of Liberec, especially Ing. Karel Pejchar, for the excellent cooperation in the development and testing of electrospinning equipment and coaxial electrospinning electrodes.

I am also grateful to the team of prof. RNDr. Evžen Amler, CSc. from the Institute of Experimental Medicine of the Academy of Sciences of the Czech Republic and team of Prof. Kornev from the Clemson Univ. for their help, collaboration on experiments and for being a source of motivation.

I owe a great debt of gratitude to my family, my boyfriend and my friends for their support, unceasing encouragement and motivation throughout my studies. They have always been there for me and I am thankful for everything they have helped me achieve.

Content

List of Abbreviations and symbols

a	amplitude
a_c	capillary number
AC	alternating current
C	initial amplitude
CED	cohesive energy density
CMC	Carboxymethyl cellulose
d	diameter of nanofibers
DC	direct current
DMA	dimethylacetamide
DMF	dimethylformamide
E_e	energy of evaporation
E	electric field
Ec	critical value of the electric field
Fc	capillary force
Fe	electric force
FWHM	the full width at half-maximum
g	gravitational acceleration
G_M	Gibbs energy of mixing
H_M	Enthalpy of mixing
HA	Hyaluronic acid
HDPE	high density polyethylene
HMW	high molecular weight
HSP	Hansen solubility parameter
HV	High Voltage
i	imaginary unit
k	wave number
k_B	Boltzmann constant
l	attenuator parameter of the wave amplitude
L	length
LMW	low molecular weight

n	number of Taylor cones/polymeric jets
N	number of molecules in lattice model
p	pressure
p_c	capillary pressure
p_e	electric pressure
p_h	hydrostatic pressure
P	productivity of spinning electrodes
PAN	Polyacrylonitrile
PEO	Polyethylene oxide
PCL	Poly-ε-caprolactone
PMMA	Polymethylmethacrylate
POM	Polyoxymethylene
PVA	Polyvinyl alcohole
PVB	Polyvinyl butyrale
PVDF	Polyvinyliden fluoride
PVP	Polyvinyl pyrolidon
Q	number of possible configurations
R	universal gas constant
R_0	radius of interaction spheres in Hansen space
R_a	distance between the solvent and dissolving material
RED	relatively energy gap
RH	relative humidity
S_M	entropy of mixing
SEM	Scanning electron microscopy
T	temperature
TEM	Transmission electron microscope
U	voltage
U_c	critical voltage
U_M	internal mixing energy
U_{opt}	optimal voltage
v	velocity
v_f	feed rate

V	volume
V_0	elementary volume
z	coordination number of lattice

Greek symbols

β	enhancement factor
γ	surface tension
δ	Hansen solubility paranmeter
δ_t	Hildebrand solubility parameter
ε	interaction energy
ζ	vertical displacement
χ	interaction parameter
λ	characteristic wavelength
Γ	electrospinning number
μ	dynamic viscosity
ρ	density
υ	volume of macromolecule
υ_0	elementary volume
ϕ	speed potential
ω	angular frequency

1 Introduction

The thesis is focused on the coaxial electrospinning. This work examines and describes the process of electrospinning itself, the development of special coaxial spinning electrodes and the analysis of the core-shell structure of formed nanofibers. Parameters of the process for coaxial electrospinning are investigated as a fundamental basis for a design and development of the new coaxial spinning electrodes. Significant part of this work is aimed at an optimization of needleless coaxial spinning electrodes for productivity enhancement of core-shell nanofibers. The development of new methods and spinning electrodes is complicated task requiring well cooperating team of experts from the ranks of engineers, technologists, scientists and designers. Many spinning electrodes mentioned in this work were developed in collaboration with other experts from the Department of Nonwovens and Nanofibrous materials and the Department of Textile Machine Design at Technical University of Liberec and with Audacio Company. Detailed analysis and investigation of the coaxial electrospinning process were done and new knowledges were obtained within this work. This knowledge is necessary to ensure the optimal formation of core-shell nanofibers. Onset of the electrospinning process is observed with the focus on formation of a bi-component droplet or a polymeric two-layer at a needle or a needleless case, respectively. The overall course of the electrospinning process is investigated in a great detail. Morphology analysis of the core-shell structure of produced nanofibers is the next goal of this thesis. An optimization of the process and materials parameters of the coaxial electrospinning leading to the core-shell nanofibers formation and a determination of the suitable and easy methods for an experimental proof of core-shell nanofibrous structure are main goals of this thesis.

There is a growing interest in nanofibers as a material for biomedical applications in the last years. Nanofibers are unique materials with a low area weight and a high specific surface area. It means, they are composed of very fine fibers with diameters ranging from 100 nm to 1 μm and with high porosity and very small inter-fiber pores. Due to these unique properties and their structure, which is similar to the extracellular matrix, nanofibers can be used in medicine as a replacement of a damaged tissue obtained. These specific properties allow their usage in biomedicine as scaffolds (H.-J. Jin, 2002), wound dressing (Bornat, 1987) or materials for drug delivery system (E.R. Kenawy, 2002). They can also be used in electronics, optics, filtration, as composite materials or as special probes (A.G. MacDiarmid, 2001; Song, 2006; Dumas, 2007; Greiner, 2007).

Development and technology of the electrospinning and especially coaxial electrospinning are the main subjects of the chapter 1.2 - State of the art. Spinning electrodes and counter-electrodes (collectors) are described in the chapter 1.3 and 1.4. Electrospinning and coaxial electrospinning setup providers are listed in the chapter 1.5. The chapter 1.6 states application of the core-shell nanofibers. The general description of the coaxial electrospinning technology is introduced in the theoretical part (Chapter 2.1). Basics of the hydrodynamics, where fundamental dispersion laws are described and derived are given in the chapter 2.2 and 2.3. Chapter 2.4 deals with relaxation time of the electrospinning process and examines a behavior of liquids in the high voltage electric field. Thermodynamics of polymer solutions is introduced in the last chapter of the theoretical part (Chapter 2.5). Appropriate selection of the core and the shell materials is critical for coaxial electrospinning. These materials should be compatible, not precipitate and premature diffusion cannot occur. Experimental part introduces used polymers, methods and equipment (chapter 3.1 and 3.2). Developed needle and needleless coaxial spinning electrodes of different shapes and designs are listed in chapter 3.3 and 3.4. Process parameters are being investigated and compared with the theoretical prediction. Chapter 3.5 deals with electrospinning of the biopolymers realized using developed coaxial spinning electrodes. Visualization of the electrospinning process and especially coaxial electrospinning process is the topic of the chapter 3.6. Detailed investigation of the electrospinning process and behavior of the electrospun liquids in the high voltage electric field is the necessary part of the precise production of the nanofibers with the desired properties. The last chapter of the experimental part is devoted to the proof of the core-shell structure of produced nanofibers (Chapter 3.7). Methods for the easy and fast analysis of the core-shell structure were searched, investigated and verified. The last chapters of this work are Evaluation of results and insights and Summary of the conclusions (Chapter 3 and 4).

Benefits of this work can be seen in the expansion of knowledge about the coaxial electrospinning and in the possibility of application of this technology in industrial production. Needleless coaxial spinning electrodes increase the productivity of core-shell nanofibers manufacturing. Equipment presupposing the use of the coaxial electrospinning on an industrial scale were developed within this work. The process of the electrospinning and its coaxial variant was investigated in detail and visualization methods were established and verified. Numerous analyzes providing the proof of the core-shell structure of the produced nanofibers were designed and tested.

1.1 Main goals of the work

1. The development and experimental testing of needle coaxial spinning electrodes;
2. The development and experimental testing of needleless coaxial spinning electrodes;
3. Investigation of process and materials parameters of needle and needleless coaxial electrospinning;
4. The analysis of the core-shell structure of produced nanofibers;
5. Description of dispersion laws for viscose liquids and derivation of dispersion laws for non-viscose liquids for free surface of layer;
6. The examination of a relaxation time of needleless electrospinning;

1.2 State of the art

Electrospinning is a relatively simple nanofibers producing technique known since the beginning of the former century (Formhals, 1934), (Zeleny, 1914). This is a process that employs electrostatic forces to produce ultra-fine fibers with diameters ranging from micrometers down to hundreds of nanometers. This is currently quite well known technology for ultra-fine fibers formation through using the action of an external and internal electric field. Polymer solution, or melt respectively, is delivered through needle or needleless spinning electrode usually connected to the positive high voltage source and it is drawn and elongated by electric forces to form nanofibers (Moghe, 2008). Nanofibers are collected on collector with opposite charge. Electrospinning is currently ranked in the forefront of many laboratory and industrial sectors. Ultra-fine fibers formation by electric forces is intensively investigated area for many applications such as: filter materials, highly functional textiles, protective clothing, scaffolds for tissue engineering, materials for drug delivery system, wound dressing, fiber reinforced composite materials, special probes, sensors and electrodes for use in electronics and optics or sound insulators (Li, 2004), (Ma, 2005), (Huang, 2003), (Moghe, 2008).

The coaxial electrospinning is less widespread in industry. Currently this is primary laboratory method for the development of sophisticated nanofibrous systems for special applications such as tissue engineering, drug delivery system or special probes for example. Since 2003 to October 2016, the Web of Knowledge published 779 articles dealing with the

coaxial electrospinning and the production of core-shell nanofibers, taking an interest in this subject is increasing, as can be seen in Figure 1.

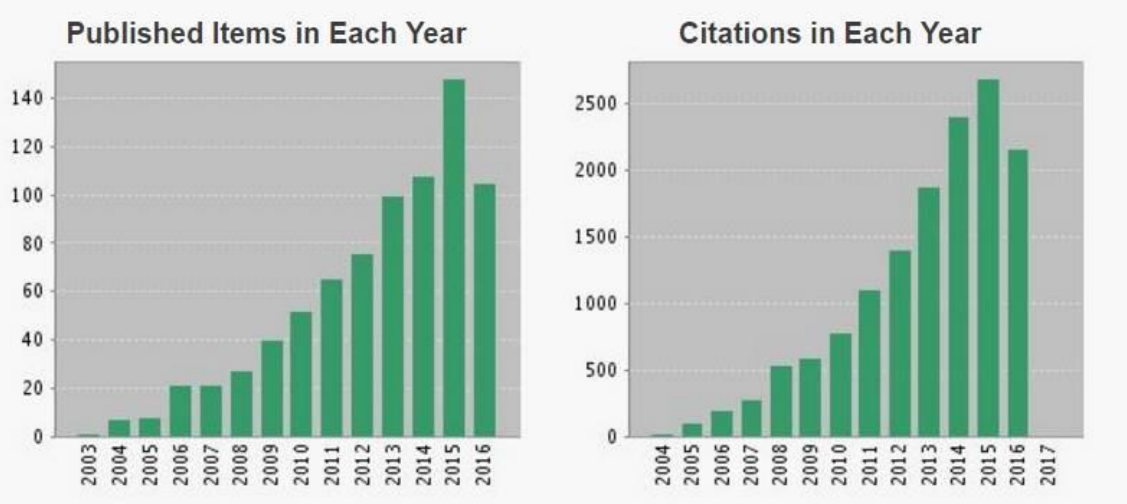

Figure 1 *Number of published articles and their citations on the coaxial electrospinning and core-shell nanofibers topic by Web of Knowledge. Data obtained on October 9, 2016.*

Technology of electrospinning was described in a range of articles (Doshi, 1995; MacDiarmid, 2001; Dzenis, 2004; Yarin, 2004; Reznik, 2006; Moghe, 2008; Sill, 2008, Lukas, 2009). This work is focused on the coaxial electrospinning. Therefore, the conventional electrospinning will be described only in general terms, without detailed explanation.

Production of nanofibers by electrospinning is a dynamic process. Polymer jets are drawn from the polymer solution or melt, then passing through the whipping/ instability zone to form nanofibers. Needle or needleless technology is used to a produce of nanofibers by electrospinning. Polymer solution is delivered through the needle or the needleless spinning electrode and is subjected to high voltage (HV) field. A free liquid surface of a polymer droplet or a layer, respectively, is destabilized by HV external field. High voltage is applied on the polymer solution after turning on the HV source and a charge is injected into this solution. The polarization of polymer solution occurs because of the positive charges attracted to the counter-electrode. The polymer solution is then destabilized by the HV external field. The instability of surface waves categorized as the Larmor-Tonks-Frenkel one (Frenkel, 1955; Tonks, 1935; Larmor, 1890) has its nature in the self-organization by the mechanism of the "fastest forming instability." This mechanism plays a key role in selection

of the fastest growing capillary wave with a characteristic wavelength λ. The electrospinning process starts by achieving certain critical value of the electric field strength E_c (Lukas, 2009). *Taylor cone* (Taylor, 1964) is created on the top of the polymer layer. The cone is typically erected in semi vertical angle 49,3° (a whole angle of 98,6°), as shown in Figure 2. Taylor cone develops into a polymer jet. This jet passes through so-called whipping instability zone, this is drawn and elongated by external and internal electric forces to form of nanofibers (Moghe, 2008). The solvent evaporates and nanofibers are deposited on the oppositely charged collector located at a defined distance from the electrode (Yarin, 2004). A nonwoven textile for nanofibers collecting may be located under the collector.

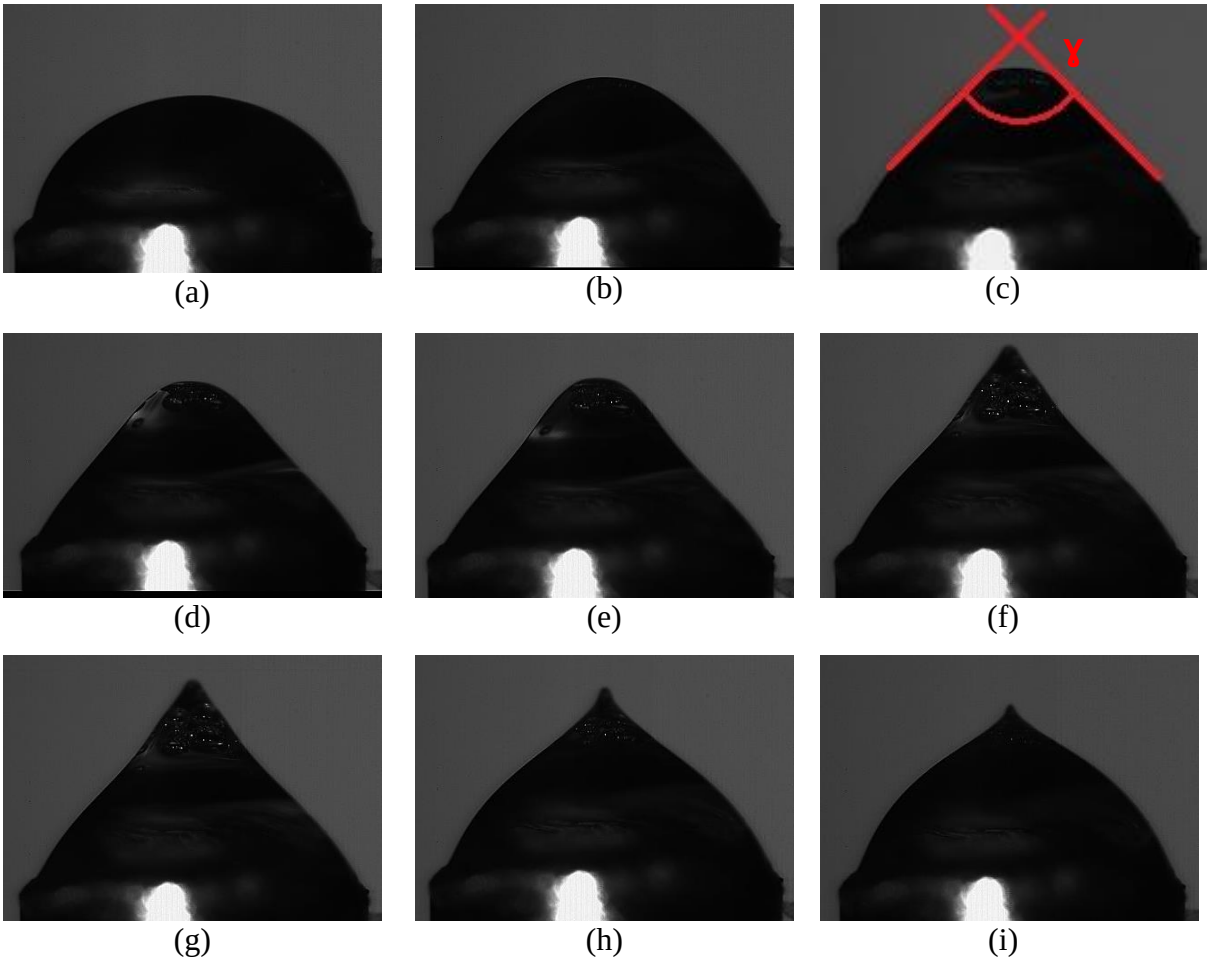

Figure 2 *The Taylor cone formation from the free polymer layer and the start of the electrospinning process: Taylor cone formation (a – c), relaxation of polymer droplet (d – i). Start of the electrospinning process (i). Reaction of electric and capillary forces can be observed, (c) The angle of the Taylor cone ɣ (a whole angle of 98,6°).*

A briefly history of core-shell electrospinning

The technology of the formation of synthetic fibers using electric forces is known for more than 100 years (Sill, 2008). But the first record of the electrostatic attraction of liquids observed by William Gilbert dates back to the 1600. Gilbert, English physician and scientist, investigated the movement of a charged spherical drop due to the charged amber rod. In 1749, French physicist Nollet examined a decay of charged fluid jet. Both inventors have come across to problem with inadequate high voltage for their experiments. In 1887 Charles Vernon Boys described "*the old, but now apparently little-known experiment of electrical spinning*."He devised a method of drawing a fiber using a crossbow. This method consisted in a location of a fused quartz to the crossbow, heating this quartz and its firing using the crossbow. He obtained a very uniform glass thread 90 feet long (Boys, 1887). In 1899 Cooley applied for a patent of his technology for producing of very fine fibers using electrostatic forces. His method has been patented in 1900 and 1902 (Cooley, 1902). His coaxial spinning electrode consists of two separated chambers. It was the first device enabling the manufacture of core-shell structures. In 1900, American physicist Morton developed equipment for a very fine fibers formation using electrostatic forces. This equipment was patented in 1902 (Morton, 1902). John Zeleny laid the foundations of modern electrospinning. In 1914, he developed a needle equipment to study liquid's electrical discharges (Zeleny, 1914; Lukas, 2009). Formhals is called the father of modern technology of electrospinning (Lukas, 2009). In 1934, he designed a device for the production of very fine fibers by electric field with collected of fibers on coils for textile industry (Formhals, 1934). Formhals patented more than 22 patents in the field of electrospinning during his lifetime. It cannot be possible to talk about nanofibers formation until the 1931, because by this time there was not any technology to enable their observation. The first prototype of electron microscope was developed in the 1931 by German physicist Ruska and electrical engineer Knoll. In 1938, Rosenblum and Petrianov-Sokolov developed filter materials for gas masks using electrospinning technology (Filatov, 1977; Lukas, 2009; Tucker, 2012). Taylor laid basics of theoretical analysis of the electrospinning process. He has tackled this topic between the years 1964 – 1969. In the early 90s of the 20th century Reneker proved the possibility of the electrospinning of a wide spectrum of polymeric materials including the possible applications for produced nanofibers (Doshi, 1995).

Yarin and Zussman brought a revolutionary idea (Yarin, 2004) of needleless electrospinning allowing increase in nanofibers productivity. Technology of mass production

of nanofibers and commercialization of the needleless electrospinning was developed and patented under the brand name Nanospider^{TM} in 2005 (Jirsak, 2005).

The first equipment for coaxial electrospinning has already been patented in the early 20th century under the name Apparatus for electrically dispersing fluids (Cooley, 1902), see in Figure 3. The principle of this equipment is a feeding of two liquid materials independently through the coaxial capillary, i.e. spinneret, to its orifice. A composite polymeric droplet is created in an orifice of this spinneret. *Taylor cone* (Taylor, 1964) is created on the top of the composite droplet and both liquids in common are drawn and elongated by electric forces and collected on the grounded collector as nanofibers with a core-shell structure (Reznik, 2006). This technology is known as the needle coaxial electrospinning.

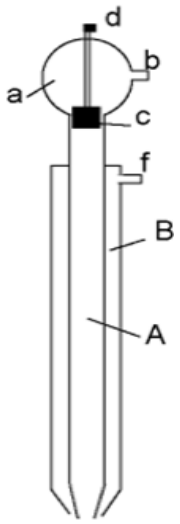

Figure 3 *Cooley's equipment for coaxial electrospinning: (A) the core capillary, (B) the shell capillary,(a) the chamber, (b) the input of core liquid, (c, d) control valves, (f) the input of shell liquid. Adapted from (Lukáš, 2009)*

Research teams began to examine coaxial electrospinning in more detail at the turn of the 20th and 21st centuries. Yarin and Zussman dealt with the combination of organic and inorganic materials (Sun, 2003). They found an incorporation of various kinds of polymeric and non-polymeric materials into nanofibers as a major advantage of coaxial electrospinning. This technology makes it possible to create unique systems with specific properties for using in cosmetics, medicine or electronics. The application of core-shell nanofibers in the industry area is paid to detail the Chapter 1.6.

Hollow nanofibers can be also produced using this technology as introduced in (Dror, 2009; Li, 2004). Two materials with different solvents are formatted into nanofibers using the coaxial electrospinning and follow the removal of the core part by a treatment of its solvent system.

The coaxial electrospinning is not just the only option to form core-shell nanofibers. An emulsion electrospinning is another way to production of nanofibers with the core-shell structure. Bazilevsky described so-called co-electrospinning in 2007 (Bazilevsky, 2007). His single-nozzle technique allows production of the core-shell nanofibers from a polymeric mixture of immiscible liquids. The mixture of polymethylmethacrylate (PMMA) and polyacrylonitrile (PAN) dissolved in dimethylformamide (DMF) is used in his work. This technology is based on the electrospinning of PAN as the shell with droplets of PMMA as the core, see in (Figure 4).

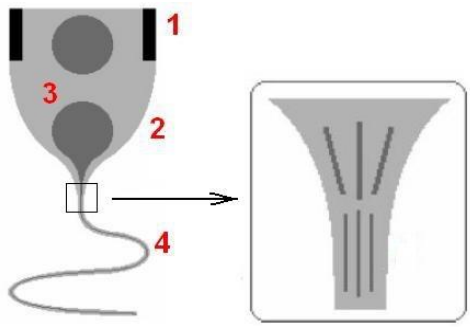

Figure 4 *Co-electrospinning of PMMA/PAN in DMF emulsion. Emulsion is needed to the needle orifice (1). The Taylor cone is created on the top of PAN shell droplet (2) and droplets of PMMA (3) are elongated by shell in electric field. Core-shell polymeric jet (4) is created (Bazilevski, 2007).*

A development of needleless coaxial electrospinning

Generally, the needle is the most commonly used electrode for the electrospinning. A disadvantage of the needle coaxial electrospinning is a very low production of core-shell nanofibers. As described by Haitao (2009), a needle can mostly create only one polymer jet and the productivity of nanofibers is less than 300 mg/h per needle. Higher productivity can be reached by increasing the number of needles (Ding, 2004). However, this so-called multiple-jet setup has a problem with non-uniform electric field, a large operating space is necessary and the cleaning of a spinning electrode is more demanding (Vysloužilová, 2010). A new idea of needleless electrospinning to increase productivity of nanofibers was

introduced by Yarin and Zussman in 2004 (Yarin, 2004). They investigated the behavior of a thin polymeric layer located above a silicon oil-based magnetic fluid in electro-magnetic field. The main aim of their work was a realization of multiple upwards jets from a free surface of polymeric solution without any needles. Needleless coaxial electrospinning uses production of core-shell nanofibers from a free surface of a polymeric two-layer. Technology of mass production of nanofibers and commercialization of the needleless electrospinning was developed in 2003 at Technical University of Liberec (TUL) in cooperation with Elmarco Ltd. and patented under the brand name Nanospider^{TM} in 2005 (Jirsak, 2005).

First apparatus for the needleless coaxial electrospinning was developed at TUL and patented in 2009 under the name "Weir spinner" (Pokorný, 2009). This technology is based on the electrospinning from a very thin two-layer of polymer solutions flowing over the electrode as is shown in Figure 5. This technology was called the weir spinner due to its similarity to the weir on a river (Vysloužilová, 2010).

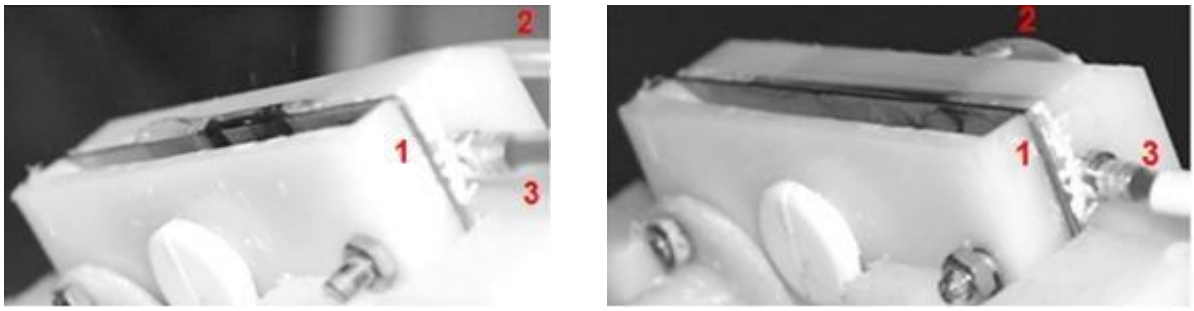

Figure 5 *The weir spinner: polymer two-layer flowing over the edge of spinning electrode (1), feed of the shell polymer solution (2), feed of the core polymer solution (3), (Vyslouzilova, 2010).*

Unique equipments for the industrial production of nanofibers and core-shell nanofibers (Spinner 1 and Spinner 2) were developed at Department of Nonwovens and Nanofibrous materials and Department of Textile Machine Design at TUL in 2012 within this work and the cluster Nanoprogres. Spinner 1, see in Figure 6 was developed for coaxial electrospinning. Followed the development of Spinner 2 based on the experience gained from the Spinner 1. Spinner 2 (Figure 6 b, c) is unique equipment allowing the production of nanofibers and core-shell nanofibers in cleanroom in grade A (European Standard). This is certificated inside the electrospinning chamber of this equipment. An integral part of the Spinner 2 is a laminar box ensuring the cleanroom in grade B (European Standard). The uniqueness of this highly productive equipment can be assessed by the fact that only a few

other institutions are currently deals with the development of the needleless coaxial electrospinning. These institutions are listed in the Chapter 1.5.

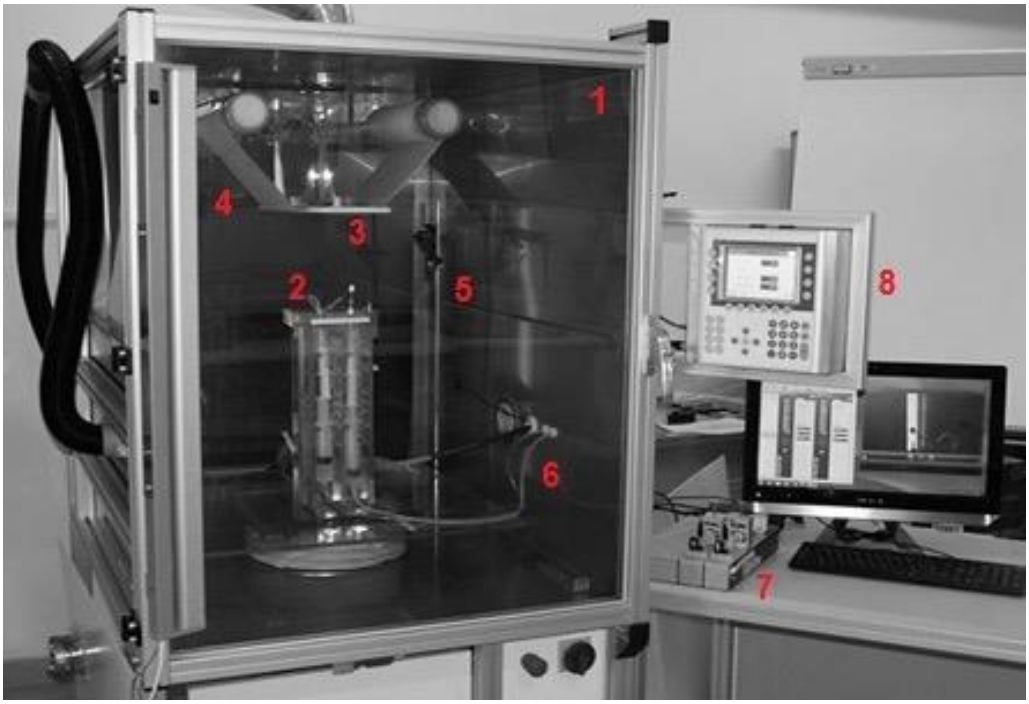

(a)

(b)

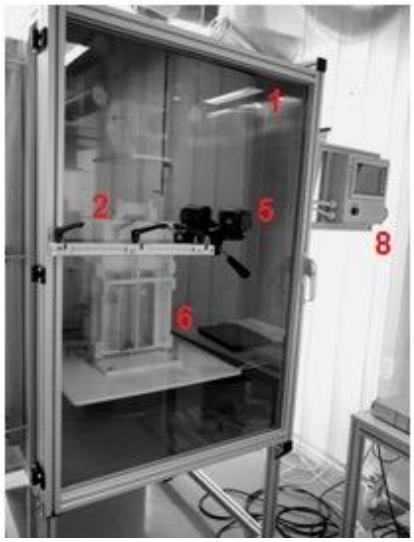

(c)

Figure 6 *Unique equipment for industrial production of nanofibers and core-shell nanofibers developed within this work and cluster Nanoprogres, z.s.p.o.: (a) Spinner 1, (b, c) Spinner 2 for clean rooms: The coaxial equipment (1), the coaxial spinner in the holder (2), the collector (3), a nonwoven spun-bond material is used as a substrate to collect nanofibers (4), a camera (5), a hydraulic dosing system (6), dosing syringes (7), the control panel (8), a laminar flow box (9).*

In 2012, American Society Arsenal Medical, Inc. introduced a high-performance slit electrode for core-shell nanofibers formation (Yan, 2012). This needleless spinner consists of two triangular shaped troughs that are aligned to a single vertical plane to form a slit-surface. The core slit is set to be slightly below that of the shell slit, see in (Figure 7). In 2014, a Contipro Company introduced 4SPIN device for the production of composite nanomaterials and core-shell nanofibers (Contipro, 2014).

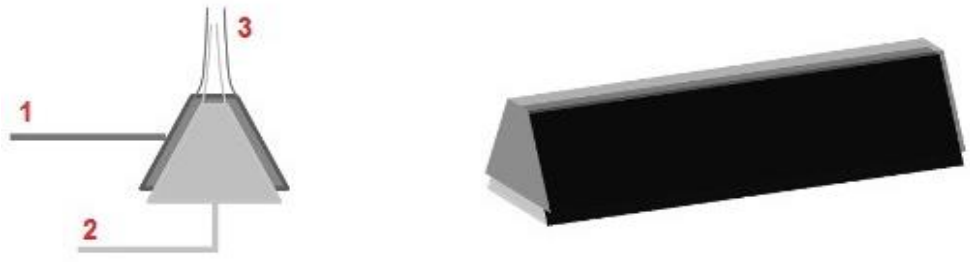

Figure 7 *Schematic of the high-throughput, needleless electrospinning fixture for core-shell nanofibers formation: the shell polymer solution (1), the core polymer solution (2), the core-shell polymeric jet (3), adapted from (ElectrospinTech, 2013).*

In 2013, Forward *et al.* described a coaxial electrospinning technology using a wire electrode. The principle of their technology is a passing of a wire through two immiscible solutions. The wire is coated with two-layer of polymeric solutions and core-shell nanofibers may be formed as is shown in the Figure 8 (Forward, 2013).

In 2014, Jiang and Qin introduced a high throughput one stepped pyramid-shaped spinneret. The productivity of this device is about 4 g/h, which is several hundred times higher than that of conventional sigle-needle electrospinning (Jiang, 2014). This technology is based on the electrospinning from a polymeric solution flowing over the electrode (Figure 9). The electric field is very heterogeneous and high as is shown in Figure 9c. The cascade construction of this electrode allows the increase of the productivity of core-shell nanofibers.

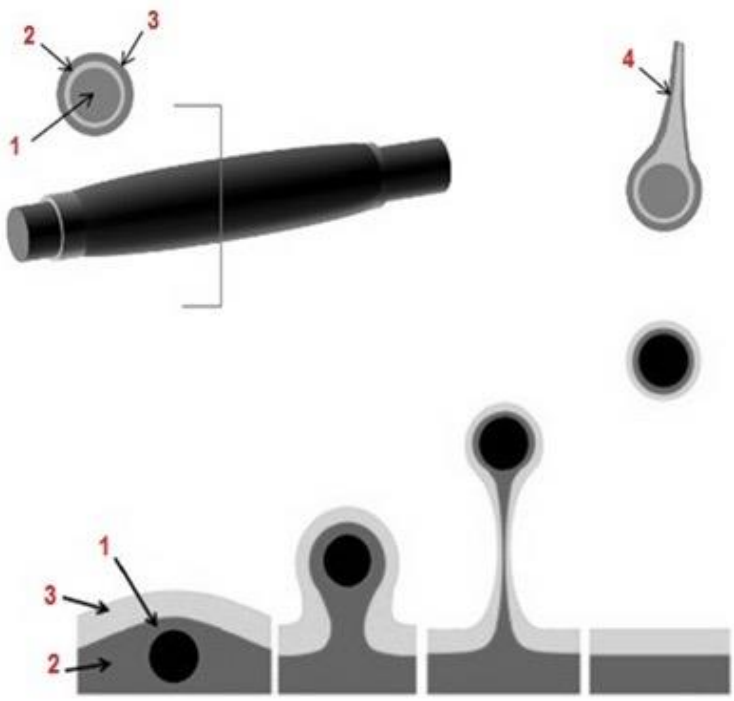

Figure 8 *Schematic of the wire needleless coaxial electrospinning for core-shell nanofibers formation: wire electrode (1), the core solution (2), the shell solution (3), coaxial jet (4), adapted from (Forward, 2013).*

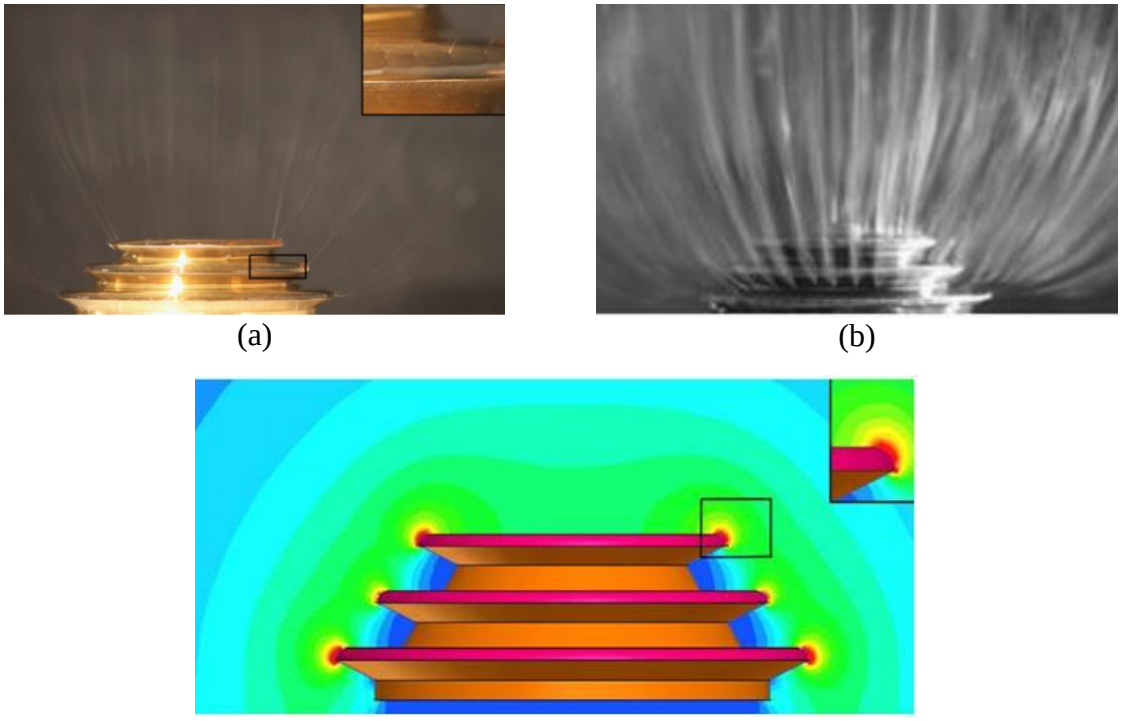

(a) (b)

(c)

Figure 9 *One stepped pyramid-shaped spinneret, adapted from (Jiang, 2014): coaxial electrospinning using the pyramid-shaped spinneret (a, b), Simulation of electric field distribution (c).*

In recent years, an interest in the highly productive coaxial spinning electrodes is greatly higher. An increasing number of both local and foreign institutions deal with the idea of core-shell nanofibers formation.

Advantages of coaxial electrospinning

Coaxial electrospinning has a several main advantages. Bi-component nanofibers with a core-shell structure for special application in the broad field of the laboratory or industry sector can be produced. Two different polymers can be electrospun together into one composite nanofiber. Great advantage is the possibility of the electrospinning of so-called "unspinable" polymers as the core part of the core-shell nanofiber.

Incorporated materials are protected from the outside environment by the shell material. The coaxial electrospinning also eliminates any damage caused by direct contact of the incorporated drug with organic solvents or harsh conditions during emulsification (Jiang 2014).

The great advantage of the core-shell nanofibers is uniformly distributed active agent (drug respectively) in nanofibrous scaffold and their so-called gradual release. The agent can be release from the scaffold gradually at the time and not all at once throughout at batch.

1.3 Electrospinning electrodes

Spinning electrodes (spinners) can be categorized according to several criteria. The most widely used classification is according to the continuity of the polymer solution dosing and the electrospinning process on the continuous and discontinuous spinning electrodes. The last one is classification according the technology on the needle or needleless spinning electrode.

Continuous or discontinuous spinning electrodes can be used depending on course of electrospinning process. Discontinuous method does not have a continuous supply of polymer solution. A defined volume of polymer solution is put on the top of spinner before electrospinning and this part of process is repeated depending on the desired nanofibrous layers. *A metal rod* developed by Filip Sanetrník (KNT, FT, TUL) or the slit electrode (Pejchar, 2013) are examples of discontinuous spinner for electrospinning show in Figure 10 a, b. A great advantage of discontinuous spinning electrodes is their use for initial tests of new polymer solutions. Just a small amount of polymer solution is necessary for this

technology. It is advantageous for the development of new polymer solution and for expensive materials. The next advantage of this method is a very short operation time and easy and quick preparation for testing. A disadvantage of this one is a very small productivity of nanofibers. Discontinuous spinning electrode is unsuitable for higher productivity of nanofibers and for formation of homogeneous nanofibrous layer. The polymer solution is continuously supplied to a spinner orifice throughout the electrospinning process in case of continuous technology. This technology is used for continuously feeding the polymer solution and electrospinning process. The advantage of this technology is less frequent refilling polymer solution and more uniform formation of nanofibrous layer. Needles, rotating cylindres, hollow metal rod, slit electrodes etc. fall into this category. The examples of these spinning electrodes are shown in Figure 10 c, d, e.

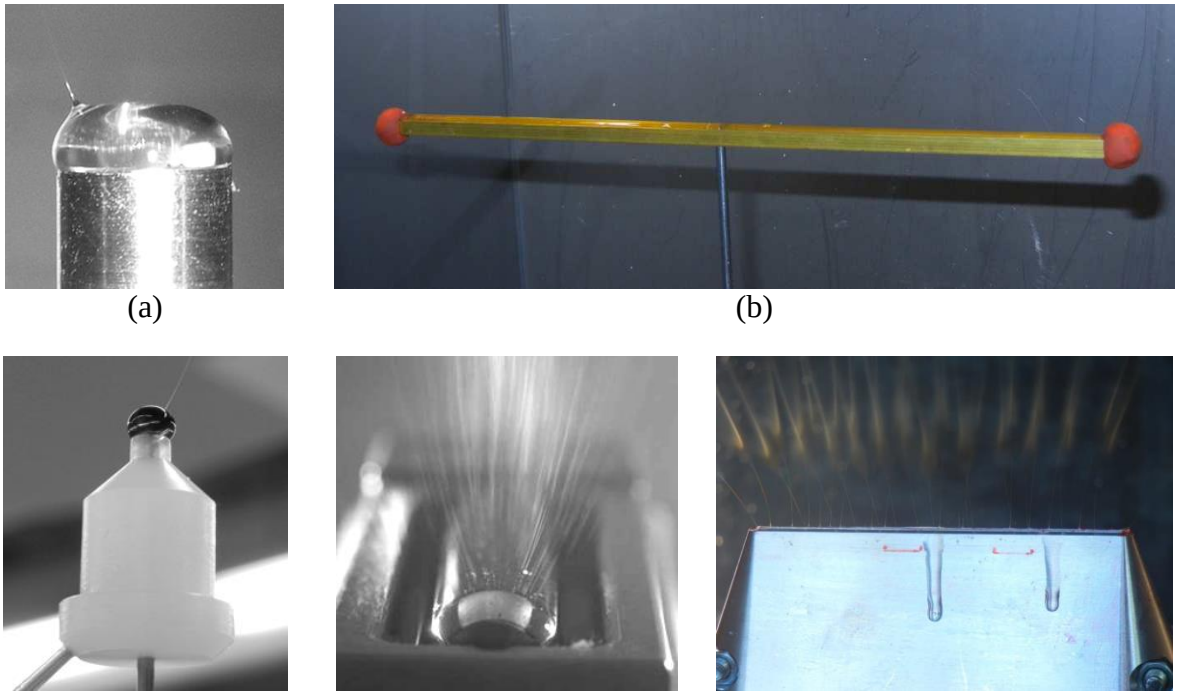

Figure 10 *An example of discontinuous and continuous spinners: The discontinuous electrospinning realized using (a) the metal rod spinner and (b) the slit spinning electrode (Pejchar, 2013), the continuous electrospinning realized using (c) the needle, (d) the rotating cylinder NANOSPIDER^{TM} technology - adapted from (Elmarco, Ltd.), (e) the slit spinning electrode (Nanoprogres)*

Needle (Figure 10 c) or needleless (10 a, b, d, e) spinning electrodes can be used for electrospinning. The electrode can be wading in the polymer solution (e.g. rotating cylinder) or polymer solution can be dose through electrode (e.g., the needle/capillary, the slit

electrode). Needle technology is based on the dosing of polymer solution through the needle/capillary spinning electrode or multiple needles to its orifice. The polymer droplet is created in this place. The needleless technology uses electrospinning from a free surface of polymer layer without needles. The advantage of this one is increase of productivity of nanofibers and more uniform electric field.

Needle or needleless technology may be chosen in case of coaxial electrospinning. The needle coaxial spinner is composed of two coaxially arranged needles. The core and shell liquids are supplied to the spinning electrode orifice and the bi-component droplet is created in this place. The needleless technology uses electrospinning from the free surface of a thin polymer two-layer. The shell polymeric layer overlaps the core liquid and both materials are electrospinning together by electric forces. A large number of needle and needleless coaxial spinning electrodes were developed with this work. These electrodes are described in detail in Chapter 3.4 and 3.5.

1.4 Collectors

There are large numbers of collector modifications for collection of nanofibers. Stationary or rotating collectors of various shapes may be used. Nanofibers can be collected directed on flat or on structured collectors or on a support fabric located in front of a collector. The collector is chosen depending on the desired structure of nanofibrous layer.

Flat stationary collectors, see in (Figure 11a) can be used for collection of nanofibrous layer with randomly oriented fibers. These collectors may have rectangular or circular shape and different size. Rotating collectors allow nanofibrous orientation. Structured collectors, see in Figure 11b,c are chosen for special 3D layers and for layers with a defined structure. Special materials for various applications can be produced using these structured collectors.

Materials with a special structure may be obtained using special structured rotational collectors, see (Figure 11c). More or less aligned nanofibers can be achieved depending on rotational speed (rpm). However, too high speed of rotating collector can cause the problem with collecting of nanofibers. They can be entrained by the airflow created by the rotation of the collector.

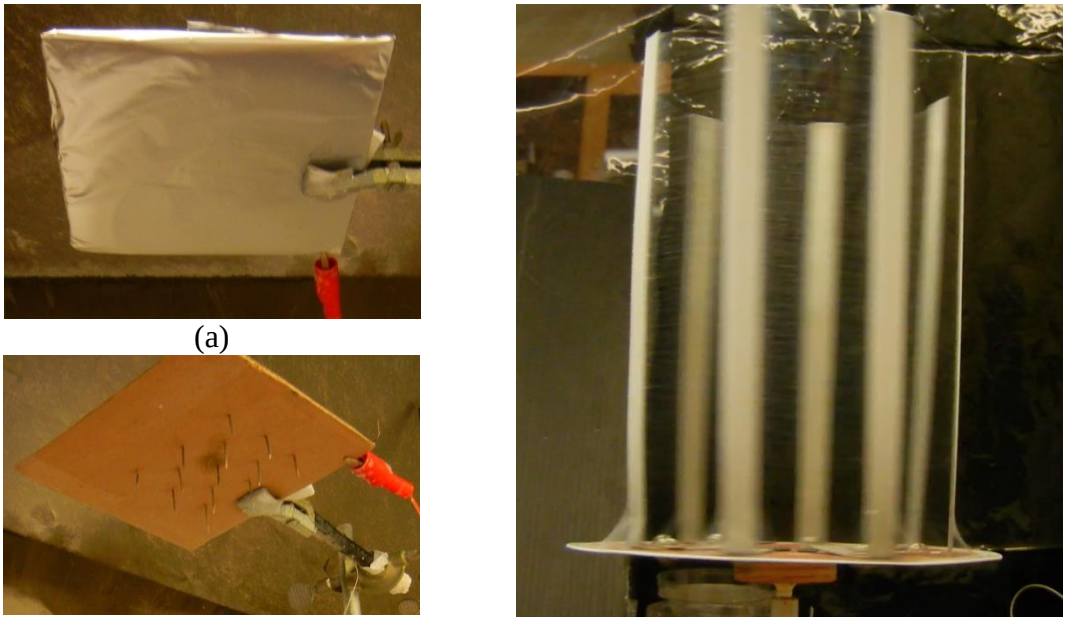

(a) (b) (c)

Figure 11 *Examples of collectors used for electrospinning: (a) flat stationary collector, (b) structured collector, (c) rotational collector.*

A special case may be electrospinning without collector. AC electrospinning is a unique method using alternating current for production of nanofibers without collector. This one is replaced by ground in close of spinning electrode (Pokorny P., 2014). Collectors used in this work are listed in the chapter 3.2 - Used methods and equipment.

(a) (b)

Figure 12 *AC electrospinning: (a) AC electrospinning equipment, (b) AC electrospinning realized using cylindrical spinning electrode. AC source (1), electrospinning electrode (2), the reservoir with polymer solution (3), nanofibers (4).*

1.5 Electrospinning setup providers

There are not many companies engaged in selling equipment for an industrial production of nanofibers. The market is relatively widely represented by companies dealing with the development and the sale of electrospinning equipment for laboratory used, but just some companies offer high productivity equipment. Currently just few companies deal with the development and the sale of electrospinning equipment for production of core-shell nanofibers. The first company offering the electrospinning devices for production of nanofibers was Elmarco Ltd. Companies engaged in developed and in selling of electrospinning equipments for production of nanofibers are shown in the Table 1 (ElectrospinTech, 2015).

Table 1 *Companies engaged in developed and in selling of electrospinning equipment*

Company	**Country**	**Laboratory Setup**	**High productivity equipment**	**Website**
Contipro	Czech Republic	yes	no	http://www.4spin.info/
ANSTCO	Iran	yes	yes	http://anstco.com/english/indexen.html
Bioinicia	Spain	yes	yes	http://bioinicia.com/, http://fluidnatek.com/
E-Spin NanoTech Pvt. Ltd.	India	yes	no	http://www.espinnanotech.com
Electrospinz	New Zealand	yes	no	http://www.electrospinz.co.nz
Electrospunra	Singapore	yes	no	http://www.electrospunra.com
Elmarco	Czech Republic	yes	yes	http://www.elmarco.cz/
Erich Huber GmbH	Germany	yes	no	http://www.ehuber.de/
Fnm Co.	Iran	yes	yes	http://en.fnm.ir/

Fuence	Japan	yes	yes	http://www.fuence.co.jp/en
HOLMARC Opto-Mechatronics	India	yes	no	http://www.holmarc.com/nano_fiber_electrospinning_station.php
IME Technologies	The Netherlands	yes	no	http://www.imetechnologies.nl/Electrospinning-n206m266
Inovenso	Turkey	yes	yes	http://www.inovenso.com
KatoTech Co. Ltd	Japan	yes	no	http://english.keskato.co.jp/products/neu.html
Linari Engineering s.r.l	Italy	yes	no	http://www.linaribiomedical.com/index.php/en/
MECC Co. Ltd	Japan	yes	yes	http://www.mecc.co.jp/en/html/nanon/list.html
MTI Corporation	USA	yes	no	http://www.mtixtl.com/
NaBond	Hong Kong	yes	no	http://www.electro-spinning.com
Nadetech Innovations	Spain	yes	no	http://www.nadetech.com/
Nano-Cat	Italy	yes	no	http://www.nanocat.it/
Nanodev Scientific	Turkey	yes	no	http://www.nanodev.com.tr
Nanoflux	Singapore	yes	no	http://www.nanoflux.com.sg
Nanomate Electrospinning	India	yes	no	http://vajendra.wix.com/indiaelectrospinning
NanoNC	South Korea	yes	no	http://www.nanonc.co.kr/
NanoStatics Corporation	Ohio, USA	yes	no	http://www.nanostatic.com/
Nasiol	Turkey	yes	no	http://www.nasiol.com/
Nanotar	Iran	yes	yes	
Physics Equipment	India	yes	no	http://www.phyeqpt.in/

Progene Link Sdn Bhd	Malaysia	yes	no	http://www.progenelink.com/
SKE S.r.l.	Italy	yes	no	http://www.ske.it/material-technologies/e-fiber-electrospinning-platform
SPINBOW	Italy	yes	no	http://www.spinbow.it/
Spraybase	Ireland	yes	no	http://www.spraybase.com
SPUR	Czech Republic	yes	yes	http://www.spur-nanotechnologies.cz/
Toptec Company Limited	South Korea	yes	yes	http://www.toptec.co.kr/
Yflow	Spain	yes	yes	http://www.yflow.com/
Zhengzhou CY Scientific Instrument Co., Ltd.	China	yes	no	http://www.zzcyky.com/

There are just few companies offering equipment for production of core-shell nanofibers, in the world. The first unique equipment enabling the production of core-shell nanofibers in the laboratory, and even in the industrial scale was developed at TUL with this work and within Nanoprogres, the Czech nanotech cluster. Other companies dealing with offers of coaxial electrospinning equipment are given in the Table 2.

Table 2 *Companies engaged in developed and in selling of coaxial electrospinning equipment*

Company	**Country**	**Laboratory Setup**	**High productivity equipments**	**Core-shell nanofibers**	**Website**
Contipro	Czech Republic	yes	no	yes	http://www.4spin.info/
Physics Equipment	India	yes	no	yes	http://www.phyeqpt.in/
Yflow	Spain	yes	yes	yes	http://www.yflow.com/

1.6 Applications of core-shell nanofibers

Core-shell nanofibers have a high potential of use in tissue engineering to replace damaged tissue or as materials for a *drug delivery system*. Coaxial electrospinning is regarded as one of the most significant breakthroughs in this field (Dzenis, 2004; Moghe, 2008). The structure of nanofibers is reminiscent of the extracellular matrix. Due to these specific properties and the possibility of incorporation of the active substance as their core part, core-shell nanofibers have an excellent usage in a medical field as a replacement of a damaged tissue (e.g. a skin, muscle tissue, or neural tissue), wound dressing or as systems for drug delivery. Materials with incorporated drugs, antibiotics, disinfection, enzymes, liposomes, spheres or even with DNA can be created and used in this field. They can be used as nanofibrous scaffolds enabling a support of cell proliferation and a creation of the new tissue. Their structure allows enough space for cell proliferation, migration and growth through the whole structure of the scaffold.

The drug delivery system is a special technology for controlled transport of drugs by the body to the treated place. The drug is located inside of core-shell nanofibers and this is protected by a shell part of nanofibers. The drug can be released from nanofibers gradually or suddenly in its full dose. This system of the controlled drug release can be initiated e. g. by pH changing. The drug may be transported by microcapsules or by liposomes. Liposomes are defined as the spherical formations with an aqueous volume completely closed by a membrane composed of lipid molecules (Mickova, 2015). They were first described by British hematologist, A.D. Bangham in year 1965 (Bangham, 1965). Liposomes may be used as a carrier of the drug or active agent. Their disadvantage is the necessity of the aqueous medium. Coaxial electrospinning allows incorporation of these liposomes with active agent into aqueous medium (core) and their protection by the shell.

The coaxial electrospinning also eliminates any damage caused by direct contact of the incorporated drug with organic solvents or harsh conditions during emulsification (Jiang, 2014). The high interest in core-shell nanofibers for medicine is given by the possibility of spinning of completely or hardly spinnable materials. The coaxial electrospinning can produce nanofibers with incorporated antibiotics (Huang, 2003), drug (Su, 2012), growth

factors (Liao, 2006), enzymes (Reznik, 2006) or cells (Klein, 2009). Great advantage of this technology is a core-shell formation with core and shell components represented by materials with different degradation times.

The medicine is not the only one possible field of use of the core-shell nanofibers. They can be also used in optics, filtration, as composites, electrically conductive fibers or as special probes for detection systems (A.G. MacDiarmid, 2001; Song, 2006; Dumas, 2007; Greiner, 2007).

The technology of coaxial electrospinning also allows incorporation of solid nanoparticles into nanofibers. Iron particles, silver particles, magnetic particles or nanodiamonds for example can be used as core part of the core-shell nanofibers. These systems can be suitable as special magnetic filters, sensors, special probes or they find them application in electronics (Dumas, 2007; Song, 2006). Selected fields of applications of core-shell nanofibers are listed in Table 3.

Table 3 *Selected fields of applications of core-shell nanofibers*

Categorization	**Application**	**Function**
Tissue engineering	2D nanofibrous scaffolds	damaged epithelia, bone, cartilage or organic tissues
	3D nanofibrous scaffolds	damaged epithelia, bone, cartilage or organic tissues
	structured scaffolds	damaged epithelia, bone, cartilage or organic tissues
	paralelized scaffolds	damaged nervous or muscle tissue
Drug delivery system	nanofibers with incorporated microcapsules transported drug	local controlled release of drug
	nanofibers with incorporated liposomes transported drug	local specific controlled release of drug
	nanofibers with incorporated antibiotics	local controlled release of antibiotics
	nanofibers with incorporated drug	local controlled release of drug
	nanofibers with incorporated grow factors	local controlled release of grow factors
	nanofibers with incorporated enzymes	local controlled release of enzymes
Wound dressing	nanofibers with active agent	damaged epithelia
optics	fiber optic cables	transfer of the signal
filtration	filters with active agent	layer of special filters

Categorization	Application	Function
	magnetic filters for information storage	layer of special filters
composites	composites with incorporated nanofibers	sophisticated filler in the composite
electrictronics	electrically conductive fibers	transfer of the signal
	sensors	transfer of the signal
	special probes for detection systems	transfer of the signal
electrochemical information storage	special reservoirs of information	transfer of the signal

2 The theoretical part

This chapter is focused on the theoretical principle of electrospinning, especially coaxial electrospinning. The technology of coaxial electrospinning process focusing on the bi-component droplet create is described and theoretical relations of hydrodynamics for needleless electrospinning from a free liquid surface were derived. Relaxation time of electrospinning described increasing instability of liquid, formation of Taylor cone and start of electrospinning was investigated and derived. The subchapter 2.5 deals with the thermodynamics of polymer solution, especially theory of miscibility of polymer solutions and relaxation time.

2.1 A general description of the coaxial electrospinning technology

Coaxial electrospinning, in which a special spinning electrode is supplied by two different liquids, is a variant of electrospinning for production of core-shell nanofibers from two kinds of liquids/polymeric solutions. This is a special technology for production of bi-component nanofibers with core-shell structure as can be seen in Figure 13. The shell is most commonly a polymeric material, while the core can be composed of other polymer or of other liquids containing nanoparticles, drugs, cells, antibiotics, enzymes, DNA or growth factors (Song, 2006; Bazilevski, 2007, Sun 2003, Zussman 2011, Huang 2006, Liao 2006, Samarasinghe 2008; Li, 2004; Ma, 2005; Moghe, 2008). This method allows also incorporation of solid particles for special magnetic filters, sensors or electronic (Song, 2006). Hollow nanofibers can be produced also with this technology as introduced in (Dror, 2009), (Li, 2004). A great advantage of this technology is a production of nanofibrous materials with a different rate of degradation.

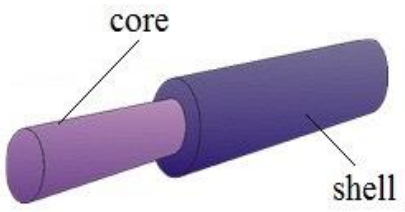

Figure 13 *Scheme of core-shell nanofiber.*

The technology of the coaxial electrospinning is a similar to the conventional electrospinning. Coaxial electrospinning set-up consists of the coaxial spinning electrode

connected to the HV source, the collector connected to the HV source, a reservoir of core and shell polymer solutions and a feeding apparatus for feed of core and shell polymer solution. The spinning electrode can be represented by coaxial needle or other coaxial apparatus allow the production of core-shell nanofibers. These apparatus are described in detail in the chapter 3.4 and 3.5. The coaxial spinning electrode is usually positively charged and located at a defined distance from the oppositely charged collector as is shown in Figure 14. Different kinds of collectors can be used for coaxial electrospinning depending on the desired nanofibrous structure. These collectors are introduced in the chapter 1.4. Usually, the support nonwovens fabric for collecting of the produced nanofibers is located under the collector.

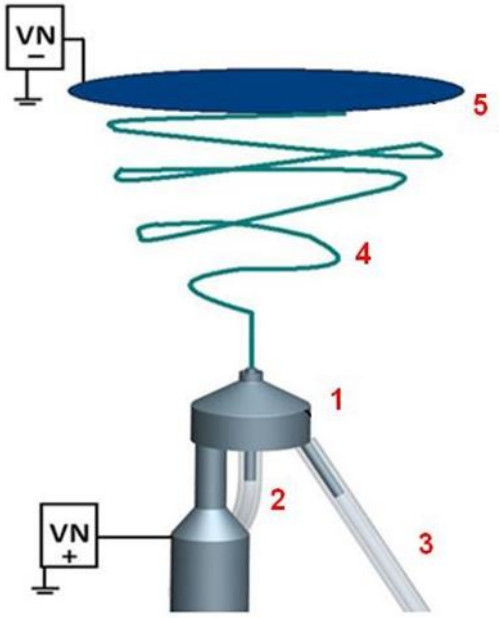

Figure 14 *The scheme of the coaxial experimental setup: the coaxial spinning electrode connected to the HV source (1), the feed of the core solution (2), the feed of the shell solution (3), whipping instability zone (4), the collector connected to the HV source (5), (Vyslouzilova, 2012).*

The feeding apparatus doped the spinning electrode with the core and shell polymer solutions. These solutions are delivered through coaxial spinning electrode to its orifice and the bi-component droplet composed of the shell and core solutions is created in this place, see in (Figure 15). After switching on the HV source is the high voltage applied on the polymer solution. There occurs a duel of the capillary and electric forces, in the electrospinning solution. Positively charged ions are regrouping to the surface of the polymer solution towards to the negatively charged collector. They are attracted to this one as is shown in

Figure 16. The polymer solution is destabilized by a high external electric field and capillary waves are created on the surface of polymeric bi-component droplet/two-layer respectively.

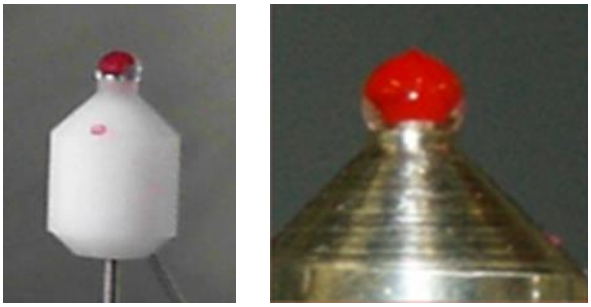

(a) (b)

Figure 15 *Bi-component droplet composed of the shell (transparent color) and the core (red color) polymer solution at the orifice of (a) the coaxial needle spinning electrode and (b) the electrospinner no. 4 (Vodseďálková, 2010)*

The Taylor cone originates from the fastest growing capillary wave with a characteristic wavelength λ on the top of the shell polymer solution. This Taylor cone pulls up the core solution and both polymer solutions are drawn and elongated together by external and internal electric forces through the zone of *the whipping instability* to production of core-shell nanofibers (Moghe, 2008). These are collected on the support nonwovens fabric located under the oppositely charged collector.

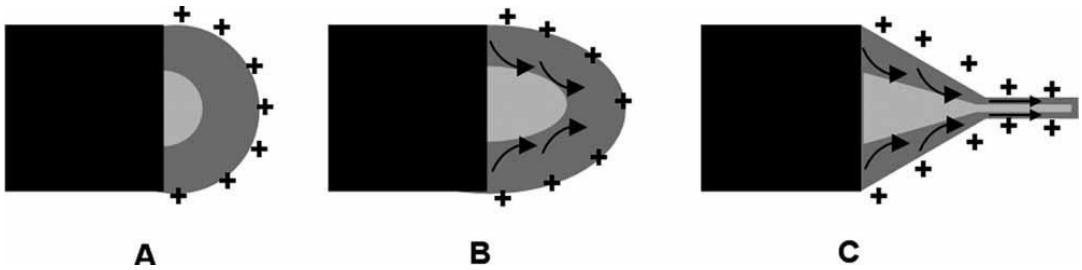

Figure 16 *Schematic illustration of bi-component droplet and the Taylor cone formation with the regrouping of the positive charge to the surface of the bi-component droplet. Adapted from (Moghe, 2008)*

2.2 Dispersion law for non-viscose liquids

The chapter deals with the behavior of liquid exposed to applied high voltage. There is a duel between electric forces F_e and capillary forces F_c after applying of the external electric field on the polymeric solution. The first Taylor cone and the first polymer jet is formed on the

liquid surface after overcoming capillary forces by electric forces $F_e > F_c$, when the critical value of electric field E_c is achieved.

Theory of continuum

A prerequisite of hydrodynamics is that a fluid is regarded as a continuous medium. This means that all elementary volumes contained within the investigated liquid have same properties irrespective on their location and on the direction of forces acting on these volumes (Landau, 1987).

The hydrodynamics considers so-called *elementary volume* of a liquid v_0, see in (Figure 17). This volume contained constantly moving particles. This one is infinitesimally small in macroscopic term but still much bigger compare to the size of contained particles. This elementary volume in the liquid is during the investigation of its movement considered to be almost a point. This mean, that *the fluid particle* and *the point in the fluid* are to be understood in a similar sense (Landau, 1987).

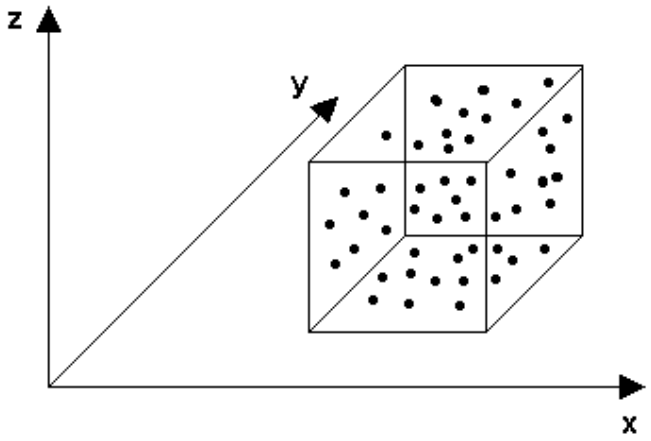

Figure 17 *The elementary volume v_0: The volume is infinitesimally small in macroscopic term but still much bigger compare to the size of contained particles.*

Theory of waves

The derived of dispersion laws is an indispensable part of hydrodynamic necessary to understand of behavior of liquids during electrospinning process. A dependence of an angular frequency ω of a capillary wave occurring on the surface of a liquid on a wave number *k* can

be expressed using dispersion laws. The capillarity plays an important role on capillary waves behavior (Levich, 1962). *Capillary waves* have a period[1] shorter than 0.5 s. A surface tension and gravity forces are at the equilibrium in capillary waves. In bigger waves are gravity forces dominant. These waves are called *gravitational waves* and they are formed after overcoming of the equilibrium. The waves of amplitudes *a*, which one considerably smaller than the wavelength λ, $a \ll \lambda$, see in (Figure 18) will be investigated in this work.

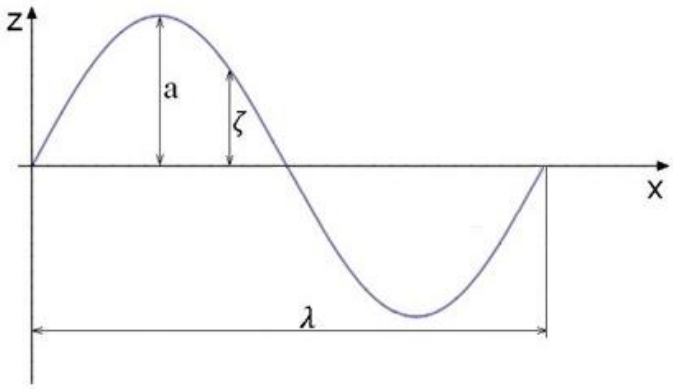

Figure 18 *The wave in the 2D system: The wave is characterized by its wavelength λ and by the amplitude a. The symbol ζ denotes the vertical displacement of the free liquid surface.*

Dispersion law

An *ideal fluid* is defined as a completely incompressible medium and non-viscous fluid without an internal friction (Landau, 1987). The dispersion law may be derived on the basic of three basic equations of hydrodynamics:

$$\rho = const., \tag{2.1}$$

where ρ denotes liquid density.

$$\vec{\nabla}\,\vec{v} = 0 \tag{2.2}$$

is the continuity equation expresses the law of conservation of the mass, where $\vec{v}$ denotes velocity field of fluid. The symbol $\vec{\nabla}$ is Hamilton operator and *t* denotes the time.

$$\rho \frac{d\vec{v}}{dt} = -\vec{\nabla}p \tag{2.3}$$

[1]Period of wave is the time for a particle on a medium to make one complete cycle. This indicates the time to copying the trajectory of the wave performs wavelength.

is Euler equation based on the Newton's Second Law of Motion. This describes a motion of the ideal fluid. The introduced form of the Euler equation is derived using the assumption that $a \ll \lambda$.

The Laplace equation for the velocity potential $\Delta\phi = 0$ may be obtained after the substituting of the velocity potential ϕ into the continuity equation. The symbol Δ denotes the Laplace Operator. The form of the Laplace equation in Cartesian coordinates is $\Delta = \left(\frac{\partial^2}{\partial x^2} + \frac{\partial^2}{\partial y^2} + \frac{\partial^2}{\partial z^2}\right)$.

The movement of capillary waves on the free surface of liquid assuming of uniform waves is investigated. The solution may be the dispersion law describing the behavior of gravitational waves on the free surface of the liquid

$$\omega^2 = gk, \tag{2.4}$$

where ω denotes the angular frequency, g is the gravity acceleration, k is the wave vector. The relation shows the squared of the angular frequency directly proportional to the wave vector. The period is growing with increasing of the wavelength. The dispersion law describing the behavior of capillary (or capillary-gravity respectively) waves on the free surface of the liquid is given by

$$\omega^2 = gk + \frac{p}{\rho}k^2. \tag{2.5}$$

The dispersion law for the non-viscose liquids is given as

$$\omega^2 = gk + \frac{p}{\rho}k^2 - \frac{\varepsilon_0 E^2}{\rho}k^2, \tag{2.6}$$

where $\varepsilon_0$denotes permittivity of vacuum and E is field strength.

2.3 Dispersion law for viscose liquids

Viscose fluids are real liquids with shear tension that is impossible to neglect in hydrodynamics. When two adjacent layers of the real fluid have different speed, the shear stress τ is formed at interface between them. The shear stress (2.7) is causes by the emergence of the friction between these layers causes by the viscosity of liquid.

$$\tau_{xz} = \mu\frac{\partial v_x}{\partial_z}, \tag{2.7}$$

where μ denotes dynamic viscosity. The symbol ∂v_x decides the speed difference of adjacent layers along the *x*-axis, while *z* is the distance between these layers. Figure 19 shows the fluid flow between parallel flat plates (Feynman, 2001). The one flat plate is firmly fixed, while the last one moves in the direction parallel with the velocity v_0.

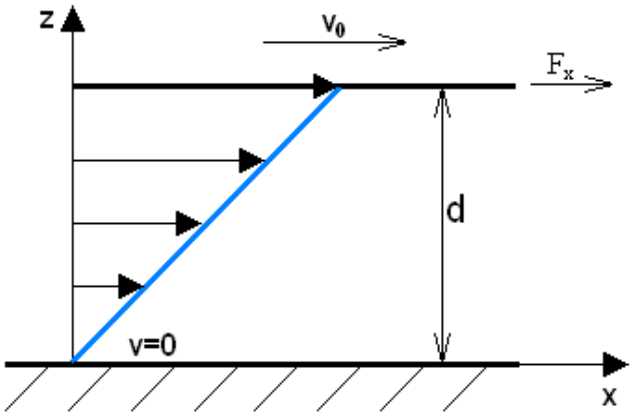

Figure 19 *The fluid flow between two parallel flat plates: The lower plate is firmly fixed, the upper plate moves with the velocity* $\boldsymbol{v_0}$ *along the x-axis. The liquid near the surface of the bottom plate has the zero velocity, while the liquid layer adjacent to the upper plate moves with it.*

The dispersion law for the gravity wave of viscose fluids is based on the linearized Navier-Stokes equation (2.8). A diffusion equation for the velocity curl will be obtained by taking a curl of this equation.

$$\frac{\partial \vec{v}}{\partial t} = -\frac{\vec{\nabla} p}{\rho} + \nu \Delta \vec{v} \tag{2.8}$$

Levich decomposes the velocity field $\vec{v}$ into two components $\vec{v} = \overrightarrow{v_0} + \vec{u}$ (Levich, 1962). The first part of this relation $\overrightarrow{v_0}$ expresses the potential part of the fluid flow and $\vec{u}$ describes the non-potential part of the liquid velocity field expressed by the curl of a liquid flux. The velocity field may be expressed using a velocity potential ϕ for 2D system of the flow in the plane (x, z) as $\vec{v} = \vec{\nabla}\phi = \left(\frac{\partial \phi}{\partial x}, 0, \frac{\partial \phi}{\partial z}\right)$ and using a scalar field ψ as $\vec{u} = \vec{\blacksquare}\psi = (-\frac{\partial \psi}{\partial z}, 0, \frac{\partial \psi}{\partial x})$. The symbol $\vec{\blacksquare}$ denotes a symbolic operator $\vec{\blacksquare} = \left(-\frac{\partial}{\partial z}, 0, \frac{\partial}{\partial x}\right)$ and the symbol ψ is called a flow function. The velocity potential ϕ fulfills the Euler equation. The continuity equation is valid assuming incompressibility of the fluid. The Laplace equation is then given:

$$\Delta \phi = 0 \tag{2.9}$$

A function ϕ may be given as the solution of the Laplace equation in the exponential form:

$$\phi = Ae^{kz}e^{ikz}e^{-i\omega z}, \tag{2.10}$$

where *A* represents an amplitude of the velocity potential, the symbol *k* is a decay parameter as well as a wave number, *i* denotes an imaginary unit and *ω* is the angular frequency.

The modified Navier-Stokes equation may be obtained instead of the velocity field $\vec{u}$ after substituting the flow function ψ into the Euler equation. The modified Navier-Stokes equation has the shape of the diffusion equation for the flow function ψ:

$$\frac{\partial \psi}{\partial t} = \nu \Delta \psi \, . \tag{2.11}$$

The solution of the flow function ψ has the form

$$\psi = Ce^{lz}e^{ikx}e^{-i\omega t}, \tag{2.12}$$

where *C* denotes the initial amplitude, *l* is the decay parameter of the wave amplitude, *k* represents the wave number. Substituting the flow function from equation (2.12) into the equation (2.11) one obtains the relation between the decay parameters *k* and *l:*

$$l^2 = k^2 + \frac{-i\omega}{\nu} \tag{2.13}$$

The boundary conditions on a free surface of the viscous liquid (2.14) are now established to obtain the dispersion law. The balance of the vertical and horizontal stress components acting in the surface layer of the fluid is described there. The pressure applied on this surface consists of the hydrostatic, electric and capillary pressure and by components of shear stress p_{zz} and p_{xz}. This shear stress is causes by the non-zero liquid viscosity and by the pressure induced by a movement of the fluid $\rho \frac{\partial \phi}{\partial t}$. The pressure applied on this surface consists

$$\rho \frac{\partial \phi}{\partial t} = -p + p_{zz}, \tag{2.14a}$$

$$p_{xz} = 0, \tag{2.14b}$$

wherein $p_{zz} = 2\mu \frac{\partial v_z}{\partial z}$ and $p_{xz} = \mu \left(\frac{\partial v_x}{\partial z} + \frac{\partial v_z}{\partial x} \right)$. The pressure p composes of three parts: the hydrostatic, capillary and electric part, i.e., $p = \rho \zeta g - \gamma \left(\frac{\partial^2 \zeta}{\partial x^2} \right) - \varepsilon_0 k E^2 \zeta$ (Landau, 1987; Lukas, 2009). There is obvious that the hydrostatic pressure counteracts the capillary pressure, in the equation (2.14a).

The needleless electrospinning applies principle of electrospinning from a free surface of polymeric layer. In the environment of high external electric field the electro-spun liquid is destabilized (Lukas, 2009). The effect of instability is described as Larmor-Tonks-Frenkel one (Frenkel, 1955; Tonks, 1935; Larmor, 1890). This effect has its nature in the self-organization by the mechanism of the "fastest forming instability," i.e., of the fastest growing capillary wave (Larmor, 1890; Tonks, 1935; Frenkel, 1955). The electric field applied on the free surface of the polymer layer causes growth of capillary waves, which have very small amplitude compared to wavelength, on the beginning of the process (before applying of external electric field). The electrospinning started from the faster forming wave. This is intended by a negative (a minimal) value of the angular frequency ω^2. Conditions of the formation of instability on the free fluid surface in 2D space are investigated. The vertical wave deflection ζ is described by relation $\zeta = A\, exp[i(kx - \omega t)]$, vide (Lukas, 2009). The relation between the vertical wave deflection ζ and scalar fields ϕ and ψ has the form

$$\zeta = \int \frac{\partial v_z}{\partial z} dt = \int \left(\frac{\partial \phi}{\partial z} + \frac{\partial \psi}{\partial z}\right) dt \cong 0. \tag{2.15}$$

This is geometric boundary condition. It may be say, that the wave is instable with the condition $-i\omega < 0$. Landau (1987) shows that the solution of boundary conditions (2.14) and (2.15) is the dispersion law for viscose fluids:

$$(-i\omega + 2\nu k^2)^2 + \omega_0^2 = 4\nu^2 k^4 \sqrt{\frac{-i\omega}{\nu k^2} + 1}\,. \tag{2.16}$$

2.4 Relaxation time of electrospinning

The relaxation time of electrospinning *T* can be determined on the bases of the dispersion law for viscose fluids (2.16). This is the time necessary to Taylor cones formation and start of electrospinning process after applying of the high voltage on the electrospun liquid. The electric forces deformed the free liquid surface and Larmor-Tonks-Frenkel instabilities are formed (Frenkel, 1955; Tonks, 1935; Larmor, 1890). The electrospinning originates from the fastest growing instability when the critical value of the electric strength E_c is overcoming. Levich (1962) introduced the solution of the dispersion law (2.16) in the case of the low viscosity liquids and long wavelengths, $\frac{-i\omega}{\nu k^2} \gg 1$ as:

$$-i\omega \cong -i\omega_0 - 2\nu k^2. \tag{2.17}$$

The solution of the dispersion law (2.16) for highly viscous liquids and short wavelengths, $\frac{-i\omega}{\nu k^2} \ll 1$, is given as (Levich, 1962):

$$-i\omega \cong -\nu k^2 \pm \sqrt{\nu^2 k^4 - \omega_0^2} = -\frac{\omega_0^2}{2\nu k^2}\,. \tag{2.18}$$

Electrospinning originates from the fasters growing instability on the free surface of the liquid. This process is managed by the dispersion law (2.16). The instability occurs for a root of this equation with $-i\omega > 0$. The reciprocal value of this growth rate $\tau = \frac{1}{-i\omega}$ can be taken as a characteristic time of the Taylor cone formation.

It is advantageous to introduce dimensionless variables and relations for further adjust:

$$\Omega_0^2 = \omega_0^2 \cdot \frac{a}{g}\,,\ A = -i\omega\sqrt{\frac{a_c}{g}}\,,$$

$$K = a_c k,\ O_h = \sqrt{\frac{\nu^2}{g a_c^3}}\,, \tag{2.19}$$

where A is the dimensionless growth rate, K denotes the dimensionless wave number, a_c denotes capillary number $a_c = \sqrt{\gamma/\rho g}$ and O_h is the *Ohnesorge number*[2]. The dispersion relations (2.18) and (2.6) can now be rewritten respectively as:

$$(A + 2O_h K^2)^2 + \Omega_0^2 = 4O_h^2 K^4 \sqrt{\frac{A}{O_h K^2} + 1}\,, \tag{2.20}$$

$$\Omega_0^2 = K^3 - 2\Gamma K^2 + K \tag{2.21}$$

We want to gain dimensionless growth rate A according K. The equation (2.20) can be rewritten using a new dimensionless variable $x = A/(O_h K^2)$ as:

$$(x+2)^2 - 4\sqrt{x+1} + \Omega_0^2/O_h^2 K^4 = 0. \tag{2.22}$$

The first term is dominant for large values of x and the second one can be linearized for $x \to 0$ using $\sqrt{x+1} \cong 1 + x/2$. In this approximation, the dimensionless dispersion relation (2.22) can become a quadratic function in x, $x^2 + 2x + \Omega_0^2/(O_h^2 K^4) = 0$. The dimensionless growth rate A can be then obtained as its positive root:

[2] The Ohnesorge number is a dimensionless constant that describes liquid cohesion. This number relates the viscous forces to inertial and surface tension forces.

$$A = -O_h K^2 + \sqrt{O_h^2 K^4 - \Omega_0^2}\,. \tag{2.23}$$

Now, we need to obtain the relations between the dimensionless wave number *K* and the electrospinning number $\Gamma = \frac{a\varepsilon E^2}{2\gamma}$ (Lukas, 2008). The condition for maximization of the growth rate *A* follows from the (2.23) rewritten in the form of an implicit function. Then, the conditions for extremes of this implicit function *f(K,A)* are:

$$f(K,A) = A^2 + 2O_h K^2 A + K^3 - 2\Gamma K^2 + K = 0, \tag{2.24a}$$

$$\frac{\partial f(K,A)}{\partial K} = 4O_h AK + 3K^2 - 4\Gamma K + 1 = 0. \tag{2.24b}$$

By analyzing the roots of (2.24) we can obtain the relations between the electrospinning number Γ and the dimensionless wave number *K*. This one is valid in case of the maximal growth rate *A*. In the first step, the (2.24b) can be rewritten as $\Gamma = O_h A + 3K/4 + 1/(4K)$ and $= O_h AK + 3K^2/4 + 1/4$. The equation for ΓK, together with that for $f(K,A)$, (10a), gives $A = \sqrt{(K^3 - K)/2}$. Thus, substituting *A* from here back into (2.24b) we obtain the resultant Γ-*K* relationship (2.25) and maximal *A* value for medium viscosity liquids. This relationship is compared to the one for non-viscous liquids (2.26):

$$\Gamma = \frac{3}{4}K + \frac{1}{4K} + O_h\sqrt{\frac{K^3 - K}{2}}\,, \tag{2.26}$$

$$\Gamma = \frac{3}{4}K + \frac{1}{4K}\,. \tag{2.27}$$

The equation (2.23), together with the inversion of the equation (2.26), i.e., $K = K(\Gamma)$, gives the dependence of the maximal value of *A* on the electrospinning number Γ for a given O_h. The relation $A = A(\Gamma)$ means that the theoretical results can be compared with experimental data, see in (Chapter 3.3), on the dimensionless time of Taylor cone formation, $T = 1/A$:

$$T = \frac{1}{-O_h K^2 + \sqrt{O_h^2 K^4 - K^3 + 2\Gamma K^2 - K}} \tag{2.28}$$

2.5 Miscibility of polymer solutions

Coaxial electrospinning process is influenced by a number of process and system parameters. The interrelationship of used electrospun materials (core and shell liquid) plays among other an important role in the study of the issue of this technology. This chapter focuses on the miscibility of polymer solutions. Suitable selection of compatible electrospun solutions, their

solvent systems respectively, to prevent of coagulation at their interface and also to avoid their undesired mixing is an indispensable matters for the correct formation of core-shell nanofibers.

2.5.1 Miscibility

Miscibility and solubility of polymers is a known issue discussed in numerous publications since the 40s of the 20th century (Huggins, 1940; Huggins, 1941, Flory, 1941; Guggenheim, 1952; Hildebrand, 1950). Polymer dissolution and an understanding of this process plays a key role during a selection of a suitable solvents and setting of suitable parameters of experiment (Miller-Chou, 2003). This issue deals with a number of authors, e.g. Hildebrand and Scott (1950), Huggins (1940, 1941), Flory (1941), Utracki (1989) or Hansen (2004). However, only a few authors deals with miscibility in coaxial electrospinning. In general, authors states that core and shell solutions should be immiscible for formation of the core-shell structure of nanofibers (Kurban 2010; Sun Z. 2003; Zhang 2004). As described Sun Z. et al. (2003), states that the coaxial electrospinning process must to be sufficiently fast to avoid blending of the core and shell liquids (Sun Z. 2003). By contrast, Sun B. et al. (2006) states that there should be at least partially miscibility between the core and the shell liquid in case of coaxial electrospinning. He explains that the surface tension between these liquids would be reduced, resulting in the formation of very fine bi-component nanofibers with core-shell structure.

Most of the polymer solutions are immiscible or hardly miscible, resulting in the creation of two separate phases. Immiscibility/bad miscibility of the polymers depends mainly on the polarity of polymers, their molecular weight and crystallinity (Utracki 1989). There occurs separation of polymers and the separate phases are created in case of differing polarities of polymers. Results of a high molecular weight is a low entropy of the polymeric system. Independently crystallizing polymers leads to the formation of the separate phase which is rarely miscible with the second polymer. Polymers classified according to the polarity can be divided into *non-polar polymers* - saturated hydrocarbons; *polarizable polymers* - unsaturated and aromatic hydrocarbon polymers (PS); *polar polymers*- polymers containing ether, ester, nitrile, chlorine or fluoride; *highly polar polymers* - polymers, containing higher concentration of amide, urethane, urea, amine, carboxyl, hydroxyl or iron groups (Meissner, 1987).

2.5.2 Miscibility of polymer solutions, coaxial electrospinning

Separation of core and shell liquids in case of coaxial electrospinning is an undesirable effect, because this leads to the formation of non-coaxial nanofibers. Core and shell liquids are electrospun separately and bi-component nanofibers with a side-side structure or nanofibrous layer with two types of nanofibers (from core and shell solutions) are produced. However, on the other hand, there must not occur either premature mixing of these two materials. Result is a blend of core and shell liquids and non-coaxial nanofibers are formed in this case.

Selection of suitable solvents for both of the electrospun polymers is the primary step in preparation of core-shell nanofibers (Yu 2004; Moghe 2008). Unsuitable selection of solvent systems has resulted in a coagulation after contact of the core and the shell of the polymer solutions at the orifice of the coaxial spinning electrode. The emphasis is on the reduction of interfacial tension at the interface of the selected polymer solutions. The choice of the same solvent for both of the used polymers is an usual solution eliminating of the coagulation. The interfacial tension is very low in this case and core-shell nanofibers can be created. There should not happen undesired premature mixing of these liquids during coaxial electrospinning process, because the characteristic time τ_1 expressing a movement of the polymeric jet through the whipping zone is considerably shorter than diffusion or mixing of the used polymeric materials (Sun, 2003). Sun (2003) states that should not happen to premature mixing of the miscible polymer solutions during coaxial electrospinning, because τ_1 is in milliseconds. This value is significantly less than the time for diffusion or mixing of the polymer solutions (Sun, 2003).

Sun B. et al. (2006) described the production of very fine core-shell nanofibers caused by partially miscibility of solutions in case of lower interface tension. There is a sharp boundary between the core and the shell due to the immiscibility of these solutions in the bi-component nanofiber. Core-shell nanofiber from partially miscible solutions will be significantly finely. Polyvinyl pyrrolidone (PVP) as the core and polylactide acid (PLA) as the shell was used for their experiment. N,N-dimethylformamide (DMF) and ethanol (ratio 50:50) were used as a solvent for PVP. Solutions at concentrations of 4, 6, 8 and 10 % (w/v) were prepared. Surface tension of these solutions changed slightly as the concentration was increased, ranging from 27,44 mN/m (4%) to 28,12 mN/m (10%).

Produced nanofibers were analyzed using transmission electrode microscope (TEM). Images from this analyses show finely nanofibers in case of higher concentration and surface

tension of PVP (Figure 20). There are shown beaded defects in case of the too lower concentration of PVP, see (Figure 20 a, b).

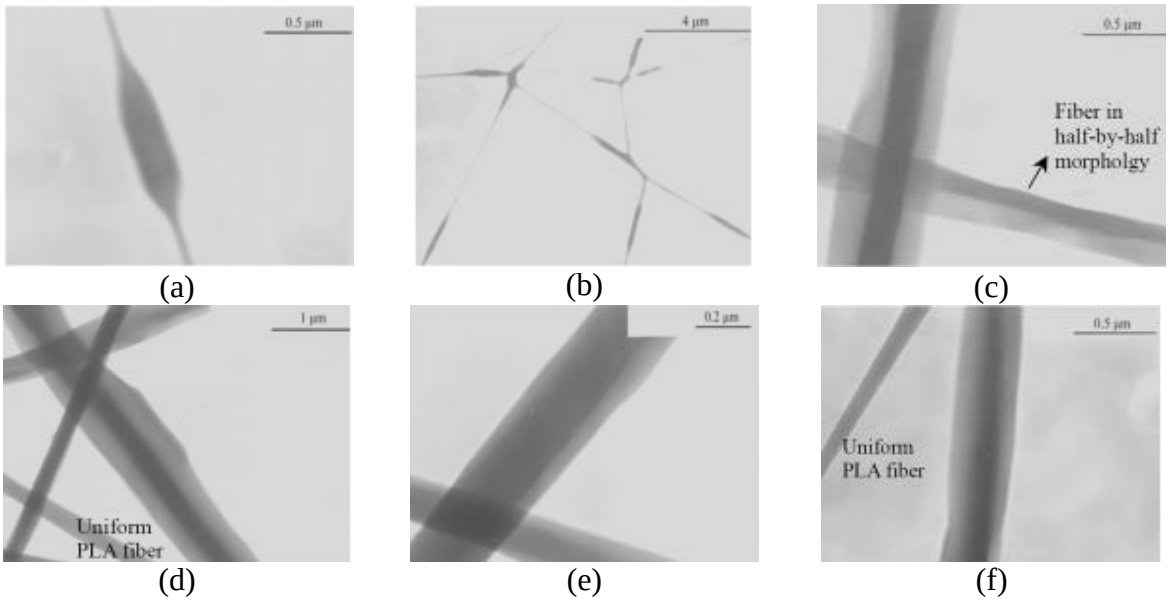

Figure 20 *TEM images of bi-component nanofibers PLA/PVP at different concentration of PVP: (a, b) 4 % (w/v), (c, d) 6 % (w/v) , (e) 8 % (w/v), (f) 10 % (w/v), Adapted from (Sun B. 2006)*

Li and Xia (2004) used immiscible solutions for production of hollow nanofibers. The solution composed from 0,3 g of PVP, 3 g of ceramic precursor $Ti(OiPr)_4$, 2 ml of acetic acid and 5 ml of ethanol are used as the shell. The mineral oil was used as the core. Coaxial electrospinning was used for production of core-shell nanofibers from these immiscible liquids. In the next step, the oil was extracted from the core-shell nanofibers and hollow nanofibers were produced as is shown in (Figure 21 a). The nanofibrous layer was immersed in octane overnight resulting in the extraction of the oil from the core part of bi-component nanofibers.

Chan et al. (2009) used poly(methyl methacrylate), (PMMA) as the shell and mineral oil, toluene, octane or distilled water as the core. Hollow fibers realized using PMMA dissolved in chloroform/ethanol (ratio 3:1) at concentration of 20 % (w/v) are shown in Figure 21 b. Mineral oil was used as the core. Core-shell nanofibers were produced using coaxial electrospinning. The mineral oil was removed from the produced fibers their soaking in octane for more than 12 h.

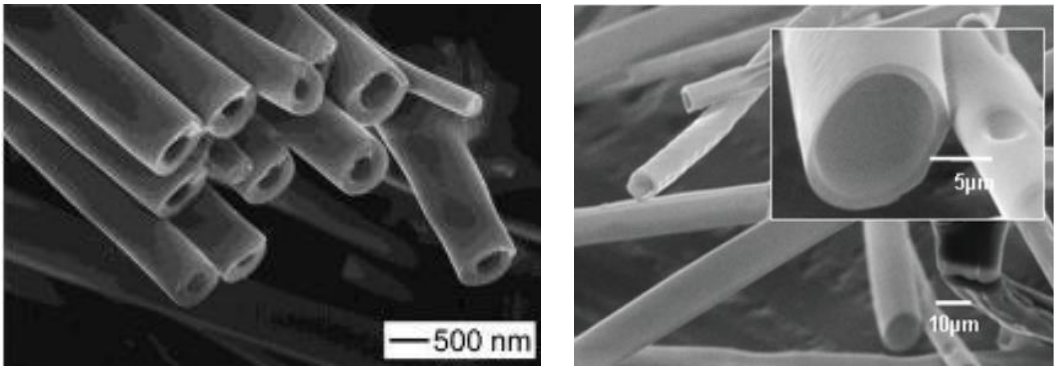

Figure 21 *(a) SEM image of hollow nanofibers PVP/ Ti(OiPr)$_4$, adapted from (Li 2004), (b) SEM image of hollow fibers PMMA, adapted from (Chan 2009).*

Miscibility of core and shell polymer solutions and appropriate selection of their solvent systems play an important role in coaxial electrospinning, because diverse core-shell structure can be formed.

2.5.3 Thermodynamic criterion of blending of polymers

The second law of thermodynamics will be used for understanding of behavior of polymer solutions during their mixing. The law deals with irreversibility of the natural processes and examines their natural course, which are under way. Changes in natural processes are happening naturally from an ordered state in an unordered state. Otherwise, the process is difficult, unnatural. The second law of thermodynamics deals with a disorderliness of the system, which is expressed entropy and says that naturally line of natural processes is a change of more ordered state to a state with higher disorderliness. Changing the state is thus accompanied by the increase of entropy.

Miscibility of the selected materials can be determined by the following methods (Utracki 1989):

- The condition of miscibility (compatibility tests of polymers)
- Measuring of the interaction parameter χ_{ij}
- Methods of the phase equilibrium

Miscibility of polymer materials depends on the balance between enthalpy and entropy of the system (Utracki 1989). The result of the high entropy of the system is easy mixing of materials. Entropy is decreasing with increasing molecular weight of polymers (Utracki 1989), (Robeson 2007). The equation to determine the change of *the Gibbs energy* ΔG_M (5.1) is a basic equation for determining miscibility of the two polymer materials. According to the

thermodynamic criteria, two polymeric materials are mutually miscible, if the Gibbs energy change during their mutual mixing is negative $\Delta G_M < 0$ (Meissner 1987):

$$\Delta G_M = \Delta H_M - T\Delta S_M, \tag{5.1}$$

where ΔG_M is the Gibbs free energy change (ie. the mixing Gibbs energy), ΔH_M denotes the enthalpy of mixing, T is thermodynamic (absolute) temperature and ΔS_M is mixing entropy of the system. The mixing enthalpy under constant pressure can be expressed as:

$$\Delta H_M = \Delta U_M + p \cdot \Delta V, \tag{5.2}$$

where ΔU_M is the internal mixing energy, p is the pressure and ΔV expresses the volume change during the mixing process. Depending on the final value of mixing enthalpy, following situations can occur during the mixing of two materials (MI, 2009):

- Zero value of the enthalpy change $\Delta H_M = 0$. The materials are completely miscible. Equal forces are applied between the particles of the same and the different kind;
- A negative value of the enthalpy change $\Delta H_M < 0$. The materials are completely miscible. Forces between the molecules of the two components are greater than the forces between molecules of the same components, the energy is released;
- A positive value of the enthalpy change $\Delta H_M > 0$. The system is separated into two phases. The forces between the molecules of different components are weaker than the forces between molecules of the same components. The mixing can occur only on condition that the resulting enthalpy change will be smaller than the entropy change ΔS_M.

Good miscibility of two polymers can be achieved by increase of entropy ΔS_M and decrease of internal energy of the system ΔU_M, as is shown in equation (5.1). Increase in the entropy can be achieved by mixing of the non-polar liquids or liquids with low polarity. In this case, disorderliness of the system is increasing and a value of the entropy term $T\Delta S_M$ in equation (5.1) results in a negative value of the change of the Gibbs energy ΔG_M. The change of the Gibbs energy will be in positive values if the mixing enthalpy will be higher than entropy in the formula. This results in the blending of polymers and the formation of separate phases. Miscibility also depends on the temperature of the system as can be seen in (5.1). The change of the Gibbs energy is decreased with increasing of the temperature.

2.5.4 Flory - Huggins theory of polymer miscibility

Flory and Huggins were the first theorists dealing with the solubility of polymers. They used *a lattice model* applied to polymer solutions, already in the 40s of the 20th century. Lattice model is a regular grid, where each node is occupied by a molecule of solvent or polymer segment, as is shown in Figure 22 (Lukas, D. 2008).

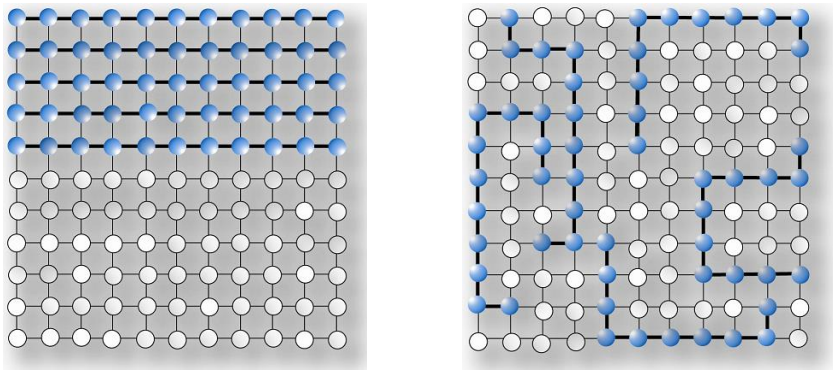

(a) (b)

Figure 22 *Lattice model of polymer chains and molecules of solvent before mixing (a) and lattice model of polymer chains surrounded by molecules of solvent after mixing (b) Blue color represents segments of polymer and white color represents molecules of solvent (Lukáš D. 2008).*

Flory - Huggins theory is based on degree of disorderliness of the system called entropy *S*. This is defined as the logarithm of the number of possible configurations *Q* in lattice model multiplied by the Boltzmann constant k_B:

$$S = k_B ln Q, \tag{5.3}$$

where *P* is the number of possible configurations of molecules of type 1 and 2 into nodes of the lattice model. The number of possible configurations *Q* is given by:

$$Q = \frac{N!}{N_1!N_2!}, \tag{5.4}$$

where N_1 is molecule of type 1, N_2 is molecule of type 2 and *N* is a total number of molecules in lattice model. Entropy of system for mixing of n_1 mol of component 1 and n_2 mol of component 2 is given by:

$$\Delta S = -k_B(n_1 ln\varphi_1 + n_2 ln\varphi_2), \tag{5.5}$$

where n_i and φ_i are molar proportions of the individual components. Assumption of the ideal solution is zero enthalpy; therefore the relation for miscibility of polymer solutions has a form:

$$\Delta G_M = k_B T(n_1 \cdot ln\varphi_1 + n_2 \cdot ln\varphi_2). \quad (5.6)$$

However, enthalpy in case of real polymer solutions has not a zero value and process of mixture is not completely random. It is necessary to take into account dependence on the thermodynamically most advantageous interactions. Real polymer solutions used *Flory-Huggins theory* of the mixing, which gives the relation for change of Gibbs energy in the following form:

$$\Delta G_M = k_B T(n_1 \cdot ln\varphi_1 + n_2 \cdot ln\varphi_2 + \chi \cdot n_1 \cdot \varphi_2), \quad (5.7)$$

where $\chi \cdot n_1 \cdot \varphi_2$ is a enthalpy member and χ is interaction parameter. This gives the energy interaction between the molecules. This is given by:

$$\chi = \frac{z\Delta\varepsilon}{k_B T}, \quad (5.8)$$

where *z* is a coordination number of lattice indicating the number of interacting nearest neighboring nodes on the grid, ε denotes the interaction energy, k_B is the Boltzmann constant and *T* is the thermodynamic temperature.

2.5.5 Solubility parameter

Polymer dissolution is analogous process to the mixing. This process has some main phases. The first phase of polymer dissolution is a swelling. Increased mobility of the solute occurs and this diffuses out of the polymer into the surrounding fluid (Miller-Chou, 2003). The swelling of the polymer is caused by the different diffusion rate of small molecules into the polymer solvent and polymer molecules into the emerging solution. Polymer chain segments are successively moving away until the segments are sufficiently distant to each other. This is accompanied by complete dissolution of polymer in solvent.

The solubility parameter is known since 1950 by Hildebrand and Scott (1950). Hildebrand solubility parameter δ_t is derived from the heat of vaporization of the components of the system and is defined as the square root of the cohesive energy density CED $[Jcm^{-3}]$:

$$\delta_t = \sqrt{CED} = \sqrt{(\Delta E_e / v)}, \quad (5.9)$$

where $\Delta E_e[J]$ is energy of evaporation and $v[cm^3]$ is volume of macromolecule.

The cohesion of the polymer is caused by so-called non-bonding forces acting between the molecules of one macromolecule with neighboring molecules. Degree of

cohesion is the energy needed to the complete separation of molecules called *energy of evaporation*. Cohesive energy of materials with low-molecular weight can be determined by measuring the heat of evaporation. However, polymers not occur in the gas phase and the cohesive energy can be determined only by indirect methods precisely on the solubility parameter. The principle is the determination of the solubility parameter of the polymer by the known solubility parameter of a solvent which dissolves the polymer as is shown in Figure 23 (Meissner 1987). In the first step, the polymer is slightly crosslinked to be insoluble. Followed by swelling of the polymer in a number of low-molecular substances with known solubility parameters and the equilibrium degree of swelling of the polymer network in these substances is determined. The value of solubility parameter of investigated polymer has the same value as the solubility parameter δ_t of the solvent in which degree of swelling has the highest value.

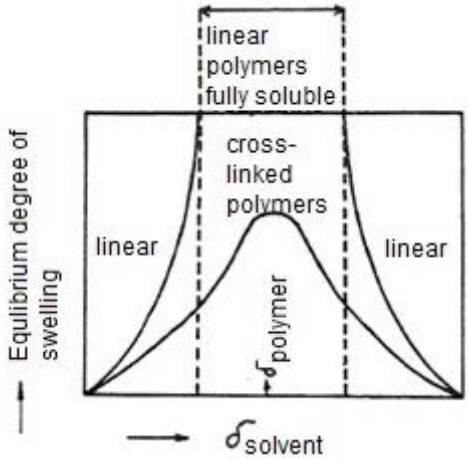

Figure 23 *Scheme of determination of the solubility parameters of polymers. Adapted from (Meissner, 1987)*

Hansen solubility parameter

Hansen solubility parameter (HSP) widely used to determine the compatibility between two substances is known since 1967 (Hansen, 2004; Launay, 2007). This says substances with the same value of HSP have suitable mutual affinity (Launay, 2007). Unlike the Hildebrand solubility parameter, Hansen uses a more detailed view of the issue of solubility and miscibility. His solubility parameter is composed of three components depending on the polymer solubility, polarity and hydrogen bridges. Evaporation of liquids is accompanied by breaking cohesive bonds. Non polar bonds, permanent dipole-dipole bonds and hydrogen bonds are broken by the evaporation process (Hansen, 2004). All of these knowledges are

includes in the Hansen solubility parameter. This is composed of a solubility parameter of dispersion component δ_D, solubility parameter of polar component $\delta_P\left[MPa^{1/2}\right]$ and solubility parameter of hydrogen bonding $\delta_H\left[MPa^{1/2}\right]$:

$$\delta^2 = \delta_D^2 + \delta_P^2 + \delta_H^2 \tag{5.10}$$

Table 4 shows examples of HSP values of selected solvents most commonly used for the preparation of polymer solutions for electrospinning. Tables of the ability of mutual miscibility of selected liquids are listed in the range of contributions, e.g. in (Pallav, 2013).

Table 4 *Values of HSP of selected solvents (Hansen, 1967)*

solvent	**δ**	**δ_D**	**δ_P**	**δ_H**
methanol	14,28	7,42	6,00	10,90
ethanol 99,9%	12,92	7,73	4,30	9,50
glycerol	21,10	8,46	_	_
acetone	9,77	7,58	5,10	3,40
dimethyl formamide	12,14	8,52	6,70	5,50
chloroform	9,21	8,65	1,50	2,80
water	23,50	6,00	15,30	16,70
acetic acid	10,50	7,10	3,90	6,60
formic acid 90%	12,15	7,00	5,80	8,10

Radius of interaction spheres in Hansen space R_0 is the next parameter necessary to determine of the polymer solubility. The visualization by plotting the individual components of the solubility parameter into the 3D graph is the most graphic way leading to the determination of the HSP of polymers; see in (Figure 24). The intersection of these three components determines the center of the sphere defined by radius R_0. Sphere defines a space for so-called good and bad solvents. The value of the HSP inside of this sphere indicates the *good solvent*. This solvent dissolves the polymer. Otherwise, if the occurrence of the solubility parameter detected outside this sphere, it is called the *bad solvent* unsuitable for the polymer (Hansen, 2008). The assessment of whether the solvent is good or bad is determined by the distance between the solvent and dissolving material R_a. The distance R_a can be determined in the following way (Launay 2007; Hansen, 2008):

$$(R_a)^2 = 4(\delta_{D1} - \delta_{D2})^2 + (\delta_{P1} - \delta_{P2})^2 + (\delta_{H1} - \delta_{H2})^2 \quad (5.11)$$

The ratio between R_0 and R_a is given so-called relatively energy gap (RED), see (5.12). Zero value of RED is found for no energy difference between the substances. The value of RED number less than 1 indicates high affinity. These solvents are called good one. Value of RED number equal to or close to 1 is a boundary condition. Higher RED number indicates lower affinities. Such solvents are called bad one.

$$RED = \frac{R_a}{R_0}. \quad (5.12)$$

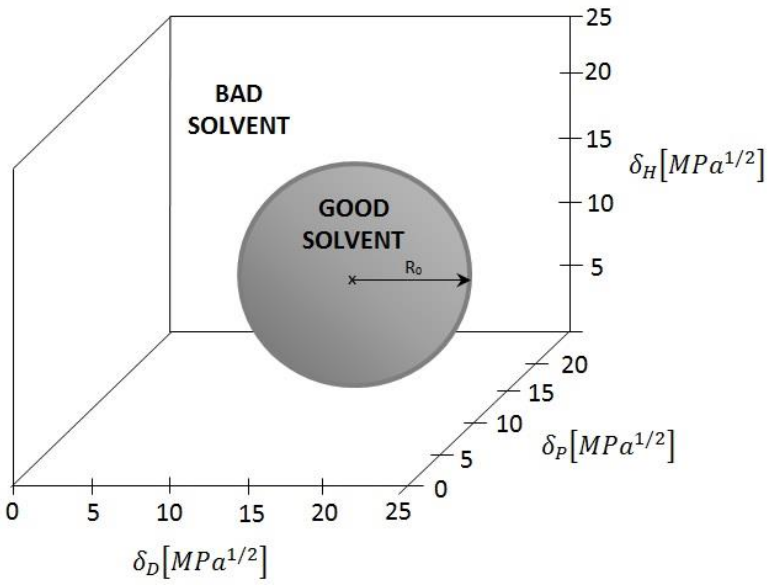

Figure 24 *3D graph of HSP with radius of interaction spheres in Hansen space R_0.*

Good and bad solvents

Distribution of solvents into good and bad depends on the conformation that the polymer chains can possess in this solvent. Polymer chains can take shape of so-called *coil* (Figure 25 a), when the polymer chain is more uncoil or shape of so-called *globule* (Figure 25 b) in case of more clamped/compact polymer chains. In the latter case, phase separation occurs, as is shown in Figure 25. According to this criterion solvents can be divided (Stoklasa 2005):

- *Ideal solvents* - polymer coil completely straighten, resulting in a maximum surface surrounded by solvent molecules chains. Solutions have high viscosity in this case. These solvents practically not exist.

- *good solvents* - polymer coil is significantly spread and polymer segments are surrounded by solvent molecules chains.
- *bad solvents* - polymer chains are in state of the globule, they are compact and phase separation occurs

However, classification of solvents into good and bad is also influenced by the temperature at which dissolution of the polymer in solvent occurs. There are solvents, which can be classified as the good solvents suitable for selected polymer at a specific temperature but they behave as bad one when the temperature changes.

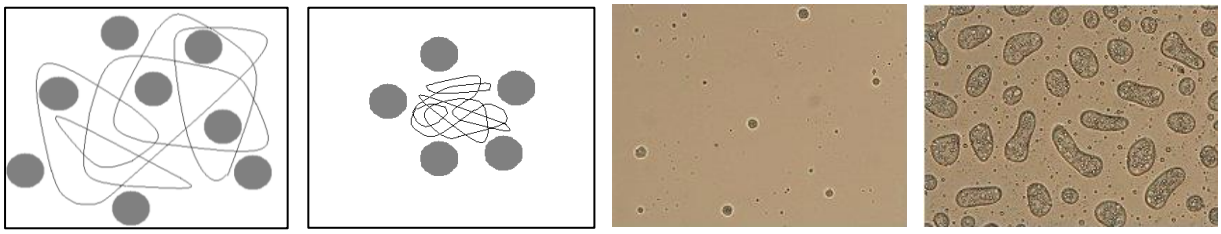

Figure 25 *The good and the bad solvent: The coil of the polymer chain in case of the good solvent (a), the globule in case of the bad solvent (b), the system with the good solvent observed using Nuclear Magnetic Resonance spectroscopy (c), the system with the bad solvent observed using Nuclear Magnetic Resonance spectroscopy (d), adapted from (Macromolecular Physics, 2011).*

3 Experimental part

The main goals of this work were a development of special needle and needleless spinning electrodes for coaxial electrospinning and their optimization based on of lessons learned from their testing. In the next step, the analysis of core-shell structure was verified. The analysis of core-shell structure of very fine fibers is not easy. Suitable methods for analysis were designed, tested and verified in this work.

3.1 Used polymers

Water soluble polymer polyvinyl alcohol (PVA) for initial testing of spinning electrodes was used. This polymer is nontoxic, biocompatible, inexpensive and well-spinnable using electrospinning technology. Polyvinyl butyral (PVB), polyethylene oxide (PEO), polycaprolactone (PCL), polyvinyliden fluoride (PVDF) and polyvinyl pyrolidon (PVP) were used for next experiments with development spinning electrodes.

In the last step, nature polymers for the anticipated use in medicine were chose. Nanofibers from natural biopolymers (e.g. silk fibroin, chitosan, collagen and hyaluronic acid) have a high potential to be utilized in biomedicine, because these are biodegradable, biocompatible and non-toxic materials. Chitosan, Hyaluronic acid (HA) and its sodium salt were used. Carboxymethyl cellulose (CMC) was used as inexpensive variant of HA for initial experiments.

Polyvinyl alcohol

Polyvinyl alcohol (PVA) is a colorless, water-soluble synthetic polymer with a chemical formula $[CH_2CH(OH)]_n$. This is a biocompatible, biodegradable, nontoxic, inexpensive and well-spinable polymer using electrospinning. There are not any health risks for people working with this polymer. PVA has a wide range of applications. This can be used in e.g. in a fisheries, in the food industry for the preparation of jelly, as a surfactant in food supplements, in chemical industry as a protective colloid for the suspension polymerization, as a thickening agent for coating materials, for the production of adhesives and impregnation materials resistant to petrol, oils, greases and solvents. This can be used as wrappers, surgical threads, textile fibers, seals, tubing and other products (Ducháček, 2011).

Polyvinyl alcohol is a polymer in that it is not built up in polymerization reactions from monomers, because of its instability. Instead, PVA is produced by alkaline hydrolysis of polyvinyl acetate (PVAc) in an alcohol (e.g. in methanol) with an alkaline catalyst such as sodium hydroxide. Polyvinyl alcohol always contains a certain number of vinyl acetate groups from the PVAc molecules. This results its variable properties (Duchacek, 2011).

This polymer is soluble in water, slightly soluble in ethanol. Its solubility in water depends on the degree of hydrolysis and molecular weight. This is insoluble in non-aqueous liquids due to strong intermolecular and intramolecular hydrogen bonding (Chetri, 2008). The solubility parameter of the PVA is 25,78 $MPa^{1/2}$ (Mark, 1999).

Polyvinyl butyral

Polyvinylbutyral (PVB) is the synthetic polymer with a chemical formula $(C_8H_{14}O_2)_n$. This is prepared from PVA by reaction with n-butyraldehyde. This is polymer with specific technical properties for technical applications. One of its major applications is laminated safety glass for automotive windshield. PVB resin can be used in wood coating, structural adhesives, as inks/dry toners or as a binder for ceramics and composite fibers (IHS, 2013). This polymer has good water resistance, elasticity and optical transparency.

PVB is soluble for example in most alcohols, ketones, in dimethylacetamide (DMA), dimethylformamide (DMF), N-Methyl-2-pyrrolidone (NMP), Acetic Acid, chloroform, tetrahydrofuran (THF) and 1,4-Dioxane. Theoretical estimate of dispersion, polar and hydrogen bonding contributions to solubility parameter is δ_D = 7,72 $MPa^{1/2}$, δ_P = 2,90 $MPa^{1/2}$, δ_H = 3,26 $MPa^{1/2}$ and δ_{total} = 8,87 $MPa^{1/2}$ (Mark, 1999).

Polyethylene oxide

Polyethylene oxide (PEO) is the synthetic crystalline polyether with chemical formula $(CH_2CH_2O)_n$. It is available in a wide range of molecular weights, wherein PEO with Mw <100,000 are usually called polyethylene glycol (PEG). This polymer is produced by catalyzed by acidic or basic catalyst from ethylene oxide with water, ethylene glycol or ethylene glycol oligomers. This is used e.g. as a thickening agent of latexes, water-soluble packaging material or a precipitating agent in water treatment (Ducháček, 2011). This is biocompatible polymer with a low toxicity and this can be used in pharmaceutical and

medical applications such as tablet coating, tissue engineering or drug delivery system with controlled release.

PEO is soluble in water and in organic solvents such as ethanol, acetone, chloroform and toluene (Ramakrishna, 2005). The solubility parameter of the PEO is 20,2 ± 0,2 $MPa^{1/2}$ (Mark, 1999).

Polycaprolactone

Polycaprolactone (PCL) is the synthetic biocompatible polyester with chemical formula $(C_6H_{10}O_2)_n$. This has a good miscibility with a large range of other types of polymers, good bond to a wide range of substrates and very good processing and mechanic properties. This is flexible polyester with elastomer properties. PCL can be used as e.g. an additive for resins, for modeling or for 3D Printing. This is biocompatible and biodegradable polymer with a low toxicity and this can be used in medical applications such as tissue engineering or drug delivery system.

PCL is not water-soluble polymer. This is high soluble in chloroform, also in dichlormethane, DMF, THF or toluene. The solubility parameter of the PCL is 17 ± 0,9 $MPa^{1/2}$ (Bordes, 2010).

Polyvinylidenfluoride

Polyvinylidenfluoride (PVDF) is a partially fluorinated thermoplastic polymer with chemical formula $(C_2H_2F_2)_n$ produced by the polymerization of vinylidene difluoride. This polymer has excellent chemical resistance, high stiffness, piezo and pyroelectric properties, extremely good resistance to aging and the large temperature range of application. This can be used e.g. for construction of chemical containers, as an insulation on electrical wires or in the production of composite electrodes for lithium ion batteries. PVDF is a good material for transducers in devices such as headphones, microphones, and sonic detectors. This polymer is widely used in medical applications such as filters and membranes, biomedical sensors or in tissue engineering for example as a replacement of artificial muscles.

PVDF swells in strongly polar solvents such as acetone or ethyl acetate and it is partially soluble e.g. in DMF, dimethyl sulfoxide (DMSO) or THF. Solubility parameters of

PVDF are δ_D = 17 $MPa^{1/2}$, δ_P = 12 $MPa^{1/2}$, δ_H = 10 $MPa^{1/2}$. Solubility parameter of PVDF dissolved in DMF is 14, 4 $MPa^{1/2}$ and 18,4 $MPa^{1/2}$ in DMSO (Mark, 1999).

Chitosan

Chitosan is a biodegradable, biocompatible and non-toxic nature linear polysaccharide composed of randomly distributed β-(1-4)-linked D-glucosamine and N-acetyl-D-glucosamine extracted from the shell of crustaceans, arthropods and mollusks, as well as the cell walls of certain fungi (Liu, 2006; No, 2002). Its chemical formula is $(C_{18}H_{35}N_3O_{13})_n$. Chitosan is produced by alkali deacetylation of chitin using sodium hydroxide as a reagent and water as a solvent (Vavříková, 2009). This has the ability to connect to each other heavy metals and other agents. This is biocompatible, biodegradable and nontoxic polymer. This can be used for example in food industry, as food preservation, for water filtration as a part of a filtration process, in biomedicine, pharmacy such as bioactive agent, cosmetic, agrochemistry or in textile industry as impregnation of textiles. This can be used in tissue engineering or in drug delivery system with control release of drugs (Vavříková, 2009).

Chitosan is insoluble in water and most organic solvents. This is soluble in acidic environment and in low concentration mineral acids; its solubility is affected by nature of the anion (Kumar, 2000; Pillai, 2009). Solubility parameter of α-chitin is 25 – 26 $MPa^{1/2}$ and 23 – 26 $MPa^{1/2}$ for β-chitin (Barton, 1991).

Hyaluronic acid

Hyaluronic acid (HA), also called hyaluronan, is a biodegradable, biocompatible and non-toxic nature polymer of glycosaminoglycan (GAG) with chemical formula $(C_{28}H_{44}N_2O_{23})_n$. This is a major component of the extracellular matrix. One of the components of the connective tissue is epithelial and nerve tissue. Hyaluronic acid occurs particularly in cartilage and synovial liquid which imparts stiffness and resilience. Hyaluronic acid is a natural polysaccharide consisting of alternating disaccharide units of a α-1,4-D-glucuronic acid and β-1,3-N-acetyl-D-glucosamine with a molecular weight range from 103 to 107 (Lodish, 2004, Laurent, 1995, JI, 2006). HA is a linear, unbranched polymer (Lapčík, 1998), is a major component of the ECM and imparts stiffness, resilience and lubricating quality to many types of connective tissue such as joints (Lodish, 2004).

Sodium hyaluronate is the sodium salt of hyaluronic acid. This material was used in this work. Sodium hyaluronate 'Hyalgan' (Fidia Farmaceutici S.p.A., Abano Terme, Italy) and 'RenehaVis' (Hyaltech Ltd., UK) were used as core part of core-shell nanofibers. Hyalgan contains 20 mg Natrii hyaluronas (Mw = 5 – 7.3 x 105 Da), RenehaVis is composed of two parts of Sodium Hyaluronate - low molecular weight (LMW) with Mw = 1 x 106 Da and of high molecular weight (HMW) with Mw = 2 x 106 Da. LMW contains 15.4 mg of Sodium Hyaluronate and HMW contains 7 mg of Sodium Hyaluronate. Nanofibers from this polysaccharide can be used as the scaffolds in tissue engineering.

Carboxymethyl cellulose

Hyaluronic acid and its sodium salt is a relatively expensive polymer material. Carboxymethyl cellulose (CMC) is a cellulose derivative with carboxymethyl groups (CH_2COOH). Its structure is similar to Sodium Hyaluronate. It is reason why CMC was chose as a model material simulating electrospinning of hyaluronan. CMC is formed by reaction cellulose with sodium hydroxide and chloracetic acid (Biswal, 2004).

3.2 Used methods and equipment

Different kinds of coaxial electrospinning equipments were used in this work. New equipments for production of core-shell nanofibers were developed and their functionality was verified. Needle and needleless spinning electrodes were designed, constructed and use for experiments in this work. Nanofibers were collected on different kinds of 2D and 3D collectors in dependence of the desired structure of nanofibrous products. Visualization methods were used for record and investigation of electrospinning process. The broad range of methods was used to observed nanofibrous morphology and to analysis of core-shell structure.

Laboratory setup for coaxial electrospinning

Initial experiments were realized using laboratory set-up for coaxial electrospinning, see (Figure 26). This apparatus was designed and manufactured in our laboratory exclusively for research activity. In the next step, new unique equipment for core-shell electrospinning was developed in framework of this work within cluster Nanoprogres (Spinner 1 and Spinner 2).

Their uniqueness resides in the possibility of their using for commercial purposes and enables optimum and reproducible production of core-shell nanofibers.

Figure 26 *Laboratory set-up for the core-shell electrospinning using a coaxial needle spinning electrode: the coaxial needle spinning electrode (1) connected to the HV source with a positive charge (2), the syringe with the core polymer solution (3), the syringe with the shell polymer solution (4), the hydraulic system for the core solution (5) and for the shell solution (6), the collector with the Spunbond nonwovens (7) connected to the HV source with a negative charge (8).*

Coaxial equipment for production of core-shell nanofibers - Spinner 1

The Spinner 1, see (Figure 6a) was developed in this work for ease of use to production of homogeneous and uniform core-shell nanofibrous structure realized by the needle or needleless coaxial technology. The main aim was to develop simple, user-friendly equipment for its intended use in the industrial sector. We focused on the search for materials and individual mechanisms of Spinner 1 in accordance with the planned development of the Spinner 2 intended for cleanrooms. All of these materials and mechanism used by us were tested for the purpose of their wholesomeness for production of highly pure nanofibrous structures suitable for biomedical applications. Individual parts of Spinner 1 was designed and developed for the purpose of a produce of the unique device for production of sophisticated core-shell nanofibrous structures with the anticipated use for industrial applications.

Coaxial equipment for production of core-shell nanofibers in cleanroom - Spinner 2

Based on the knowledge acquired during the development of the Spinner 1 was designed and constructed the new coaxial equipment - The Spinner 2. This was developed within this work and cluster Nanoprogres. This unique equipment allows the core-shell nanofibers formation in cleanroom with group A (European Standard). This equipment constructed from the special biocompatible and non-toxic materials allows the production of highly pure nanofibrous structure for use in regenerative medicine. We used engineering solutions, special materials, mechanisms and HEPA Filters and we developed equipment with regard to maintaining laminar flow. Due to these parameters and technologies, we developed the coaxial electrospinning equipment with its inner space certified on the cleanroom of class A and its outer space under a laminar box certified on the cleanroom of class B. The Spinner 2 is shown in Figure 6 b, c.

Laboratory electrospinning setup for investigation of relaxation time

The experimental setup for investigation of relaxation time is shown in Figure 28. This equipment was manufactured at the Department of Nonwovens and Nanofibrous materials, Technical University of Liberec within this work. Rod spinning electrode with diameter 8.85 mm was used for this experiment and located 100 mm under the metal disc collector with diameter 150 mm. A 300 Watt High Voltage DC Power Supply (AU-60PO.5-L, Matsusada Precision Inc.) was used. The rod was connected to the positive pole of the high voltage source, while the collector was grounded. Photographic snapshots of electrospun polymeric droplets were taken using stereopticon Meopta, see in Figure 27a, and Nikon camera Coolpix 4500. Surface tension measurements were done using the digital tensiometer (Krűss K9) and viscosity of polymer solutions was obtained using viscometer Haake Roto Visco 1.

The experimental setup allows read two voltaic signals at channels 1 and 2 of the oscilloscope. The channel 1 records the switch-on state of the rod that is triggered by the switch S1. This entry is represented by a lower voltage signal on oscilloscope records, see in Figure 28. Voltage waveforms are recorded at channel 1 of the oscilloscope using voltage divider formed by resistors R3 and R2. The switch point appears as a peak at time t_1. The oscilloscope channel 1 records the voltage on the rod, and hence, on a droplet. The electric current caused by the charges reaching the collector is recorded at channel 2 of the oscilloscope and appears as a next delayed signal having its peak at time t_2. These charges are

formed in the vicinity of the Taylor cone and are accelerated by electric field pushing them toward the collector. The time of ion transport to the collector is measured in milliseconds, hence can be safely neglected here (Pokorny, 2010). Therefore the time difference $\Delta = t_2 - t_1$ is defined as the characteristic time of Taylor cone formation.

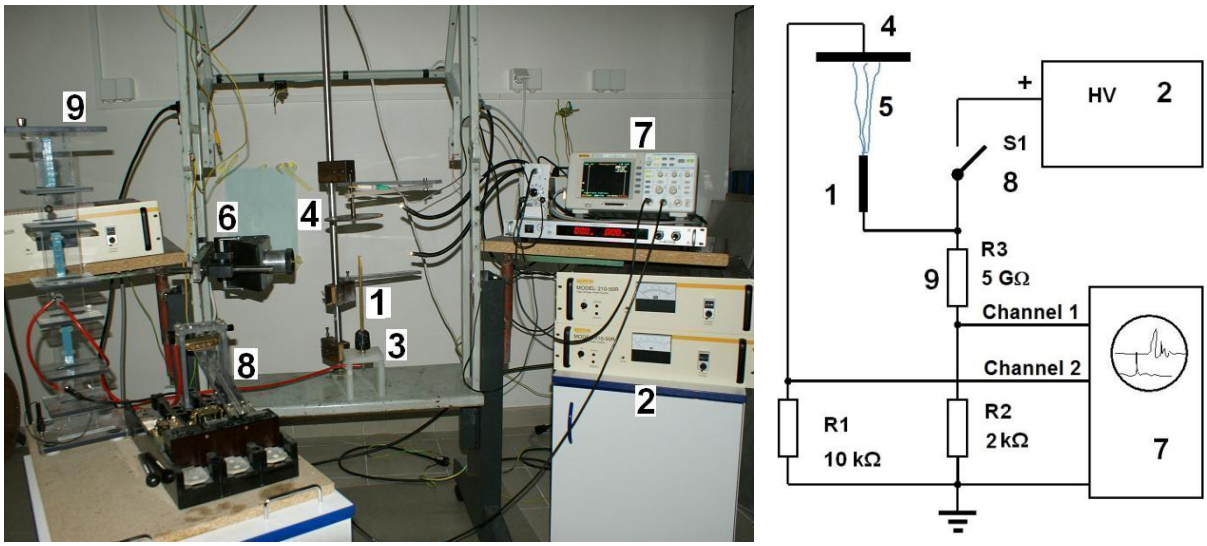

(a) (b)

Figure 27: *(a) The electrospinning setup: rod spinning electrode (1), HV source (2), chuck (3), disk collector (4), electrospinning jet (5), (b) The circuit for measurements of the characteristic time of Taylor cone formation consists of oscilloscope (7), switcher (8) and voltage divider (9).*

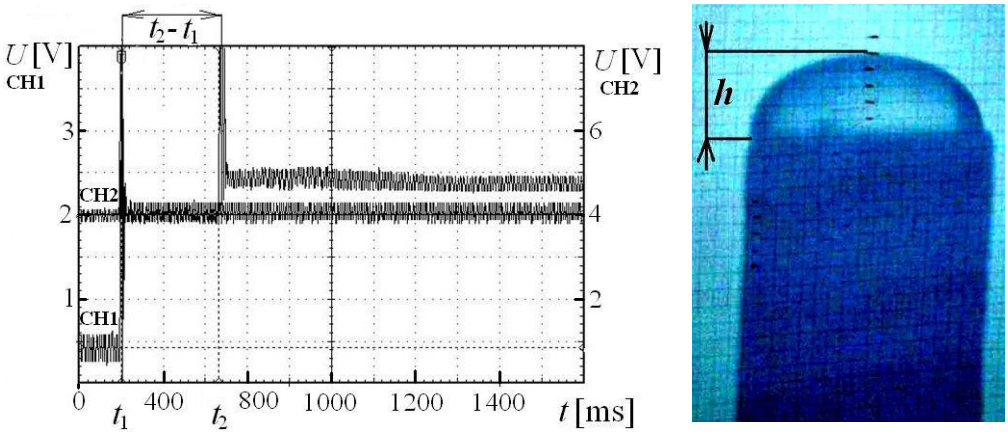

Figure 28: *(A) Oscilloscope records from channels 1 (CH1) and 2 (CH2) provide the time delay $\Delta = t_2 - t_1$ between the moments of switching on the field and the onset of jet formation. (B) The droplet of height h on the top of the electrospinning rod electrode.*

Equipment for AC electrospinning

The new equipment for AC electrospinning developed at Technical University of Liberec within Nanoprogres cluster (Pokorny P., 2014) was used in last experiments (Figure 29). This equipment uses alternating current to production of nanofibers without oppositely charged counter-electrode. Nanofibers are curried by air and collected on the support material (the yarn, the rod or other collector without the electric charge).

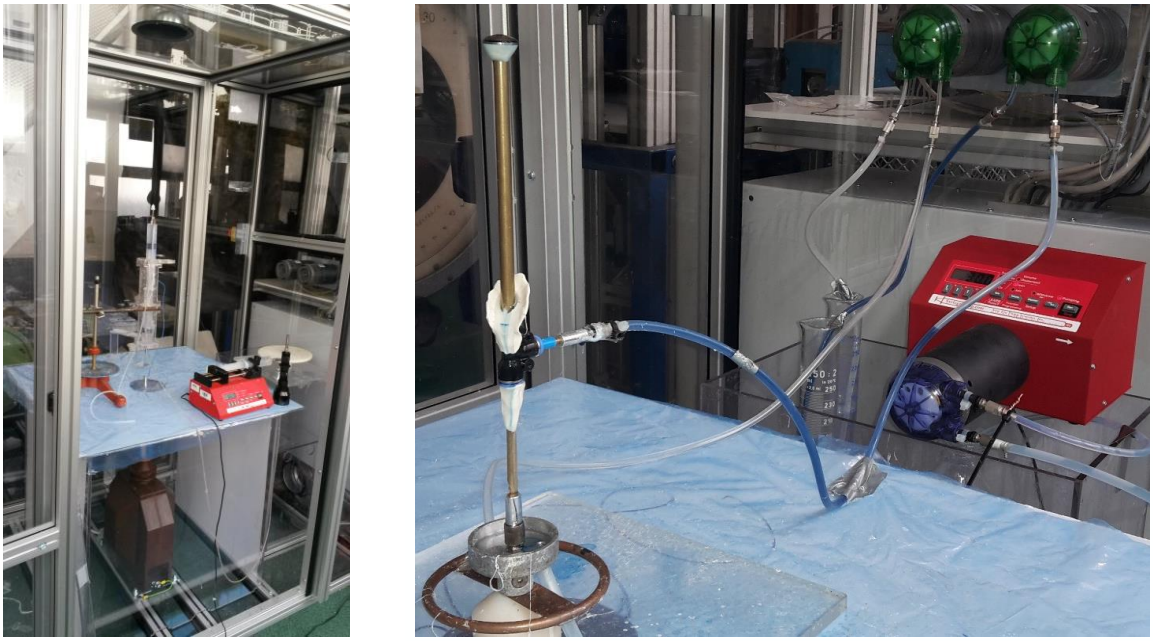

Figure 29 *AC equipment (c): the coaxial spinning electrode (1) connected to the HV source with the alternating current (2), supply of the core polymer solution (3), supply of the shell polymer solution (4), the syringe pump (5).*

Spinning electrodes

Needle and needleless coaxial electrospinning were used for production of core-shell nanofibers. Initial experiments were done using coaxial electro-spinner no. 4, see in (Figure 31b) (Vodseďálková, 2010). Based on knowledge obtained from these experiments were designed and developed new spinning electrodes in this work. These developed spinning electrodes are listed in the chapter 3.4 and 3.5.

Collectors

The disc metal collector with average of 180 mm and the stainless steel sheet with thickness 2 mm and size 160 mm x 355 mm (width x depth) were used as flat collector in this work. These collectors were used for production of randomly oriented 2D nanofibrous layers. The special rotating collector Sioux (Kornev, 2012) was used for production of nanofibrous yarn.

Visualization methods

Visualization methods were used for record of electrospinning process. Visualization of electrospinning can achieve better control of process and determine optimal conditions. Optical methods were used for observation of electrospinning process, for a formation of Taylor cones on the surface of polymer solution, polymer jets, investigated their stability and behavior throughout the electrospinning.

The web camera Microsoft LifeCam Studio with a 1080p sensor, HD camera Panasonic HC-W850 with 120 fps (Panasonic, UK) and Nikon Coolpix S8100 (Nikon, Jap.) were used for these experiments. A high speed camera iSPEED 3 with 150 00 fps (Olympus, USA) was used for recording detail of creation of polymer droplet/layer or two-layer in case of needleless coaxial electrospinning, respectively. The formation of Taylor cones and polymeric jets were investigated as well as their shape, number, stability and the distance between them (characteristic wavelength λ). Taylor cones and polymeric jets distribution and the occurrence of corona discharges were investigated using of the UV camera CoroCam 1 (Uvirco Technologies, SA).

Methods of materials and structure analyzing

Polymeric solutions were stirred with a magnetic stirrer Heidolph Vibramax 100 (Heidolph, DE) and MSH 300 (Boeco, DE). Surface tension was measured using Krűss tensiometer K121 (Krűss, DE). Pentometer was used to determine the polymeric solution density.

The morphology of nanofibrous layers was observed using scanning electron microscopy (SEM) Phenom G2 (FEI, USA), Tescan Vega (Tescan, CZ) and Carl Zeiss ULTRA plus (Zeiss, DE).

The analysis of core-shell structure was investigated using confocal laser scanning microscope Zeiss LSM 5 DUO (Zeiss, DE), transmission electron microscope High-resolution TEM – H9500 (Hitachi, Jap.) and SEM Carl Zeiss ULTRA plus (Zeiss, DE). Cuts of nanofibers was done using CryoMill, (Retsch GmbH, DE) and Jeol JSM 7600F (Jeol Ltd., DE). The spectrofotemeter Avatar 320 FT – IR (Elsichrom, SE) and Energy Dispersive X-ray Spectrometer JED 2300 (Jeol Ltd., DE) were used for detection of incorporated materials.

3.3 Investigation of relaxation time

The experimental setup for investigation of relaxation time, see (Figure 27) was used for these experiments. Solutions of PVA (Sloviol, Chemicke zavody Novaky, SK) were prepared at concentration ranging from 5 to 15 % (w/v) dissolving in distilled water. Parameters of these solutions are listed in table 5.

Table 5 *Parameters of PVA solutions. The dynamic viscosity was determined for the share rates within the range (50, 600) s^{-1}. All values were measured at temperature of 20°C.*

C [(a)]	γ [(b)] [mN/m]	η [(c)] [Pa.s]	ρ [(d)] [kg/m^3]	ν [(e)] [m^2/s] x 10^{-5}	O_h [(f)] [-]
5%	43.5 ± 0.1	0.01436 ± 0.00003	994.7 ± 0.6	1.4455	0.03290
6%	43.5 ± 0.1	0.0174 ± 0.0001	1000.7 ± 0.4	1.7521	0.06610
7%	43.5 ± 0.2	0.01897 ± 0.00002	1002.3 ± 0.4	1.8962	0.06618
8%	43.5 ± 0.1	0.0381 ± 0.0001	1003.2 ± 0.3	3.8114	0.13245
9%	43.5 ± 0.1	0.0532 ± 0.0001	1004.1 ± 0.2	5.3147	0.16567
10%	43.6 ± 0.1	0.1073 ± 0.0002	1005.4 ± 0.4	1.0686	0.36420
11%	43.7 ± 0.1	0.1220 ± 0.0001	1005.8 ± 0.5	1.2139	0.39674
12%	43.7 ± 0.1	0.2008 ± 0.0001	1006.9 ± 0.4	1.9944	0.62869
13%	43.7 ± 0.1	0.311 ± 0.002	1007.6 ± 0.4	3.1045	1.02630
14%	43.8 ± 0.1	0.4994 ± 0.0004	1008.5 ± 0.5	4.9548	1.62052
15%	44.3 ± 0.1	0.5054 ± 0.0004	1009.1 ± 0.1	5.0109	1.64030

(a) C is the weight concentration
(b) γ is the surface tension
(c) η is the dynamic viscosity
(d) ρ is the mass density
(e) ν is the kinematic viscosity
(f) O_h is the Ohnesorge number

The polymeric droplet which had a 1 ml volume was deposited on top of the rod electrode using a micropipette. The droplet profile was projected on a screen using the 20x

lenses of the stereopticon, see (Figure 27) and its height was measured as is shown in Figure 28. In the next step, the stereopticon was switched off and the delay time was measured. All experiments were conducted at the ambient temperature 19°C – 23°C. The relative air humidity varied from 35% - 51%.

The dimensionless electrospinning number $\Gamma = a\varepsilon E^2/2\gamma$ and capillary number $a_c = \sqrt{\gamma/\rho g}$ (Lukas, 2008) are necessary to characterize the process of Taylor cone and polymeric jet formations for excitation of the electrospinning process. The polymeric jet is expected to emanate from the Taylor cone when the electrospinning number exceeds the critical value. This criticality condition defines the critical field at the liquid surface $E_c = \sqrt[4]{4\gamma\rho g/\varepsilon^2}$, which depends only on the physico-chemical parameters of the liquid (Lukas, 2008).

In these experiments, the voltage *U* as a global characteristic of the electric field was defined. In the next step, the local field strength values *E* was assigned to the applied voltages *U*. The process started with the experimental determination of the so-called critical voltage U_C as the lowest voltage for which the liquid surface was destabilized and a polymeric jet appeared. The relationship between *U* and *E* is assumed to be linear for a fixed geometry of the spinner, $E = \beta U/L$, where β is a dimensionless enhancement factor and *L* is the distance between the spinning electrode and the collector. The enhancement factor β was determined from the measured critical voltage U_C and the theoretically predicted critical field E_C as $\beta = E_C L / U_C$. The experimental values of U_C were found inside the interval 12 - 30 kV. Experimental results from measurement of PVA at concentration 5% (w/v), 8% (w/v), 12% (w/v) and 15% (w/v) are shown in Table 6.

The time delay obtained from experiment was about 24 ms for low viscosity PVA solutions (5% (w/v)) with high electrospinning numbers (Γ = 6). For highly viscous solutions (15% (w/v)) and the critical electrospinning number ($\Gamma \approx 1$), the time delay increased up to 1.269 s. These time delays Δt were measured ten times for each concentration and for each value of the electrospinning number. The relationship between the experimentally determined dimensionless time delay $T_{EXP} = \Delta t\sqrt{g/a}$ and the dimensionless electrospinning number Γ is plotted in Figure 30 a-d. One polymeric jet was observed in case of low electrospinning numbers ($\Gamma \cong \Gamma_c = 1$), while for greater electrospinning numbers (Γ = 6) five polymeric jets were observed. The ability to generate multiple jets with the existing setup can be used as

evidence for the formation of nanofibers in the so-called needleless electrospinning mode (Yarin, 2004).

Table 6 *Experimental results from measurement of PVA.*

Polymer solution	U[(a)][kV]	τ[(b)] [s]	T[(c)] [-]	E[(d)] [V/m]	Γ[(e)] [-]
5% PVA	15,5			2156736,566	1
	16	0,2512	1,745877755	2226308,713	1,065556711
	18	0,0808	0,561572144	2504597,302	1,348595213
	20	0,0694	0,482340431	2782885,892	1,664932361
	22	0,0544	0,378088176	3061174,481	2,014568157
	24	0,048	0,333607214	3339463,07	2,3975026
	26	0,0344	0,23908517	3617751,659	2,813735691
	28	0,032	0,22240481	3896040,248	3,263267428
	30	0,0264	0,183483968	4174328,837	3,746097813
8% PVA	13,9			2161329,36	1
	16	0,1136	0,791218401	2487861,134	1,324983179
	18	0,092	0,640775466	2798843,776	1,676931836
	20	0,0696	0,48476057	3109826,417	2,070286217
	22	0,0608	0,423469004	3420809,059	2,505046323
	24	0,04	0,278598029	3731791,701	2,981212153
	26	0,0392	0,273026068	4042774,342	3,498783707
	28	0,0376	0,261882147	4353756,984	4,057760986
	30	0,0256	0,178302738	4664739,626	4,658143989
12% PVA	14,4			2165801,76	1
	16	0,4792	3,336848709	2406446,4	1,234567901
	18	0,4776	3,325707311	2707252,2	1,562499999
	20	0,2808	1,955315354	3008058	1,929012345
	22	0,223	1,55283235	3308863,8	2,334104937
	24	0,1096	0,763185765	3609669,6	2,777777777
	26	0,0744	0,518075008	3910475,4	3,260030863
	28	0,0736	0,512504309	4211281,2	3,780864196
	30	0,0624	0,434514523	4512087	4,340277776
15% PVA	13			2174383,987	1
	14	1,269	8,811254049	2341644,294	1,159763314
	16	1,133	7,866943135	2676164,907	1,5147929
	18	0,5512	3,827236589	3010685,52	1,917159764
	20	0,3272	2,271900965	3345206,134	2,366863906
	22	0,2048	1,422021142	3679726,747	2,863905326
	24	0,156	1,083180167	4014247,361	3,408284025
	26	0,108	0,749893962	4348767,974	4,000000001
	28	0,0912	0,63324379	4683288,587	4,639053256
	30	0,0752	0,522148388	5017809,201	5,325443788

[a] U is the voltage
[b] τ is the relaxation time
[c] T is the dimensionless time delay
[d] E is the electric field
[e] v_u is the dimensionless electrospinning number

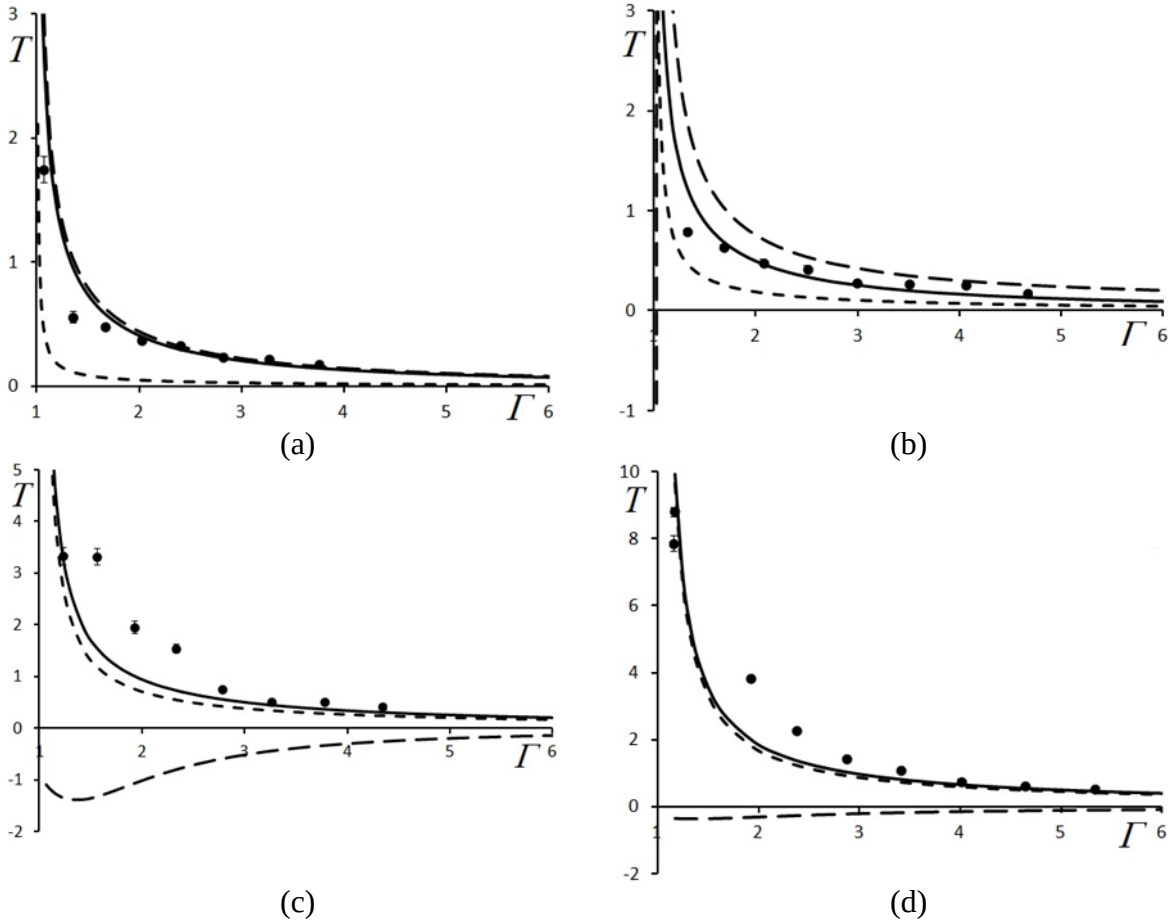

Figure 30 *The time delay T as a function of electrospinning number Γ. Experimental data points correspond to the mean values averaged over 10 measurements each. (a) PVA solution at concentration of 5 % (w/v), Oh = 0.033, (b) PVA solution at concentration of 8 % (w/v), Oh=0.132, (c) PVA solution at concentration of 12 % (w/v), Oh=0.628 (d) PVA solution at concentration of 15 % (w/v), Oh=1.640.*

Values of the time delay were obtained from the experimental measurement for different concentration of PVA solution. This time delay denotes the time required to the build of Taylor cone. There were founded that experimental data corresponds to the theoretical results.

3.4 Needle coaxial spinning electrodes

A needle coaxial electrode consists of two coaxially arranged capillaries, see in (Figure 31). The composite droplet creating in an orifice of this spinning electrode forms a composite Taylor cone that pulls up both the shell polymer and the core polymer. Then, both polymers together are drawn and elongated by the electrospinning jet and collected on the grounded collector (Moghe, 2008).

(a) (b) (c)

Figure 31 *Coaxial needle spinning electrodes: (a) The model of spinning electrode, (b) the electro-spinner no. 4 (Vodseďálková, 2010), (c) the spinning electrode from polyoxymethylene (Vysloužilová, 2012); (1) the coaxial head, (2) the input of shell liquid, (3) the input of core liquid.*

The electro-spinner no. 4 was constructed with two coaxially arranged needles wherein the inner needle is firmly protruding from the orifice of the outer one by 1/3 of the outer needle diameter. In this work, coaxial spinning electrodes with the choice of the protruding from the orifice were developed. The reason is the choice of the protrusion depending on used spinning polymer solutions and liquids.

Many variants of needle spinning electrodes were developed in collaboration with Audacio, Ltd. Company. We designed electrodes from duraluminium, teflon, polypropylene (PP), polyoxymethylene (POM) and high density polyethylene TIVAR 1000 (HDPE). The reason for choosing of a wide range of construction materials was a finding of optimal spinning electrodes allows electrospinning of broad range of materials. Spinning electrodes from conductive and non-conductive construction materials were designed a developed for the purpose of easy manipulation, maintenance and with respect to chemical and mechanical resistance by intended use. In the next step, the investigation was focused on the shape of construction of a spinneret orifice. Spinnerets with a different shape of the orifice and an angle were developed.

Water-soluble PVA (Sloviol, Chemicke zavody Novaky, SK) was used for initial experiments with new needle coaxial spinning electrodes. Solution of PVA was prepared at concentration of 12 % (w/v) solvent in distilled water and used as the shell polymer. Solution of PVA was prepared at concentration of 4 % (w/v) solvent in distilled water and used as the core polymer. The red pigment was added to core polymer for better observation of electrospinning process. Surface tension of 12% PVA was 40,1 ± 0,1 mN/m 36,8 ± 0,2 mN/m for 4% PVA. Dynamic viscosity was 0,647 Pa.s (12% PVA) and 0,014 Pa.s (4% PVA).

In the second step, PCL (M_n = 45.000, Sigma Aldrich, UK) was used for next experiments. The reason for choice of PCL was its insolubility in the water and its possibility for used in the medicine and tissue engineering. Polycaprolactone at concentration of 14 % (w/v) was prepared dissolving in chloroform/ethanol (8:2) and used as shell polymer solution. Polycaprolactone at concentration of 5 % (w/v) was prepared dissolving in chloroform/ethanol (8:2) and used as core polymer solution. Surface tension of the 14% PCL was 23,6 ± 0,1 mN/m 24,2 ± 0,1 mN/m for 5% PCL. Dynamic viscosity was 0,149 Pa.s (14% PCL) and 0,013 Pa.s (5% PCL).

In the last step, electrospinning of PCL/PVA was tested using coaxial spinning electrodes. The reason for chose of PCL with incorporated water soluble polymer solution was the preparation of drug delivery system. Biocompatible, nontoxic and water-insoluble PCL protects the water-soluble core material. This one may contain drugs, liposomes, enzymes and other liquids stored in water environment. PCL at concentration of 14 % (w/v) dissolved in chloroform/ethanol (8:2) was used as the shell material. PVA at concentration of 8 % (w/v) dissolved in distilled water/ethanol (5:5) was used as the core material. This dissolving system was chose to better compatibility of core and shell liquid. This avoids the mutual coagulation core and shell liquid at their interface.

The first experiments with designed coaxial spinning electrodes from duraluminium, PP, POM and teflon were realized using laboratory set-up for coaxial electrospinning. These spinning electrodes were investigated with focus on the optimal construction material, design and process parameters. Based on knowledge gained of the experiments were designed new coaxial spinning electrodes from POM and HDPE. These electrodes were developed in collaboration with Audacio, s.r.o. within project Nanoprogres and they were tested in the Spinner 1. Different shape of electrodes orifice were designed and their suitability for production of core-shell nanofibers were tested in this work.

The laboratory set-up in air conditioned digestion was used for testing of these spinning electrodes, see in (Figure 26). The core needle of coaxial spinning electrode was mounted on the syringe with the core polymer solution. The shell needle was mounted on the syringe with the shell polymer solution. The inner needle was protruding from the orifice of the outer one by 0,1 – 1 mm of the outer needle diameter. The coaxial spinning electrode was connected to a HV source (Spellman Sl100) and positively charged. The electrode was located 100 mm below the negatively charged disc collector with a diameter of 180 mm. Process parameters from the testing of coaxial spinning electrodes are listed in Table 7.

Table 7 *Process parameters of coaxial electrospinning realized using developed needle spinning electrodes*

Material of the spinning electrode	**U_1[a] [kV]**	**U_2[b][kV]**	**T[c] [°C]**	**RH[d] [%]**	**v_s[e] [ml/h]**	**v_c[f] [ml/h]**
Duraluminium	(+)15 - 20	(-)10 - 15	21	39	0,4 – 0,7	0,5 - 1
Polypropylene	(+)14 - 20	(-)10 - 15	20	38	0,5 – 1	0,4 – 0,9
Teflon	(+)14 - 20	(-)10 - 15	20	38	0,5 – 1	0,4 – 0,9
Polyoxymethylene	(+)14 - 20	(-)10 - 15	20	38	0,5 – 1	0,4 – 0,9

[a] U_1 is the voltage on the spinning electrode
[b] U_2 is the voltage on the collector
[c] T is the temperature
[d] RH is the relative humidity
[e] v_s is the feed rate of the shell polymer solution
[f] v_c is the feed rate of the core polymer solution

Electrospinning of PVA and PCL ran pretty well. The polymeric bi-component droplet was created at the orifice of the spinning electrode and core-shell nanofibers were formed in all cases of the developed spinning electrodes, but some disadvantages were observed during testing. The duraluminium coaxial spinning electrode is made from the electrically conductive material. The electric charge is not focused only to the polymeric droplet but this is distributed throughout the spinner. Next disadvantage of this electrode is a polymeric droplet slumping. The polymeric droplet of larger volume is not stable throughout electrospinning. There is a problem with a maintaining the droplet throughout the process. The problem with a stability of the polymeric bi-component droplet was also in the case of the PP spinning electrodes. Teflon is a tough and fatty material. The inserting of needles with

different diameters into the spinning head was difficult. Except this shortage, the work with this spinning electrode was without problems and electrospinning ran pretty well.

There were some problems with combination of PCL and water-soluble PVA as its core part during electrospinning process. The combination of these materials caused coagulation at the orifice of the spinning electrode after a few of minutes of electrospinning process. Stopping of the process and the cleaning of the orifice of the spinning electrodes was necessary before the next continuation of electrospinning.

Needle coaxial spinning electrode from polyoxymethylene

The POM spinning electrode, see (Figure 32) appeared to be most satisfactory. Manipulation with this one was easy; polymer bi-component droplet was stable throughout electrospinning process and the electrospinning process was continuous. There weren't observed any slumping of polymer solution during process. An advantage of this electrode is non-conductive material. The electric charge is concentrated on the polymer droplet and this is not on the body of spinning electrode as in case of metal spinning electrode. The next advantage is undemanding preparation of spinning electrode for electrospinning process. This electrode allows easy manipulation and cleaning from the polymer solutions after electrospinning. This needle spinning electrode was selected as the best one and used for the further experiments.

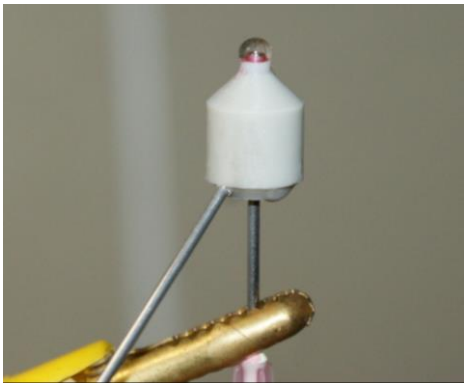

Figure 32 *The detail of the needle spinning electrode from POM with the bi-component polymeric droplet.*

In the next step, the new equipment for production of core-shell nanofibers developed in framework of this work and within Nanoprogres cluster was used (Spinner 1, Nanoprogres). The spinning electrode was placed on the spinning electrode holder and connected to the tubes with core and shell polymer solutions as is shown in Figure 33. The

inner needle was protruding from the orifice of the outer one by 0,1 – 1 mm of the outer needle diameter. The coaxial spinning electrode was connected to a HV source (Spellman Sl100) and positively charged. The electrode was located 100 mm below the negatively charged collector from stainless steel. Its thickness was 2 mm and size 160 mm x 355 mm (width x depth).

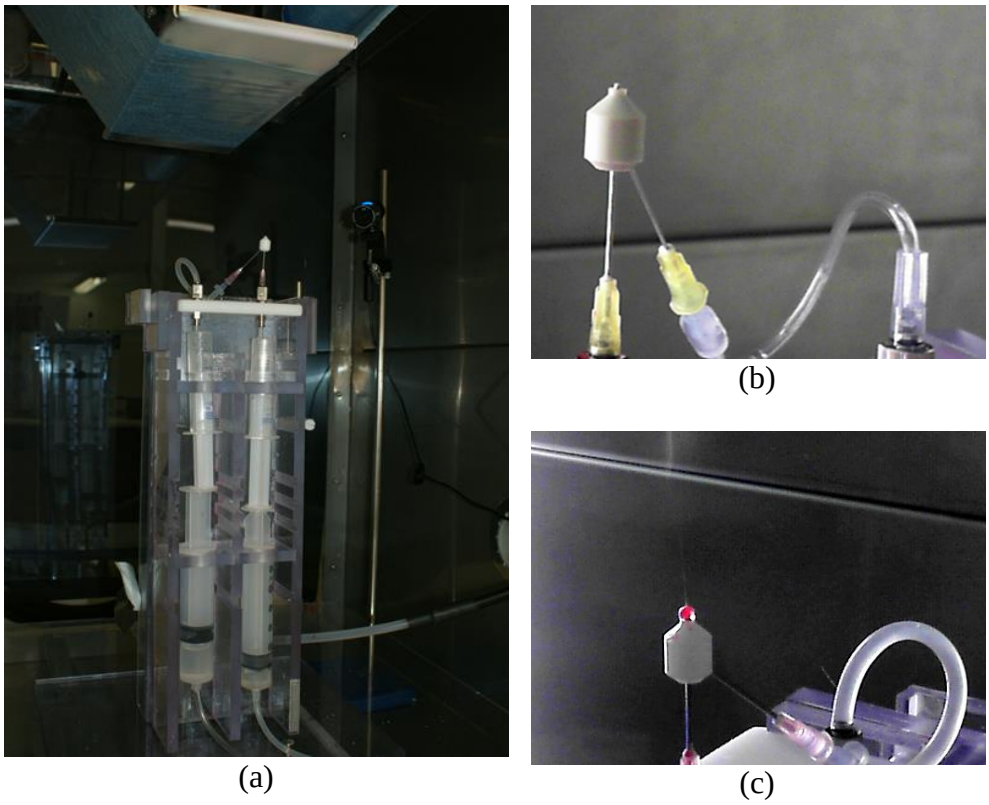

(a) (b) (c)

Figure 33 *The needle spinning electrode from POM: (a, b) the spinning electrode clamped in the holder in Spinner 1, (c) coaxial electrospinning realized by this spinning electrode (Nanoprogres).*

It was found 100 mm was not enough distance L for production of core-shell nanofibers. There was a wet track of polymer solution, on the collector. 100 mm was insufficient distance for the solvent evaporation. 150 mm was the optimal distance for production of core-shell nanofibers from PVA using Spinner 1. The distance of 180 mm was necessary in case of the coaxial electrospinning of PCL. The Spunbond nonwoven was placed under the collector. This nonwoven was unwound with constant velocity v throughout electrospinning process. Spinner 1 allows the moving of spinning electrode in z-axis. Due to this movement and unwinding of the Spunbond nonwoven, homogeneous nanofibrous layers was achieved. The experiments were carried out in a chamber with controlled atmospheric conditions; temperature was 23°C and relative humidity was 25,4 % for electrospinning of

PVA and 23,5°C and 28 % for elecrospinning of PCL. Process parameters of electrospinning of PVA are listed in Table 8 and process parameters of electrospinning of PCL are listed in Table 9.

Table 8 *Process parameters of coaxial electrospinning PVA realized using of POM spinning electrode.*

Experiment	**U[(a)] [kV]**	**v_c [(b)] [ml/h]**	**v_s [(b)] [ml/h]**	**L_0[(c)] [mm]**	**v_z[(d)] [mm/s]**	**v_u[(e)] [mm/s]**	**L[(f)] [mm]**
1	(+)20/(-) 20	2,7	5,7	55/-100	15	0,2	201
2	(+)20/(-) 20	1,3	4,7	55/-100	6	0,1	150
3	(+)20/(-) 20	0,7	2	55/-100	10	0,1	150
4	(+)20/(-) 20	0,5	1,7	50/-60	10	0,1	150
5	(+)20/(-) 18	0,3	2	50/-60	15	0,5	150
6	(+)20/(-) 18	0,3	2	65/-70	20	0,8	150

[(a)] U is the voltage
[(b)] v is the feed rate of polymer solutions
[(c)] L_0 is the limit of the spinning electrode from zero possition
[(d)] v_z is the feed rate of the spinning electrode in z-axis
[(e)] v_u is the speed of unwinding of Spunbond onnwoven
[(f)] L is the distance between electrodes

Table 9 *Process parameters of coaxial electrospinning PCL realized using of POM spinning electrode.*

Experiment	**U[(a)] [kV]**	**v [(b)] [ml/h]**	**L_0[(c)] [mm]**	**v_z[(d)] [mm/s]**	**v_u[(e)] [mm/s]**	**L[(f)] [mm]**
1	(+)20/(-) 20	1,7 core 10 shell	55/-120	10	0,1	180
2	(+)20/(-) 20	3,3 core 10 shell	60/-110	10	0,1	180
3	(+)20/(-) 20	3,3 core 10 shell	70/-110	10	0,1	180
4	(+)20/(-) 20	3,3 core 10 shell	80/-110	10	0,1	180

[(a)] U is the voltage
[(b)] v is the feed rate of polymer solutions
[(c)] L_0 is the limit of the spinning electrode from zero possition
[(d)] v_z is the feed rate of the spinning electrode in z-axis
[(e)] v_u is the speed of unwinding of Spunbond onnwoven
[(f)] L is the distance between electrodes

Needle coaxial spinning electrode from high density polyethylene TIVAR 1000

This spinning electrode, see (Figure 34) was developed within this work and project Nanoprogres and tested in the new spinning equipment Spinner 1 (Nanoprogres). The spinning electrode was placed on the spinning electrode holder and connected to the tubes with core and shell polymer solutions. The inner needle was protruding from the orifice of the outer one by 0,1 – 1 mm of the outer needle diameter. The coaxial spinning electrode was connected to a HV source (Spellman Sl100) and positively charged. The electrode was located 150 mm below the negatively charged collector from stainless steel. Its thickness was 2 mm and size 160 mm x 355 mm (width x depth). The Spunbond nonwoven was placed under the collector. This nonwoven was unwound with constant velocity v throughout electrospinning process. The experiments were carried out in a chamber with controlled atmospheric conditions; temperature was 23°C and relative humidity was 25,4 % for electrospinning of PVA and 23,5°C and 28 % for elecrospinning of PCL. Process parameters of electrospinning of PVA are listed in Table 10 and process parameters of electrospinning of PCL are listed in Table 11.

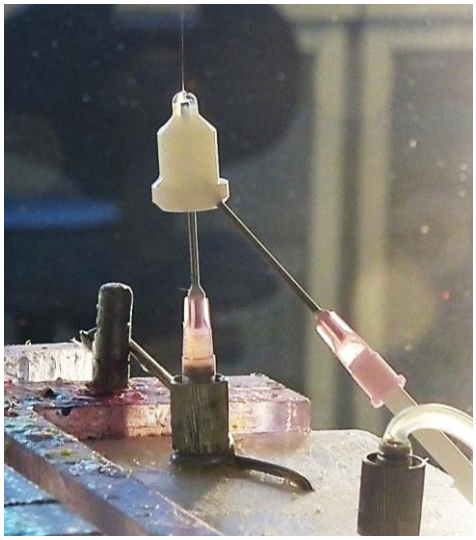

Figure 34 *The coaxial electrospinning realized by the coaxial needle spinning electrode from HDPE (Nanoprogres)*

Table 10 *Process parameters of coaxial electrospinning PVA realized using of HDPE spinning electrode.*

Experiment	**U[(a)] [kV]**	***v*** **[(b)] [ml/h]**	**L_0[(c)] [mm]**	**v_z[(d)] [mm/s]**	**v_u[(e)] [mm/s]**	**L[(f)] [mm]**
1	(+)20/(-) 18	0,3 core 2 shell	65/-70	15	0,1	150
2	(+)20/(-) 18	0,6 core 2,5 shell	70/-70	15	0,1	150
3	(+)20/(-) 18	0,6 core 2 shell	70/-70	15	0,1	150

[(a)] U is the voltage
[(b)] v is the feed rate of polymer solutions
[(c)] L_0 is the limit of the spinning electrode from zero possition
[(d)] v_z is the feed rate of the spinning electrode in z-axis
[(e)] v_u is the speed of unwinding of Spunbond nonwoven
[(f)] L is the distance between electrodes

Table 11 *Process parameters of coaxial electrospinning PCL realized using of HDPE spinning electrode.*

Experiment	**U[(a)] [kV]**	***v*** **[(b)] [ml/h]**	**L_0[(c)] [mm]**	**v_z[(d)] [mm/s]**	**v_u[(e)] [mm/s]**	**L[(f)] [mm]**
1	(+)20/(-) 20	3,3 core 10 shell	80/-110	15	0,1	180
2	(+)20/(-) 18	3,3 core 10 shell	80/-110	15	0,1	190
3	(+)20/(-) 18	3,3 core 12 shell	80/-110	15	0,1	190

[(a)] U is the voltage
[(b)] v is the feed rate of polymer solutions
[(c)] L_0 is the limit of the spinning electrode from zero possition
[(d)] v_z is the feed rate of the spinning electrode in z-axis
[(e)] v_u is the speed of unwinding of Spunbond onnwoven
[(f)] L is the distance between electrodes

The HDPE coaxial needle spinning electrode runs very well. This material is suitable for electrospinning, easily to handle and there were not any problems with core-shell

nanofibers formation during electrospinning process. Based on the knowledge gained from the testing of these coaxial spinning electrodes were designed and constructed another series of spinning electrodes from HDPE with different designs. We focused on the shape of the orifice of the spinning electrodes. New spinning electrodes with and without so-called ”neck”, with different shapes, bevel angle and diameter of the neck were designed within this work. The new developed needle coaxial spinning electrodes are shown in Table 12.

Table 12 *Developed needle coaxial spinning electrodes with different shapes of their orifice.*

				
Material: POM	Material: TIVAR 1000	Material: TIVAR 1000	Material: TIVAR 1000	Material: TIVAR 1000
With the neck	With the neck	With the neck	With the neck	Without the neck
diameter of the neck: 3 mm	diameter of the neck: 3 mm	diameter of the neck: 2 mm	diameter of the neck: 6 mm	diameter of the neck: 3 mm
Suitable electrospinning materials: universal for a wide range of materials.	Suitable electrospinning materials: universal for a wide range of materials.	Suitable electrospinning materials: containing of volatile substances.	Suitable for needle non-coaxial electrospinning of water soluble liquids.	Unsuitable for electrospinning, slumping of the polymeric droplet

The spinning electrode from HDPE with a neck, see in (Figure 35 a, b) has optimal design for electrospinning of broad spectrum of polymer solutions and other liquids, respectively. The neck allows keeping of polymeric droplet at the orifice of the spinner throughout the electrospinning process. Electrodes with a tiny orifice, see in (Figure 35 c) are appropriate for electrospinning of volatile solvents. Electrodes with a large orifice and without a neck, see in (Figure 35 d, e) are unsuitable for using. Optimal bi-component droplet can not to be created, this is slumping from the electrode and core-shell nanofibers are not produced.

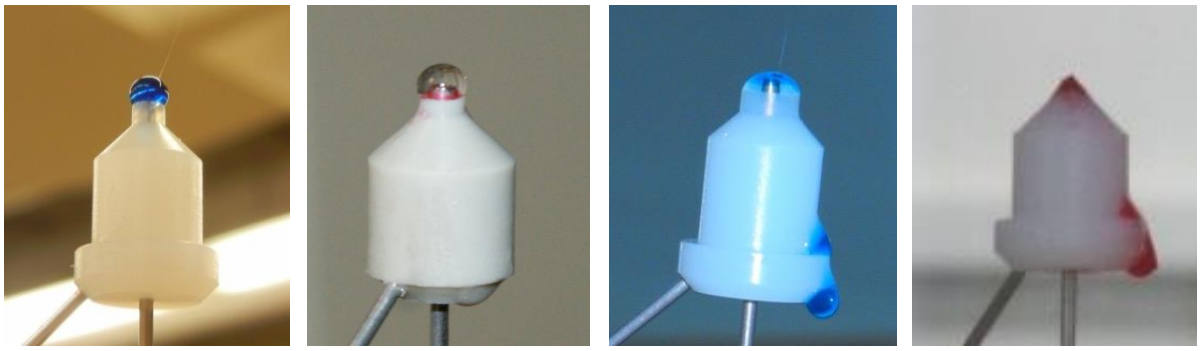

(a) (b) (c) (d)

Figure 35 *Developed coaxial needle spinning electrodes with the neck and optimal bi-component polymeric droplet (a, b), the too large of diameter of the spinning electrode orifice caused the droplet slumping (c), the spinning electrode without the neck causes the droplet slumping (d).*

In the next step, new coaxial spinning electrodes with different bevel angle of the orifice and of the upper part of the spinning electrode was designed and tested within this work. There was found, these structural modifications have no influence on the coaxial electrospinning.

Core-shell nanofibrous yarn

Water-soluble polyvinyl alcohol (PVA, Sloviol, Chemicke zavody Novaky SK) was used for the initial experiment. A solution of 12 (w/v) PVA in distilled water was prepared as shell material. The solution of 4 % (w/v) PVA dissolved in the Prussian blue was used as the core solution. The Prussian blue $[Fe_4[Fe(CN)_6]_3]$ is a dark blue pigment containing iron. It was used for a better observation of electrospinning process and to achieve phase contrast during analysis of the core-shell structure, see in Chapter 3.8.

The needle coaxial spinning electrode, see in (Figure 36 b) was used for this experiment. This one was connected to a high voltage source (Glassman, series FC) and positively charged. The grounded disc collector was located at the distance 130 and 150 mm above spinning electrode. Coaxial electrospinning set-up is shown in Figure 36 a.

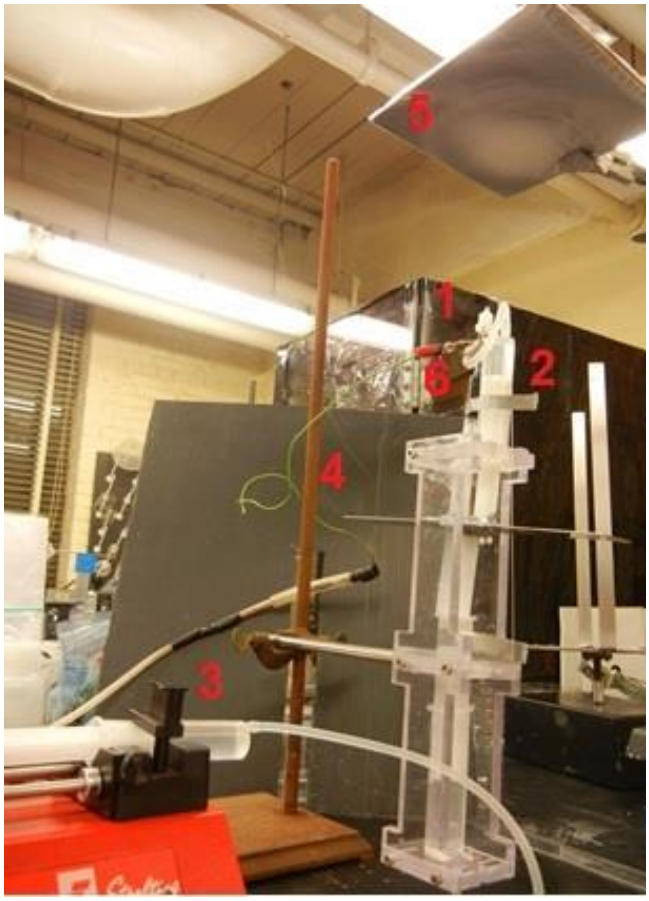

(a)

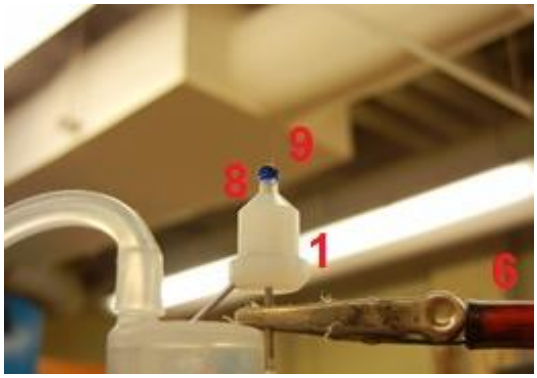

(b)

Figure 36 *Coaxial electrospinning set-up (a), coaxial spinning electrode with bi-component polymeric droplet (b)**:** coaxial spinning electrode (1), dosing system with polymer solutions (2), syringe pump (3), holder of electrospinning device (4), collector (5), HV cable (7), bi-component droplet (8), polymeric jet (9).*

Core and shell solutions were transferred into plastic syringes, empowered by a syringe pump and dosed at a rate of 0,05 – 0,1 ml/h (core) and of 0,5 – 0,7 ml/h (shell). Electrospinning started while achieving critical voltage 13,3 kV (for distance of electrodes = 130 mm) and 13,6 kV (for distance of electrodes = 150 mm). Optimal values for electrospinning process were 16 kV – 19 kV. The electrospinning was carried out at ambient temperature 25,2 ± 0,3 °C and at a relative humidity 22,5 ± 0,5 %. Core-shell nanofibers were collected on the aluminum foil located on the collector.

In order hand, a special rotating collector was used for parallel coaxial nanofibers, see in (Figure 37 a). The grounded rotating collector was located at the distance 140 and 250 mm from spinning electrode. Polymeric solutions were dosed at a rate of 0,3 – 0,6 ml/h (shell) and 0,05 ml/h (core). Electrospinning started while achieving critical voltage 14,5 kV (for distance of electrodes = 140 mm) and 15,3 kV (for distance of electrodes = 250 mm). Optimal values for electrospinning process were 19 kV. The electrospinning was carried out at ambient temperature 25,4 ± 0,2 °C and at a relative humidity 22,5 ± 0,5 %. Core-shell nanofibers were collected on the grounded rotating collector, see in (Figure 37 c).

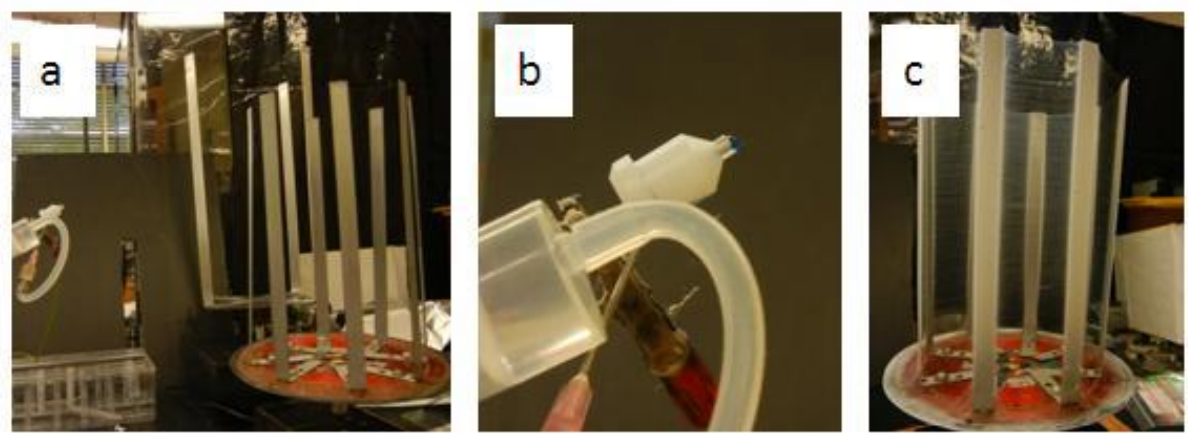

Figure 37 *Coaxial electrospinning set-up with a rotating collector (a), detail of coaxial spinning electrode with bi-component polymeric droplet (b), parallel coaxial nanofibers collected on the grounded collector (c).*

Core-shell nanofibers were taken down from the collector by special collect equipment and twisted. Core-shell nanofibrous yarns were produced, see (Figure 38).

Figure 38 *Core-shell nanofibrous yarn from PVA with incorporated Prussian Blue.*

Nanofibrous yarn was observed by SEM (Hitachi SU6600). Image from SEM analysis is shown in Figure 39. Parallel fibers may be observed in this picture. The detail analysis of this yarn is presented in Chapter 3.8.1.

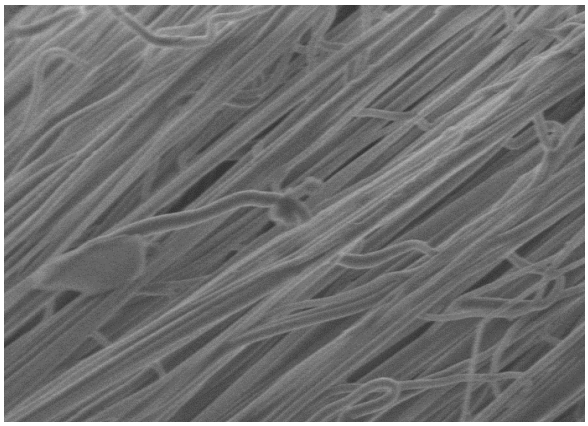

Figure 39 *SEM image of PVA nanofibrous yarn with incorporated Prussian blue*

Core-shell nanofibers with incorporated particles

PVA and PVDF with incorporated iron and magnetic particles were prepared in these experiments. PVA (Sloviol R16,Chemicke zavody Novaky, SK) was used for the first experiments. The solution of 12 % (w/v) PVA dissolved in distilled water was prepared as the shell. The solution of 10 % (w/v) PVA dissolved in distilled water was prepared as the core. Nanoparticles of iron and magnetic particles (in the next step) were added to the core solution at concentration 0.5 % (w/v).

The needle coaxial spinning electrode, see in Figure 36b was used for this experiment. This was connected to the HV source (Spellman Sl100) and positively charged (20 kV). The disc collector with diameter of 180 mm located at the distance 150 mm above spinning electrode was grounded. A nonwoven Spunbond (Pegas, CZ) for collecting the nanofibers was located under the collector.

Polymeric solutions were transferred into a 20 ml plastic syringe, empowered by a syringe pump (neMESYS, Cetoni) and dosed at a constant rate of 1.2 ml/hr (core) and of 3 ml/hr (shell). The electrospinning was carried out at ambient temperature 21°C and at a relative humidity 35 %. Core-shell nanofibers were collected on the Spunbond nonwoven, located on the collector.

Produced nanofibrous layers with incorporated iron and magnetic particles were observed using fluorescent microscopy. Detail analyzes of produced layers are listed in Chapter 3.8.6.

In the next step, coaxial electrospinning of PVDF with magnetic particles was done. First, PVDF was used as the both, shell and core material. A solution of 18 % (w/v) PVDF in dimethylacetamide (DMAc) and acetone (Ac) was prepared as the shell (ratio 8:2). The solution of 3 % (w/v) PVDF dissolved in DMAc/Ac (ratio 8:2) was used as the core one. Magnetic particles NiNP were added to the core solution. Two core solutions were prepared – solution containing 0.025 % (w/v) NiNP and solution containing 0.05 % (w/v) NiNP. The solutions were prepared at temperature of 40°C with magnetic stirring for 48 h.

The needle coaxial spinning electrode was used for experiment, see in (Figure 36b). This was connected to a HV source (Glassman, series FC) and positively charged. The grounded disc collector was located at the distance 100 - 280 mm above spinneret. Polymeric solutions were transferred into plastic syringes, empowered by a syringe pump and dosed at a

rate of 0,05 – 0,5 ml/h (core solution) and of 0,5 – 3,5 ml/h (shell solution). Electrospinning started while achieving critical voltage16 kV. Voltage 16 kV – 24 kV was used. The electrospinning was carried out at ambient temperature 25 ± 0,3 °C and at a relative humidity 22,5 ± 0,5 %. Nanofibers were not created during electrospinning process. Parameters of process were changed, but PVDF nanofibers were not created. Wet nanofibers were collected on a grounded discs collector and foil was created. Negatively charged collector was used for next experiment. Voltage from + 13/-8 kV to +19/-14 kV was applied. Very thin nanofibrous layers were created in this case. In the order hand, a special rotating collector was used. Nanofibers were not created in this case.

Second, the shell material was replaced by PVA. The core material was not changed. Coaxial spinning electrode was connected to the HV source and positively charged. This one was located at the distance 170 mm from negatively charged rotating collector. Polymeric solutions were transferred into plastic syringes, empowered by a syringe pump and dosed at a rate of 0,05 ml/h (core solution) and of 0,5 ml/h (shell solution). Electrospinning started while achieving critical voltage +11/-8 kV. Voltage +14 kV/– 8 kV was used for optimal electrospinning process. The electrospinning was carried out at ambient temperature 25 ± 0,3 °C and at a relative humidity 22,5 ± 0,5 %. Core-shell nanofibers were formed and collected on the negatively charged rotating collector. Parallel coaxial nanofibers with magnetic particles were created. The detail analysis of the produced nanofibrous structures is listed in Chapter 3.8.

3.5 Needleless coaxial spinning electrodes

Dis-continual and continual needleless coaxial spinning electrodes were developed within this work to increase of productivity of core-shell nanofibers. Dis-continual spinning electrodes were intended for a laboratory use to investigate of the coaxial electrospinning process with focus on the behavior of Taylor cones on the free surface of the polymer solution. Continual needleless spinning electrodes were developed in cooperation with Department of Textile Machine Design at Technical University of Liberec under the project Nanoprogres.

3.5.1 The pool needleless spinning electrode

The pool needleless spinning electrode, see in (Figure 40) is the electrode with simple construction using technology of the dis-continual electrospinning form the free surface of the polymeric two-layer. This electrode was developed within this work and project KONTAKT ME10145. Coaxial electrospinning is realized from a very thin film of the shell polymer solution placed on the surface of the core material. The last one fills the whole volume of the pool. Taylor cones are created on the top of the thin polymer film after applying HV. These Taylor cones pull up core material as their core-part. Both materials are drawn and elongated together through acting electric forces and core-shell nanofibers are created and collected on the oppositely charged collector.

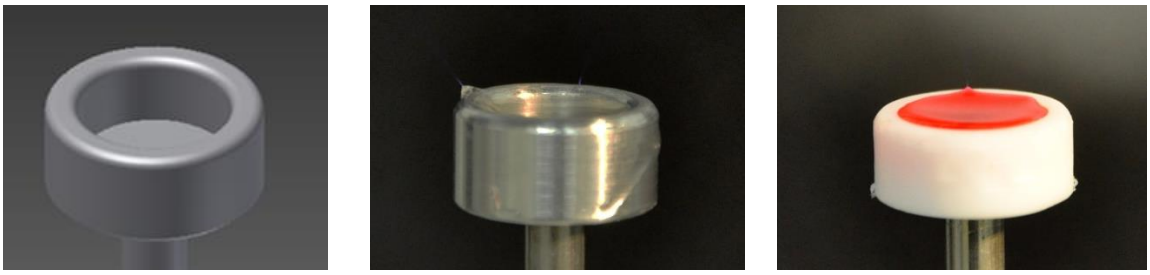

(a) (b) (c)

Figure 40 *Pool needleless spinning electrodes: The model of the pool spinning electrode (a), the pool spinning electrode from the electrically conductive (b) and electrically non-conductive (c) material.*

The pool needleless spinning electrode from electrically conductive material

The duraluminium was selected as the electrically conductive material suitable for design of this type of the pool. Dis-continual coaxial spinning electrode (Figure 40 b) with the inner diameter of 14 mm and outer diameter of 20 mm was designed, made and tested within this work. The depth of this electrode was 4 mm and its height was 9 mm. The rounded edges eliminating a local concentration of electric charge was designed for construction solution of electrode.

The whole volume of the pool electrode was filled by the core liquid of a vegetable oil and by the core liquid of a PVA at concentration of 4% (w/v) with added red food pigment for better observation in the second experiment. Very thin polymeric film of PVA at concentration of 12 % (w/v) was applied on the surface of the core liquid by an annular ring as is shown in Figure 41.

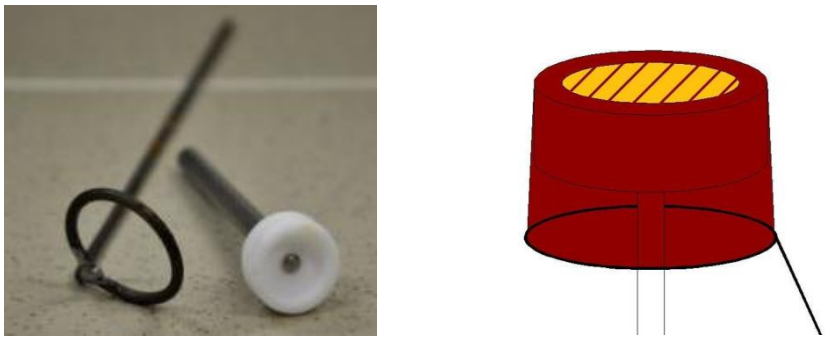

(a) (b)

Figure 41 *The pool needleless spinning electrode with the annular ring (a), the application of a thin film of the shell polymer solution on the surface of the core liquid using the annular ring (Matulová, 2011).*

Electrospinning did not run very well as can be seen in Figure 42. The conductive material of the pool electrode caused concentration of electric charge on the body of this electrode. Polymer solution was slumping from the spinning electrode. A uniform distribution of electric charge across the entire of the surface of the shell polymer solution is necessary to needleless electrospinning. Based on these observations it has developed the pool spinning electrode from the electrically non-conductive material.

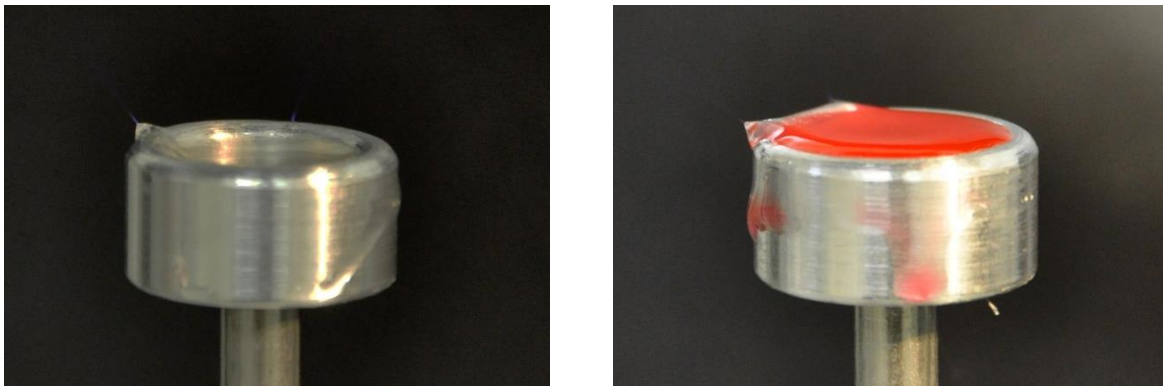

(a) (b)

Figure 42 *Coaxial electrospinning realized using the pool needleless spinning electrode from electrically conductive material (duraluminium): (a) electrospinning of the PVA/vegetable oil, (b) electrospinning of the PVA/PVA with red food pigment (Matulová, 2011).*

The produced nanofibrous layer with incorporated vegetable oil was observed using optical microscope Olympus. The images from this analysis are shown in Figure 43. Beads with incorporated vegetable oil can be seen on the fibers. This analysis is described in detail in the Chapter 3.8.2.

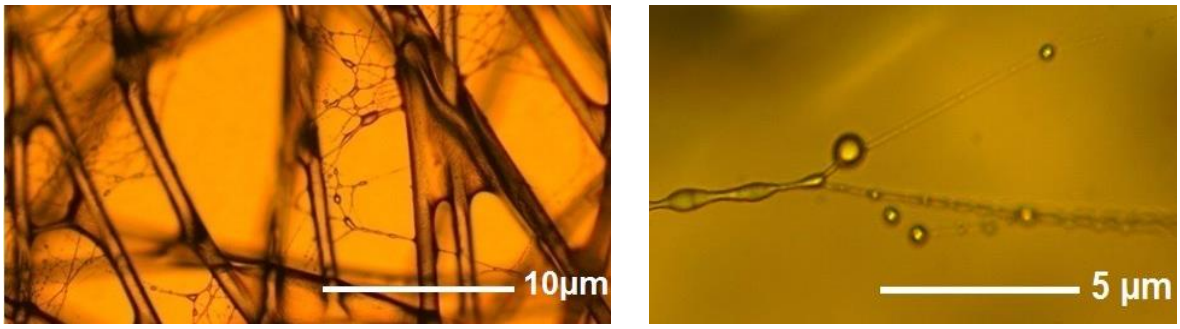

Figure 43 *Core-shell nanofibers with incorporated vegetable oil observed using optical microscope Olympus.*

The pool needleless spinning electrode from electrically nonconductive material

The Teflon was selected as the electrically non-conductive material suitable for design of this type of pool. Dis-continual coaxial spinning electrode with the same parameters as the pool electrode from the duraluminium was designed, made and tested within this work.

The whole volume of the pool electrode was filled by the core liquid of nature oil. The red food pigment was added for better observation of the coaxial electrospinning process. Very thin polymeric film of PVA with concentration of 12 % (w/v) was applied on the surface of the core liquid by an annular ring as is shown in Figure 41.

The electrospinning run very well. A large number of Taylor cones and polymeric jets were observed and nanofibrous layer was created on the collector. The produced nanofibrous layer was observed using optical microscope Olympus. The images from this analysis are shown in Figure 44. Beads with incorporated oil can be seen on the fibers. This analysis is described in detail in the Chapter 3.8.2.

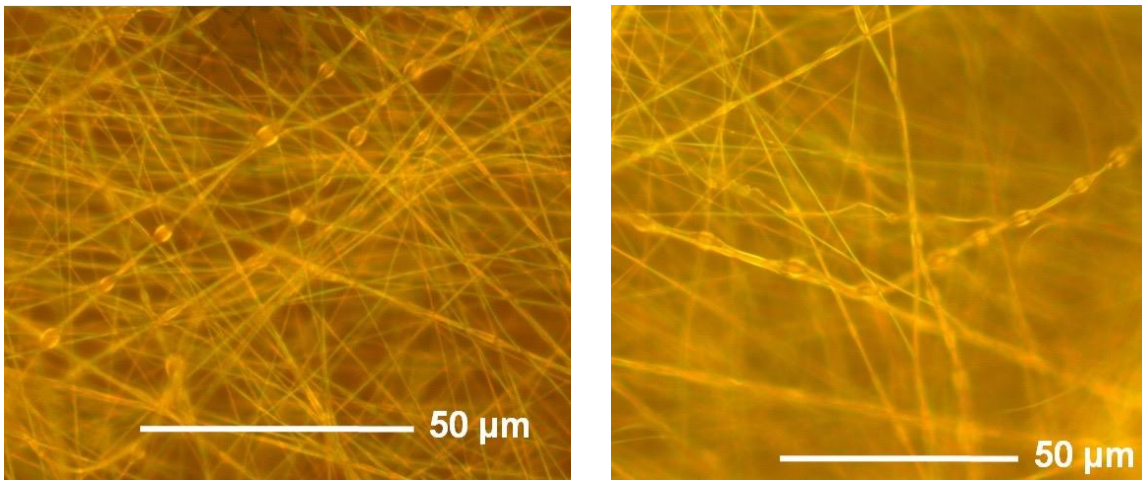

Figure 44 *Core-shell nanofibers with incorporated vegetable oil observed using optical microscope Olympus.*

3.5.2 Weir spinner

The weir spinner is the needleless coaxial spinning electrode for electrospinning from the free surface of the polymeric two-layer. Two polymers are spun together by the action of electrostatic field. Core-shell nanofibers are collected on the oppositely charged collector as is shown in Figure 45. A great number of Taylor cones and polymer jets are created on the top of free liquid surface of the polymeric two-layer.

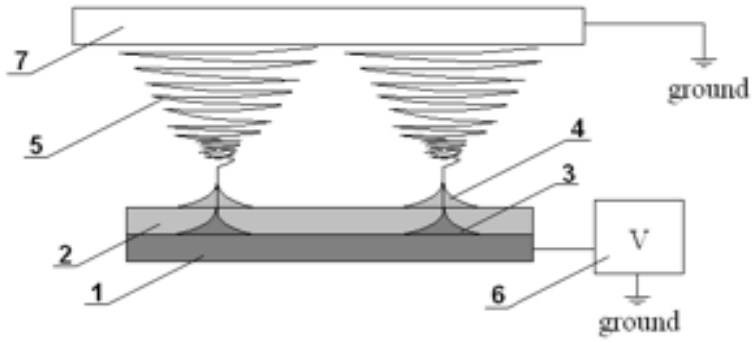

Figure 45 *The schema of the needleless coaxial electrospinning from the free surface of the polymeric two-layer: Layer of the core polymer (1), layer of the shell polymer (2), Taylor cones (3, 4), the polymer jet (5), HV supply (6), grounded collector (7).*

This spinning electrode was developed at the Technical University of Liberec and patented in 2009 (Pokorný, 2009). This technology gained its name from the similarity to the weir on the race (Vysloužilová, 2010).

The weir spinner with parameters 80 x 70 x 28 mm (weight x high x depth) consists of two feeding chambers with volume 8 ml (the shell chamber) and 7 ml (the core chamber) for dispensing of shell and core liquids and of one outflow chamber for the waste material as is shown in Figure 46. The middle part represents the plate electrode with thickness 1 mm that is placed in between two side parts. The work length of the weir spinner is 47 mm.

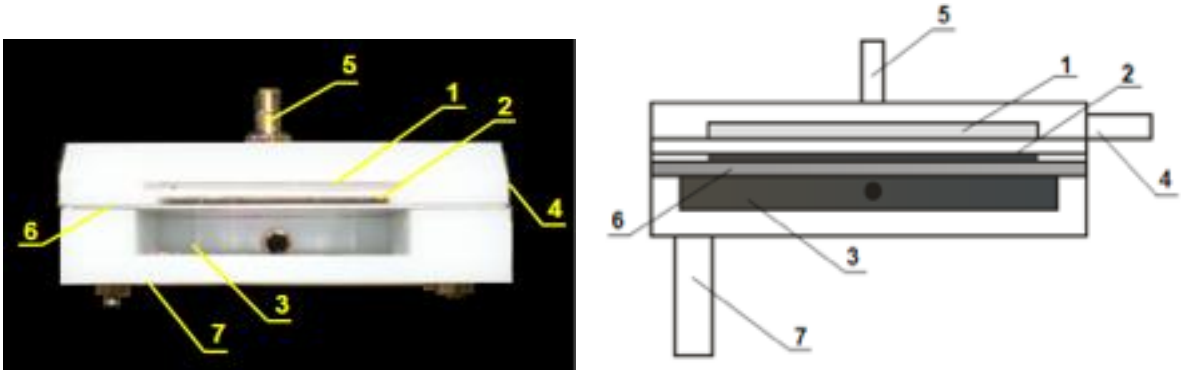

Figure 46 *The Weir spinner: the chamber for the shell polymer solution (1), the chamber for the core polymer solution (2), the outflow chamber (3), the core polymer feeding tube (4), the shell polymer feeding tube (5), the electrode (6), the holder for HV cord (7), (Vysloužilová, 2011).*

The laboratory set-up placed in air conditioned digestion was used for initial tests of the weir spinner. This one was mounted on the tubes with the core and the shell polymer solution. The weir spinner was connected to the HV Spellman Sl100 supply and positively charged. This spinner was located 100 - 160 mm below the oppositely charged disc collector with diameter 180 mm. The Spunbond nonwoven for collecting of core-shell nanofibers was located under the collector. The applied voltage was 20 - 35 kV (positive pole) and 10 – 30 kV (negative pole). The shell polymer feed rate was 5 - 15 ml/hr and the core polymer feed rate was 3 - 10 ml/hr. The experiments were carried out with temperature 21°C and relative humidity 36 %.

The experiments have shown, that this needleless spinning electrode is suitable apparatus for production of core-shell nanofibers from the free surface of the thin polymeric two-layer. The optimal distance between electrodes was 130 mm for test PVA solution. The electrospinning process started in achieving values of HV +25/-15 kV. The value of HV was increased to the +33/-15 kV for which the electrospinning process was optimal. It was founded, that the optimal feed rate is 12 ml/h for the shell and 8 ml/h for the core polymer

solution. Nanofibers were collected on the collector with the Spunbond nonwoven only. There was created the homogeneous nanofibrous layer without wet defects.

This equipment allows increasing of productivity of core-shell nanofibers, because a lot of Taylor cones and polymeric jets are created. The viscosity of the shell polymer has to be higher than the viscosity of the core polymer. The shell polymer with lower viscosity can't pull up the core polymer with higher concentration.

There were found some disadvantages of this spinning electrode design. First of all there was too large volume of feeding chambers. A lot of the spinning material has been lost due to large capacity of chambers. This is a big problem in a case of electrospinning of expensive materials such as drugs, enzymes, liposomes, special liquids with nano diamonds and others. The next disadvantage was a uneven polymer solution feed to the orifice of the weir spinner. To ensure the uniform supply of polymer solutions is crucial for production of bi-component nanofibers with core-shell structure. Based on these knowledges from electrospinning realized using this apparatus, the new optimized weir spinner was designed and tested.

3.5.3 Weir spinner of the 2nd generation

The weir spinner of the 2nd generation, see in (Figure 47) is the optimized version of the original weir spinner. This one was designed to obtain full function spinning electrode with the uniform supply of polymer solutions to its orifice that creates the homogeneous polymeric two-layer.

Volumes of feed chambers were reduced to 1 ml. This is great advantage for electrospinning of expensive and special polymers and liquids. Just small volume of these materials is as a rule necessary to electrospun by needleless technology. The next advantages of this type of spinning electrode are thin feed chambers ensuring a laminar flow of liquids. The result is the homogeneous polymeric two-layer at the spinning electrode orifice. The work length of the weir spinner of the second generation is 42 mm.

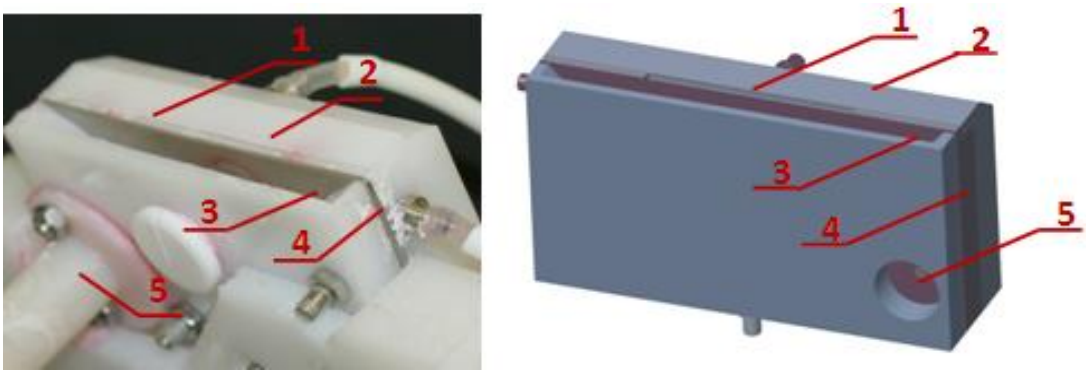

Figure 47 *The Weir spinner of the 2nd generation: the chamber for the core polymer solution (1), the chamber for the shell polymer solution (2), the outflow chamber (3), the core polymer feeding tube (4), the shell polymer feeding tube (5), the electrode (6), the holder for HV cord (7), (Vysloužilová, 2011).*

The weir spinner of the 2nd generation was tested in the air conditioned chamber. The water soluble PVA at concentration of 12 % (w/v) was used as the shell liquid and the water soluble PVA at concentration of 4 % (w/v) was used as the core liquid. The red food pigment was added to the core to better observation of the coaxial electrospinning process. The spinning electrode was placed on the spinning electrode holder and connected to the tubes with core and shell polymer solutions. The coaxial spinning electrode was connected to the HV source (Spellman Sl150) and positively charged. The electrode was located 100 mm below the negatively charged disc collector with the diameter of 120 mm connected to the HV source (Spellman Sl150). The Spunbond nonwoven was placed under the collector for core-shell nanofibers deposition.

Polymer solutions were fed to the weir spinner using the dosing pumps Nemesys 14.1 (Cetoni, DE). The feeding rate of the core and shell material was set in 1:2 ratio and ranged from 0,5 - 4 ml /h. After switching HV, the Taylor cones have been formed on the surface of the shell polymer solution and these cones pull up the core liquid as is shown in Figure 48. Electrospinning started with achieving +18/-8 kV. The applied voltage ranged from 18 to 35 kV (positive pole) and 8 to 12 kV (negative pole). The experiments were carried out in the chamber with controlled atmospheric conditions; temperature was 21±3 °C and RH was 28±5%.

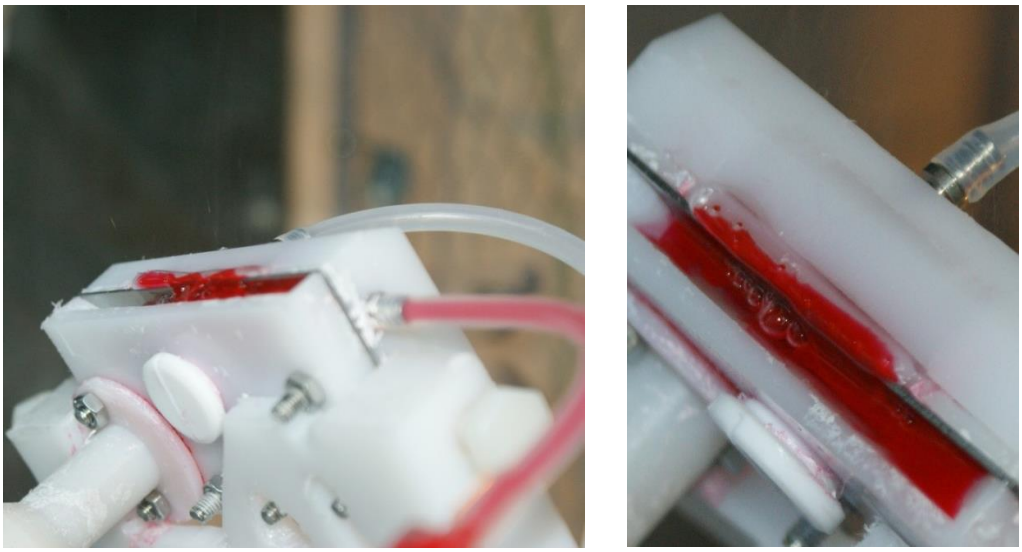

Figure 48 *Needleless coaxial electrospinning realized using weir spinner of the 2nd generation.*

The productivity of this apparatus was 2.67±0.99 g/h. It means that it is approximately 4 times more than needle technology (the productivity of the needle coaxial spinning electrode is 0.64±0.03 g/h). Productivity of the developed spinning electrodes is listed in Chapter 3.5.8 in Table 15.

3.5.4 Weir spinner of the 3rd generation

A new type of the weir spinner, see (Figure 49) was designed and made to maximize the effect of the production of core-shell nanofibers and eliminating the waste of non-spun material. Its structural design lies in the highest concentration of the electric charge on the surface of the polymer two-layer. There is considerable change in design of the new weir spinner compared to the previous two types. The spinning electrode from the stainless steel is not recessed into the body of the device, but it is exposed to the electric field. The dimensions of this apparatus are 100 x 25 mm (length x width).

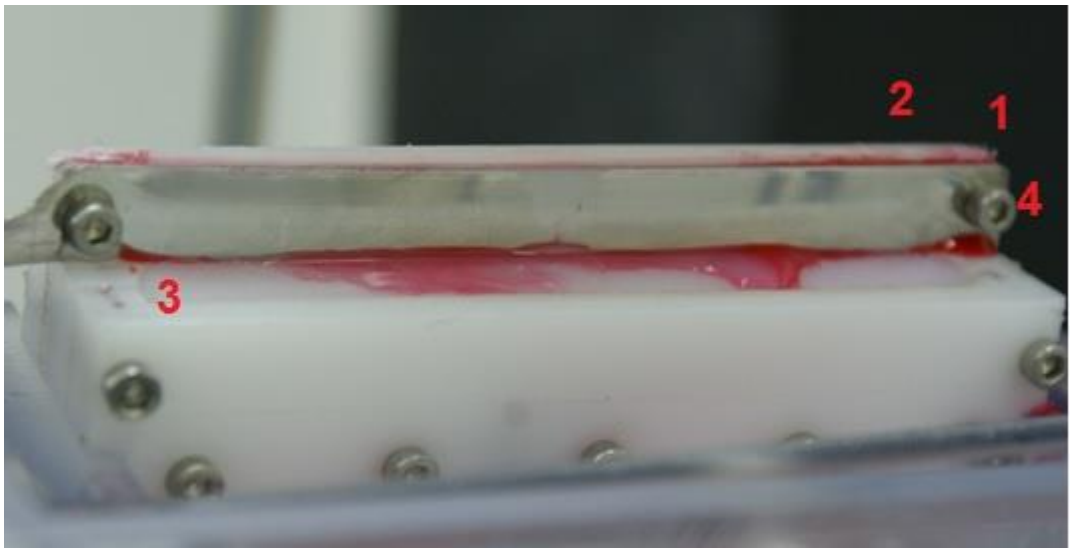

Figure 49 *The Weir spinner of the 3rd generation (Nanoprogres): the chamber for the core polymer solution (1), the chamber for the shell polymer solution (2), the outflow chamber (3), the electrode (4)*

This needleless electrode was tested in the air conditioned chamber under the same process conditions as in the case of the weir spinner of the 2nd generation. PVA at concentration of 12 % (w/v) was used as the shell material and the PVA at concentration of 4 (w/v) was used as the core material. The red food pigment was added to the core material for better observation of the coaxial electrospinning process.

Polymer solutions were fed to the weir spinner using the dosing pumps Nemesys 14.1 (Cetoni, DE). The feeding rate of the core and shell material was set in 1:2 ratio and ranged from 0,5 - 4 ml / hr. There occurred the undesirable leakage of polymer solutions under the spinning electrode as can be seen in Figure 50. Larger volume of supplied polymer solutions was therefore not supplied to the spinner orifice (spinning space of the apparatus), but this flowed away into the outlet chamber before the actual coaxial electrospinning process. After switching HV the Taylor cones have been formed and the spinning process started. The applied voltage was 18 - 35 kV (positive pole) and 8 – 12 kV (negative pole). The experiments were carried out in the chamber with controlled atmospheric conditions; temperature was 21 °C and RH was 28 %.

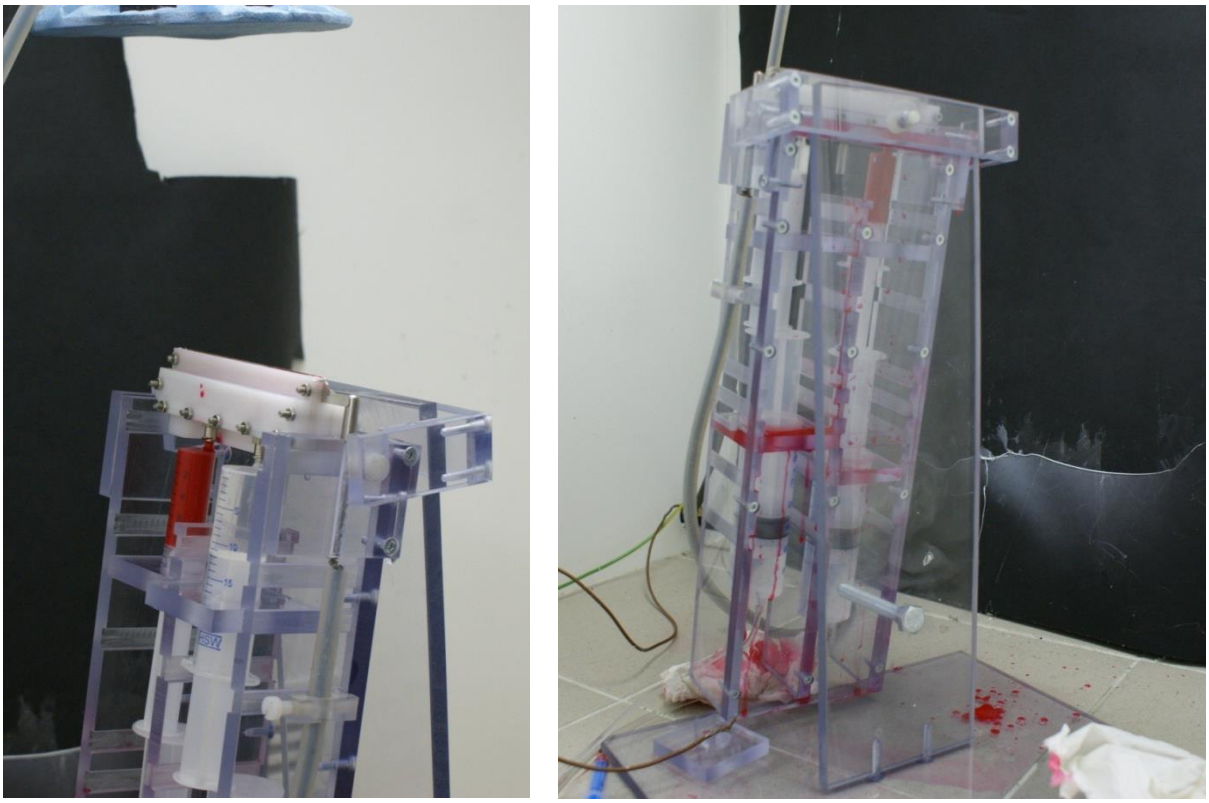

Figure 50 *Fixation of the weir spinner of the 3rd generation in the spinning electrode holder and connection to the syringes with core and shell polymer solutions. The device is placed in the holder at a given angle suitable for the optimal creation of the polymeric two-layer.*

This design of the needleless spinning electrode has proved inconvenient; the predicted spinning required effect has not been achieved. Reducing of the electrode and its location was causing the solution flowing away into the outlet chamber. The thin uniform polymeric two-layer was not formed at the orifice of the weir spinner. The negative effect on the two-layer formation had also inappropriately selected the fed of polymer solutions. It was withdraw from this design of the coaxial needleless spinning electrode.

3.5.5 Weir spinner of the 4th generation

After the experience gained from the previous experiments, the overall view of the design of spinning electrode was changed. It was necessary to expose the spinning polymer solution to an electric field, so that the maximum electrical charge was focused on it. Furthermore, it was necessary to adjust the design of the electrospinning device to avoid the electric charge conducting away by individual parts of the spinning electrode. This charge conducting away has resulted in negative effect on the electrospinning process.

The new needleless spinning electrode with parameters 35 x 155 mm (width of the base x length) was designed within this work, project SGS 28012 and Nanoprogres cluster. This new spinning electrode is shown in Figure 51. Its orifice was significantly narrowed and raised from the base of the spinning electrode to the maximal exposure of the electrospinning liquid to the electric field. The remaining part of the apparatus (the massive base of the apparatus) was inserted as deeply as possible from the action of the electric field. The aim was the maximum exposure of the electrospinning liquid to the electric field. The plate electrode was replaced by the wire electrode placed to the orifice of the core chamber. A separator plate was inserted between core and shell chamber.

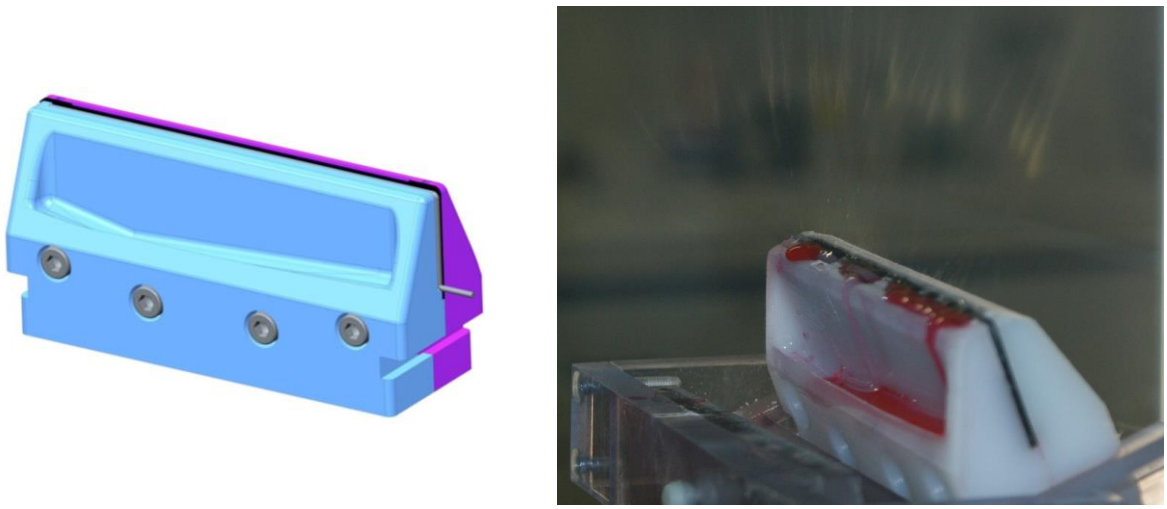

(a) (b)

Figure 51 *(a) 3D model of the weir spinner of the 4th generation, (b) electrospinning realized by the weir spinner of the 4th generation*

The new weir spinner of the 4th generation was tested in the Spinner 1 (Nanoprogres). This one was placed on the spinning electrode holder and connected to the syringes with core and shell polymer solutions. The new weir spinner was connected to the HV source (Spellman Sl150) and positively charged. The electrode was located 150 - 160 mm below the negatively charged collector from stainless steel. Its thickness was 2 mm and size 160 mm x 355 mm (width x depth). The Spunbond nonwoven was placed under the collector. This nonwoven was unwound with constant velocity 0,05 mm/s during electrospinning process. Syringe pumps NEMESYS 14.1 (Cetoni, GE) were used to feed polymer solutions into weir spinner chambers. The feeding rate of the shell polymer solution was 11 - 17 ml/hr and 8 – 13 ml/h for the core polymer solution. The applied HV ranged between 30 - 35 kV (the weir

spinner) and 30 – 35 kV (the collector). The experiments were carried out in a chamber with controlled atmospheric conditions; temperature was 23°C and relative humidity was 35 %.

The experiments showed that the thin uniform polymer two-layer is not created at the orifice of the weir spinner. This is caused by too wide spinning electrode orifice. The feeding chambers are located at a great distance from the plate electrode, resulting in evaporation of solvent from the polymer solutions before onset of the electrospinning process. The spinning electrode orifice is located close to the upper part of the spinner holder. This resulted to polymer solution dripping on this upper part and there occurs undesirable getting from these polymer droplets.

The following modifications of the weir spinner was focused on the another narrowing of the spinning electrode orifice. The thickness of the separator plate was reduced. The wire electrode was placed in close proximity to the core chamber to significantly reduce the time of the core polymer solution supply to the orifice of the spinning electrode. These modifications have resulted in reduction of the undesirable evaporation of the solvent during the transport of the electrospinning polymer solutions to the plate electrode and hence it eliminates the undesirable drying of these polymer liquids. This weir spinner modified within this work and project Nanoprogres is shown in Figure 52.

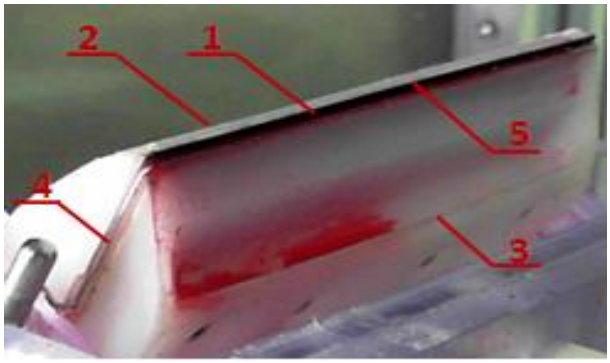

Figure 52 *The modified weir spinner of the 4th generation with the very thin orifice and thin dividing partition between the core and the shell chamber: core chamber (1), shell chamber (2), waste chamber (3), wire electrode (4), separator plate (5).*

These experiments showed that polymer solutions were supplied unevenly to the weir spinner orifice. The core solution flowed mostly from the right side of the feeding chambers, while the shell one from the left side. The uniform polymeric two-layer was not created as shown in Figure 53. The flowing of both polymer solutions occurred even in the case of the

dosage of only one of the polymers. The too narrow slits of the chambers were likely the reason of this problem.

In the next step, the screws have been loosened, the pressure between both parts of the spinner was reduced and this has resulted in more uniform feeding of the polymer solutions. The polymeric two-layer at the spinner orifice was created, but still remained inhomogeneous. The experiments with the protrusion of the dividing partition were carried out and optimal protrusion regarding the homogeneous polymeric two-layer formation was investigated. The main aim of these experiments was the location of the shell polymer above the core one and to avoid their undesirable mixing. There was observed non-coaxial electrospinning of the shell polymer solution from the edge of the separator plate after switching HW source (see in Figure 53). The dividing plate was an alignment with the upper edge of the shell chamber. Both of the polymer solutions were electrospun, but separately, non-coaxial electrospinning were observed. The optimal polymeric two-layer was not created.

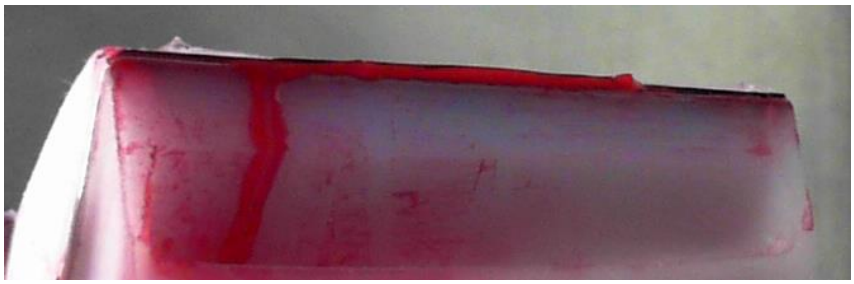

Figure 53 *Non-coaxial electrospinning realized using weir spinner of the 4th generation. The core polymer solution (red one) was flowing out from the right side of the feeding chambers and the shell one from the left side.*

Optimal protrusion of the dividing plate and inclination angle of the weir spinner were investigated in the next step. The finding of the suitable inclination angle of this spinner is necessary to the creation of the optimal polymeric two-layer and for core-shell nanofibers formation. Experiments showed that 80° is the optimal angle for the needleless coaxial electrospinning realized by the new weir spinner. Lower values of the inclination angle resulted in slumping of the polymer solutions before the polymeric two-layer formation. Optimal protrusion of the dividing plate was 0.2 mm. Higher values of protrusion caused a separation of the polymer solutions and core-shell nanofibers were not formed, see (Figure 54). Otherwise, lower values of protrusion resulted in the mixing of core and shell solutions before electrospinning.

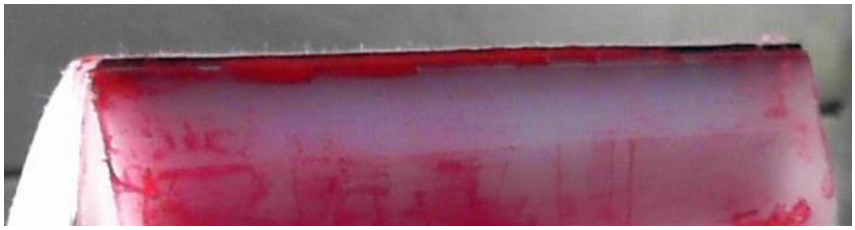

Figure 54 *Non-coaxial electrospinning of the shell polymer solution from the edge of the dividing plate protruding 1 mm above the spinner orifice. The core and the shell polymer solution stayed separation by dividing partition.*

Experiments have shown, the weir spinner is suitable spinning electrode to increase of productivity of core-shell nanofibers. The large numbers of Taylor cones and polymeric jets were created as is shown in Figure 55. The productivity of this spinning electrode is 3.45±0.83 g/h. It is approximately 5 times more than needle coaxial technology; see in Chapter 3.5.8, Table 15. The disadvantage of this spinning electrode is susceptibility to creation of spark discharges caused by its edges as is shown in Figure 55 b. Electrospinning process is accompanied by corona discharges (Figure 55). Corona discharges are generated by highly charged polymeric jet roots, so-called Taylor's cones. Sometimes, the corona discharge converts into the spark discharge. This is unsuitable for electrospinning process, since the discharge drains away energy from the technological process (Vyslouzilova, 2014).

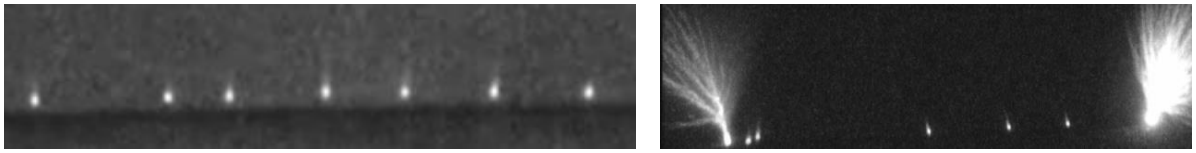

(a) (b)

Figure 55 *(a) Corona discharges and (b) spark discharges during electrospinning realized using the weir spinner of the 4th generation. Ultraviolet light spots in the figure determine the position of Taylor cones. Photographs are obtained using CoroCam I, Uvirco Technologies, SA.*

The next research was focused on the elimination of the spark discharges and it was searched the ideal solution for concentrating the maximal electric charge on the electrospinning polymer solution. It is supposed, the minimal electric charge will be conducted by the body of the spinning electrode.

3.5.6 Cleft electrode

Cleft electrode with the rounded edges, see (Figure 56) was developed at the Department of Textile Machine Design at Technical University of Liberec within this work, project SGS 21012 and project Nanoprogres as a new modification of the weir spinner. The modification increases productivity of needleless coaxial electrospinning due to the suppression of spark discharges. The idea of the cleft electrode is the elimination of a loss of electric energy caused by sharp edges of the weir spinner. This spinning electrode was designed from the duraluminium. The reason for this material was the possibility to use cleft electrode in environment of the cleanroom as in Spinner 2 (Nanoprogres). The next advantage of this construction material is its easy workability and accuracy machining.

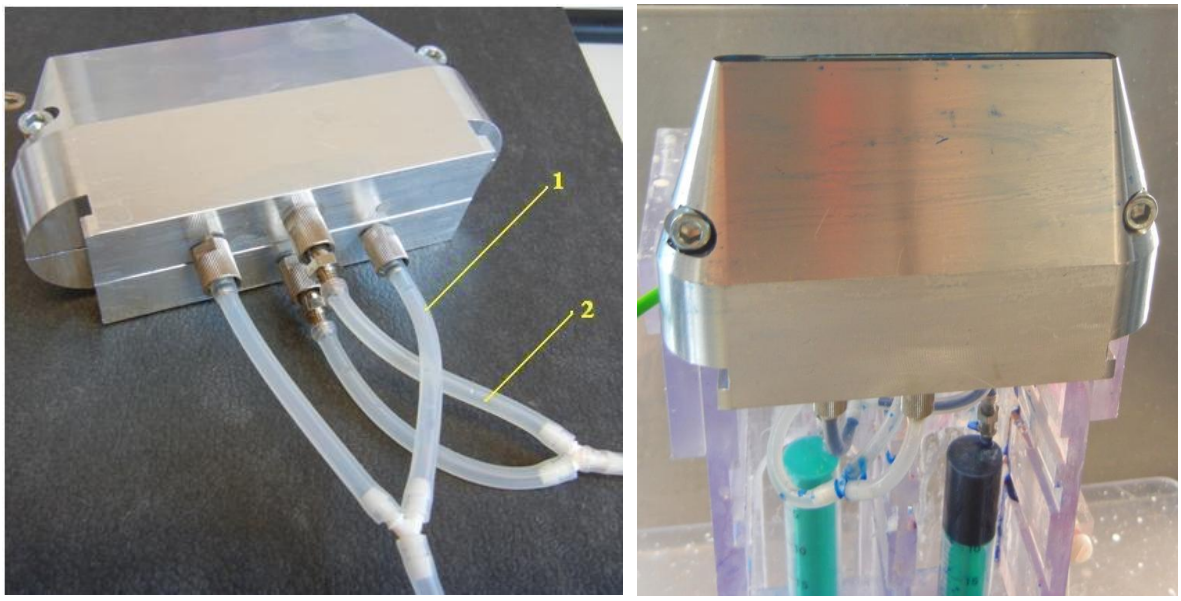

Figure 56 *The cleft electrode with a massive base and a slim orifice: Connection of the cleft electrode on the dosing system (a) and its placed into the holder in Spinner 1 (b): supply of the core material (1), supply of the shell material (2).*

The cleft electrode is composed from the two main parts tightly clamped to prevent flowing through electrospinning liquids. The cleft electrode has two chambers for the shell polymer solution (outer one) and for the core liquid (inner one). Special guide metal combs, see in (Figure 57) are located into these chambers to ensure uniform dosing of the core and shell liquids to the spinning electrode orifice. The massive base ensures the laminar flow of electrospinning liquids and the tight grip of both outer parts of the electrode. The polymeric two-layer is sufficiently exposed to the electric field due to the very thin orifice of the spinning electrode. The maximal electric charge is concentrated on the two-layer and this is not conducted by the spinning electrode body. The special dosing system was used for

uniform feeding of the electrospinning liquids. Both electrospinning materials, core and shell liquids, are supplied by the two tubing to the core and shell chambers as is shown in Figure 56. Each chamber has a special design for ensuring the laminar flow. This is important for the formation of the homogeneous polymeric two-layer at the orifice of the spinning electrode.

The experiments aiming to find the optimal geometry of the chambers of the spinning electrode were done. The uniform formation of the homogeneous polymeric two-layer was investigated. Figure 57 shows experiments with the dosing of the inner and outer chambers by polymer solutions. The special experiment with a transparent chamber was prepared and the polymer dosing of chambers was investigated. The optimal composition for the formation of the uniform polymeric two-layer was founded during these experiments.

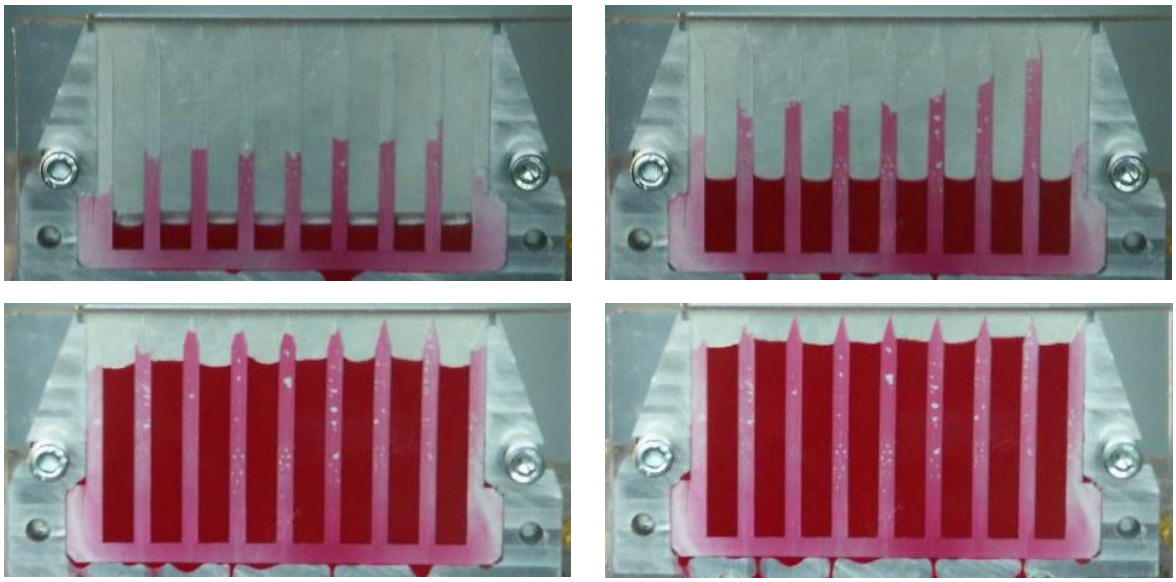

Figure 57 *Investigation of the uniformity of filling the inner and outer chambers by polymer solutions with red pigment.*

In the first step, the orifice of the core chamber was designed protruding 1 mm above the shell chamber in order to eliminate mixing of core and shell liquids before electrospinning process as is shown in Figure 58 a. Experiments showed that this design is not suitable for the formation of the polymeric two-layer as is shown in Figure 58 c. The shell polymer solution flows down from the orifice of the cleft electrode. The layer of the core liquid is above the shell one and the core-shell nanofibers are not created.

In the next step, the protrusion of the core chamber was reduced to 0,5 mm, see in (Figure 58 b). This design was suitable for the polymeric two-layer formation and core-shell nanofibers were formed in this case.

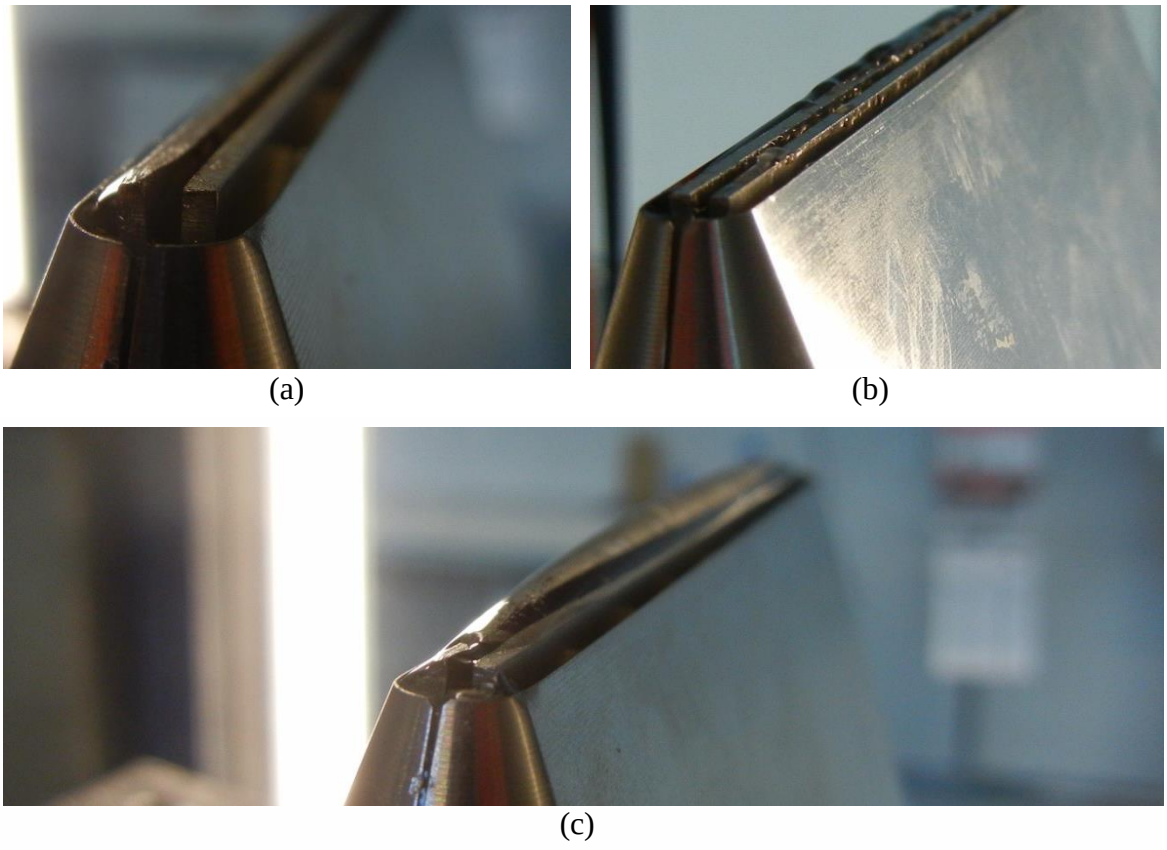

Figure 58 *The cleft electrode with a protrusion of the core chamber 1 mm (a) and 0,5 mm (b) above the shell chamber.*

Experiments were done with Spinner 1 (Nanoprogres). The cleft electrode was placed on the spinning electrode holder and connected to the system of the dosing tubes with core and shell polymer solutions as is shown in Figure 59. The PVA solution at concentration of 12 wt.% was used as the shell solution and the PVA at concentration of 4 wt.% with Prussian Blue was used as the core solution. The cleft electrode was connected to the HV source (Spellman Sl100) and positively charged. The electrode was located 150 mm below the negatively charged collector from stainless steel with thickness 2 mm and size 160 mm x 355 mm (width x depth). 150 mm proved to be optimal value for these test polymer solutions. The Spunbond nonwoven placed under the collector was unwound with constant velocity 0,05 mm/s throughout electrospinning process. Syringe pumps NEMESYS 14.1 (Cetoni, GE) were used to feed polymer solutions into weir spinner chambers. The feeding rate of the shell polymer solution was 11 - 17 ml/hr and 8 – 13 ml/hr for the core polymer solution. The applied HV was in the range of values 30 - 35 kV (the weir spinner) and 30 – 35 kV (the collector). The experiments were carried out in a chamber with controlled atmospheric conditions; temperature was 23°C and relative humidity was 35 %.

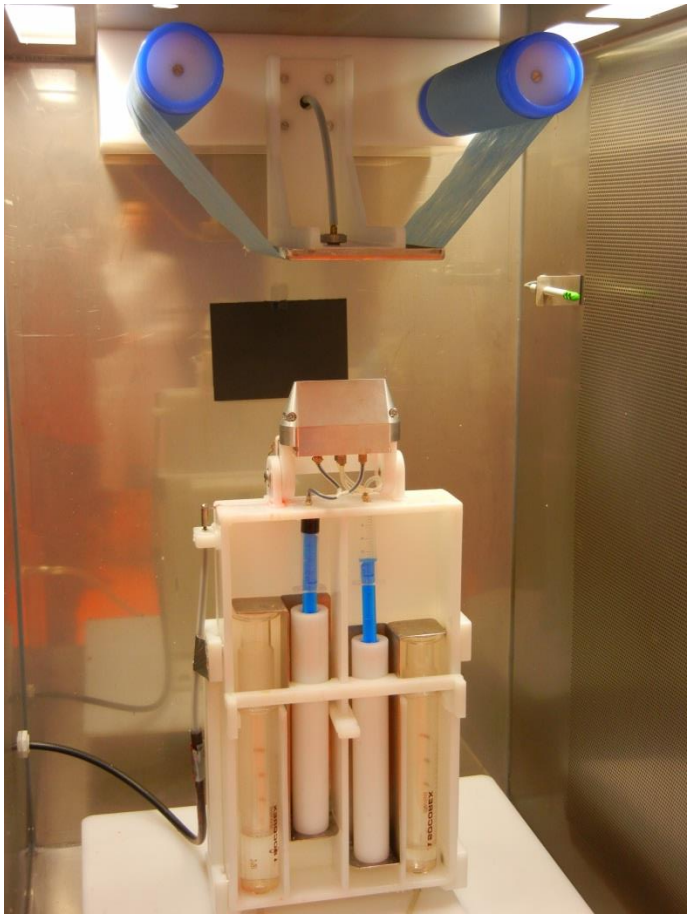

Figure 59 *Cleft electrode placed on the spinning electrode holder and connected to the system of the dosing tubes with core and shell polymer solutions in the Spinner 2.*

Thin homogeneous polymer two-layer was created at the orifice of the cleft electrode with the protrusion of the core chamber 0,5 mm. Many Taylor cones and polymer jets were observed during coaxial electrospinning process as can be seen in (Figure 60). The productivity of this needleless coaxial spinning electrode is 2.67±0.99 g/h, it means this is comparable to the weir spinner, see in Chapter 3.5.8 in Table 15.

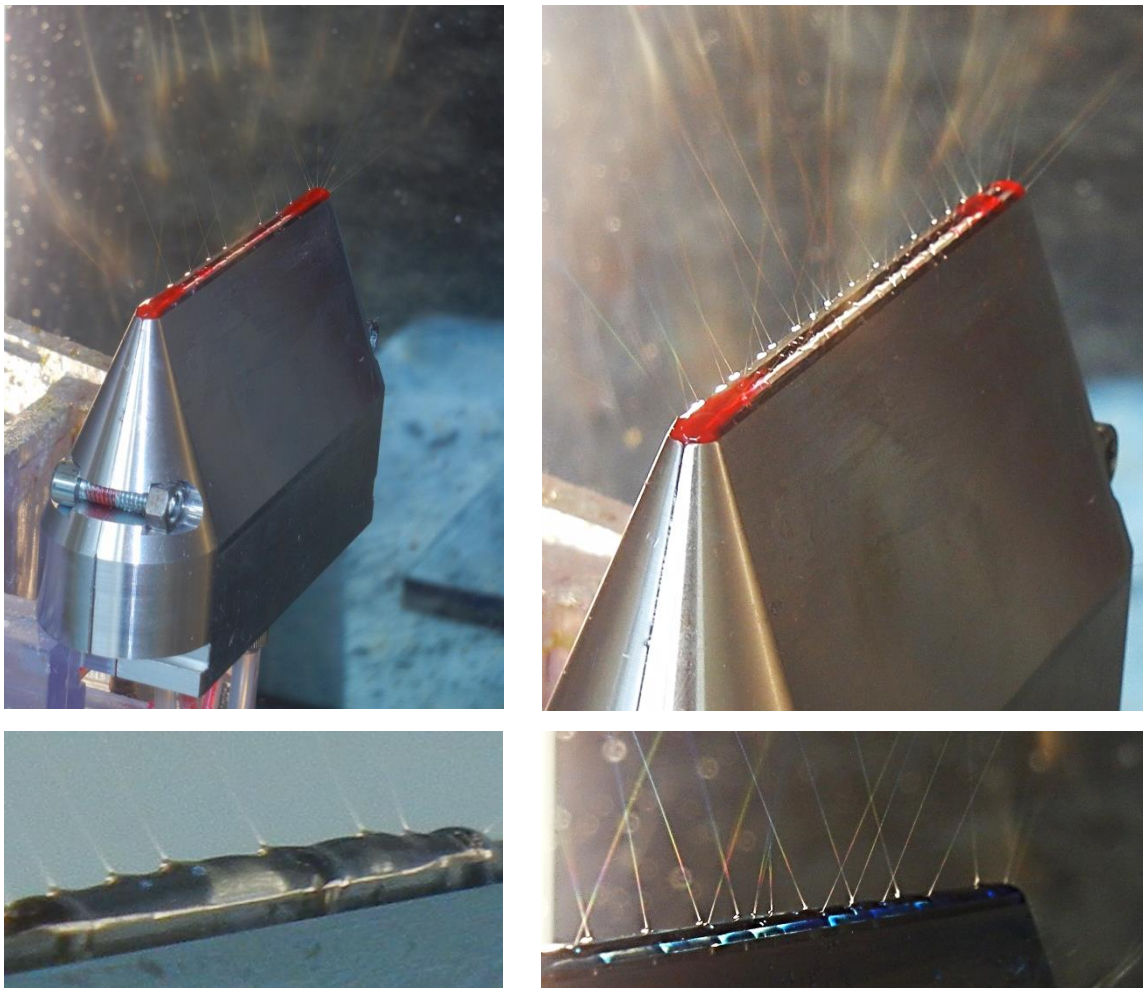

Figure 60 *The coaxial electrospinning realized using cleft electrode in Spinner 1 with the detail of polymeric jets on the polymer two-layer*

3.5.7 Cylindrical coaxial spinning electrode

Based on the results of the spinning electrode with the cleft geometry, a new design of the electrode was developed at Department of Textile Machine Design at Technical University of Liberec within this work and project SGS 21012. The aim of the new concept was to replace the linear shaped electrode by the circular one, which would eliminate problems at the ends of the cleft electrode. The cylindrical coaxial spinning electrode, see in (Figure 61) has a smooth surface and it consists of three cylindrical feeding chambers. The outer chambers are intended for the supply of the shell polymer solution, the middle one is for supply of the core liquid. The orifice of this one was located 0,5 mm below the electrode orifice. The assumption was that the core liquid overlaps the shell one. This spinning electrode used a special tubes system and feeding chambers with auxiliary distribution ring located horizontally at the bottom of the core chamber. This system supports the uniform dosing of

polymer solutions into feed chambers and the formation of the homogeneously polymer two-layer at the orifice of the spinning electrode. The tubes system is shown in Figure 61 b.

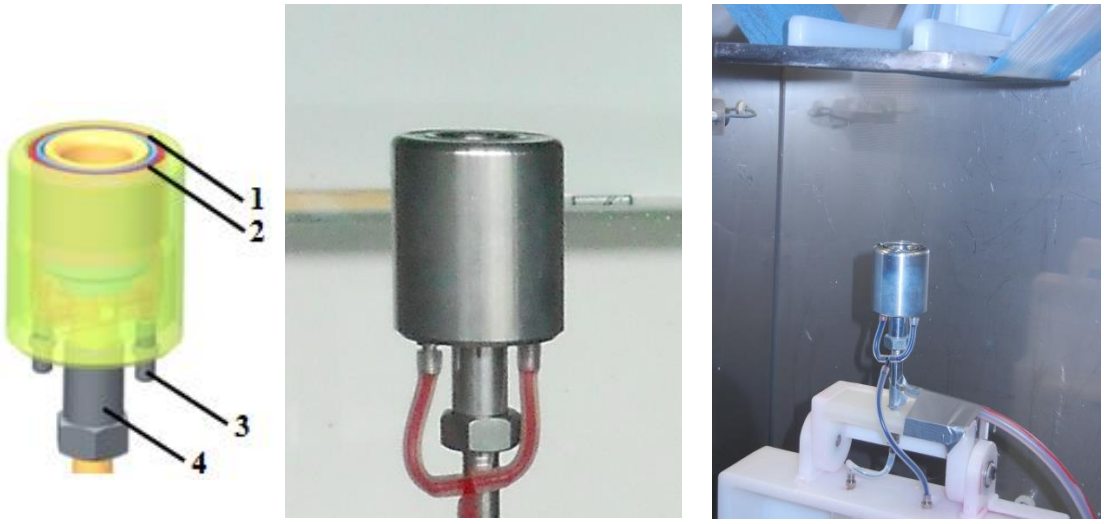

(a) (b) (c)

Figure 61 *(a) The model of the cylindrical coaxial spinning electrode, (b) the cylindrical coaxial spinning electrode, (c) electrospinning from the cylindrical electrode: (1) the outer and (2) the inner annulus, (3) the core tube, (4) the shell tube (Pejchar, 2013).*

The solution of PVA was prepared at concentration of 12 % (w/v) in distilled water and used as the shell solution. Crosslinking agent glyoxal (3 % (w/v) of dry matter of PVA) and phosphoric acid (4 % (w/v) of dry matter of PVA) were added to the PVA solution. The solution of PVA was prepared at concentration of 4 % (w/v) dissolving in distilled water and used as the core solution. The Prussian blue was added to the core solution for better observation of the electrospinning process and for analysis of the core-shell structure of produced nanofibers. This analysis is listed in detail in Chapter 3.8.

The experiments were carried out in Spinner 1 and Spinner 2 with controlled atmospheric conditions; temperature was 23±2°C and relative humidity was 32±2 %. Spinning electrode was clamped in holder and connected to the special tubes system with core and shell polymer solutions. This one was connected to the HV source (Spellman Sl100) and positively charged. The electrode was located 130 mm below the negatively charged collector from stainless steel with thickness 2 mm and size 160 mm x 355 mm (width x depth). The Spunbond nonwoven was placed under the collector and unwounded with constant velocity 0,05 mm/s throughout electrospinning process. Polymer solutions were

supplied into the chambers of spinning electrode using the syringe pumps (NEMESYS, Cetoni, GE.) and fed at a rate of 10 - 25 ml/hr (core) and of 30 - 60 ml/hr (shell).

It was found that the optimal voltage was +33/-30 kV and the optimal distance between electrodes was 130 mm for electrospinning of PVA. Electrospinning ran uniformly across the all surface of the spinning polymer solution. The optimal feed rate was 60 ml/h for the shell solution and 25 ml/h for the core solution. This higher feed rate was equal to the high productivity of this new spinning electrode. The electrospinning process was recorded by the special camera for detection of the corona discharges CoroCam 1 (Uvirco Technologies, SA) as is shown in Figure 62. The uniform distribution of polymeric jets was observed during coaxial electrospinning. The process was not accompanied by spark discharge causing loss of electric energy due to cylindrical construction and curvature of the edges of this spinning electrode. The electric charge density is constant over the entire circumference of the electrode orifice. There is no cumulating of electric charge into the areas with the local extremes as in case of the spinning electrode with the linear design.

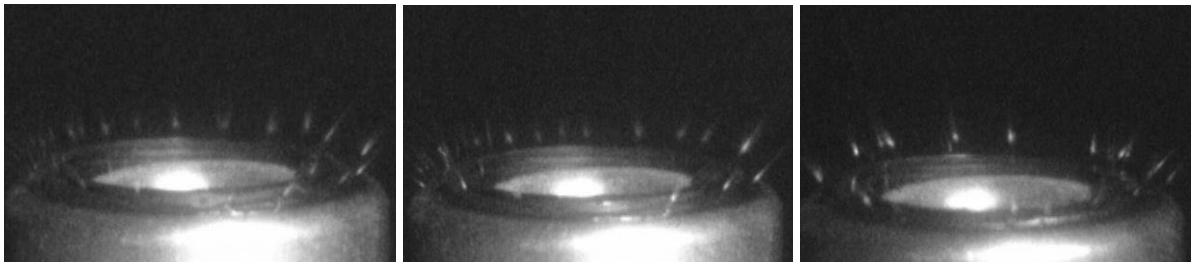

Figure 62 *Corona discharges detected during the coaxial electrospinning realized by cylindrical coaxial spinning electrode recorded by CoroCam 1 (Pejchar, 2013)*

Experiments showed that cylindrical construction of the needleless coaxial spinning electrode is very advantageous. There were not observed spark discharges causing the loss of electric energy and the feeding of polymer solutions were most evenly due to dosing systems. The homogeneous polymeric two-layer was created at the orifice of this electrode without polymeric layer slumping throughout electrospinning process (Lukáš, 2013).

Very interesting knowledge was found during experiments. The thin slits of chambers in a circular configuration cause crosslinking of the PVA with added crosslinking agent as is shown in Figure 63. A water-insoluble layer of polymer has formed. An electric cell was created by this construction of the spinning electrode. Polymer solutions without crosslinking agents were used for next experiments with cylindrical coaxial spinning electrode.

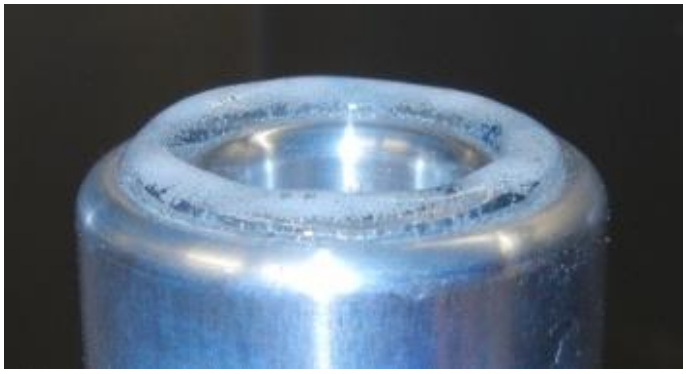

***Figure** 63 water-insoluble layer of PVA at the orifice of the cylindrical coaxial spinning electrode*

Experiments showed that higher values of HV are necessary to start the electrospinning process. Too massive orifice of the spinning electrode results in conducting away the electrical charge from the electrospinning process to the spinning electrode body. There was the problem, electric charge was not concentrated primarily only on the surface of the electrospinning polymer solution. The solution could be founded in the creation of the two-layer with higher volume overlapping the spinning electrode orifice. The construction of this spinning electrode did not allow the stable maintenance of the bulk polymer two-layer. The two-layer was slumping, see in (Figure 64).

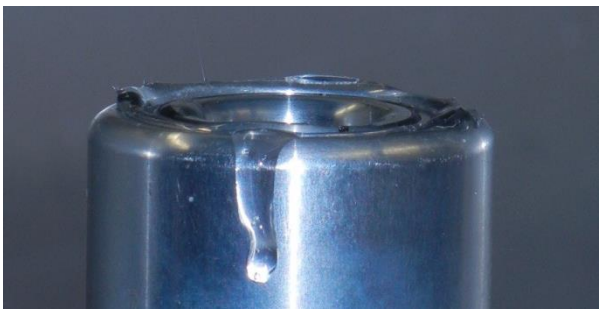

***Figure 64** Slumping of the polymer solution from the cylindrical coaxial spinning electrode during electrospinning process.*

The productivity of this spinning electrode was higher compared to the weir spinner but there was unnecessarily to high the value of HV to start the electrospinning. The process was accompanied by the formation of ozone due to this high value of HV. There was also founded, the height of the core chamber is unsuitable for the creation of the polymeric two-layer. Polymer solutions were mixed before start of electrospinning process. Therefore the

new construction of the cylindrical coaxial spinning electrode with the modified orifice was designed in the next step.

3.5.8 Cylindrical coaxial spinning electrode of the 2nd generation

The new cylindrical coaxial spinning electrode, see (Figure 65) was developed at Department of Textile Machine Design at Technical University of Liberec within this work and project SGS 21012. This new concept of the cylindrical coaxial spinning electrode is based on a smaller diameter of the outer perimeter of the spinning electrode. The new diameter of the spinning electrode orifice was 31 mm, this means about 4 mm smaller than the initial concept. It is supposed, the spinning electrode with the smaller average of the orifice can be suitable also for AC electrospinning (Pokorný, 2014). There is a limitation in the maximal value of the HV in AC electrospinning. This value of HV is insufficient to start of electrospinning realized the spinning electrode with the massive construction. The experiments showed that the average of the spinning electrode 31 mm is suitable for AC electrospinning. The core chamber was designed with the protrusion 0,5 above the shell one. This new concept should prevent premature mixing of polymers solutions. Many construction materials were taken away from the spinning electrode and this one is less massive than the initial concept of the cylindrical coaxial spinning electrode. The maximal electric intensity is located on the polymeric two-layer and the electric energy is not lost by the body of the spinning electrode.

PVA (Sloviol, Chemicke zavody Novaky, SK) at concentration of 12 % (w/v) dissolved in distilled water was used as the shell solution and PVA at concentration of 4 % (w/v) with added Prussian blue was used as the core one. In the next step, PCL (Mn = 45.000, Sigma Aldrich, UK) at concentration of 14 % (w/v) dissolved in chloroform/ethanol (9:1) was used as the shell solution and PCL at concentration of 5 % (w/v) dissolved in chloroform/ethanol (9:1) was used as the core solution. In the next step, PVB (Mowital, Kuraray, UK) at concentration of 10 % (w/v) dissolved in ethanol was used as the shell solution and PVB at concentration of 5 % (w/v) dissolved in ethanol with added Prussian blue was used as the core solution. In the last step, PUR at concentration of 15 % (w/v) was used as the shell solution and PVB at concentration of 5 % (w/v) was used as the core solution.

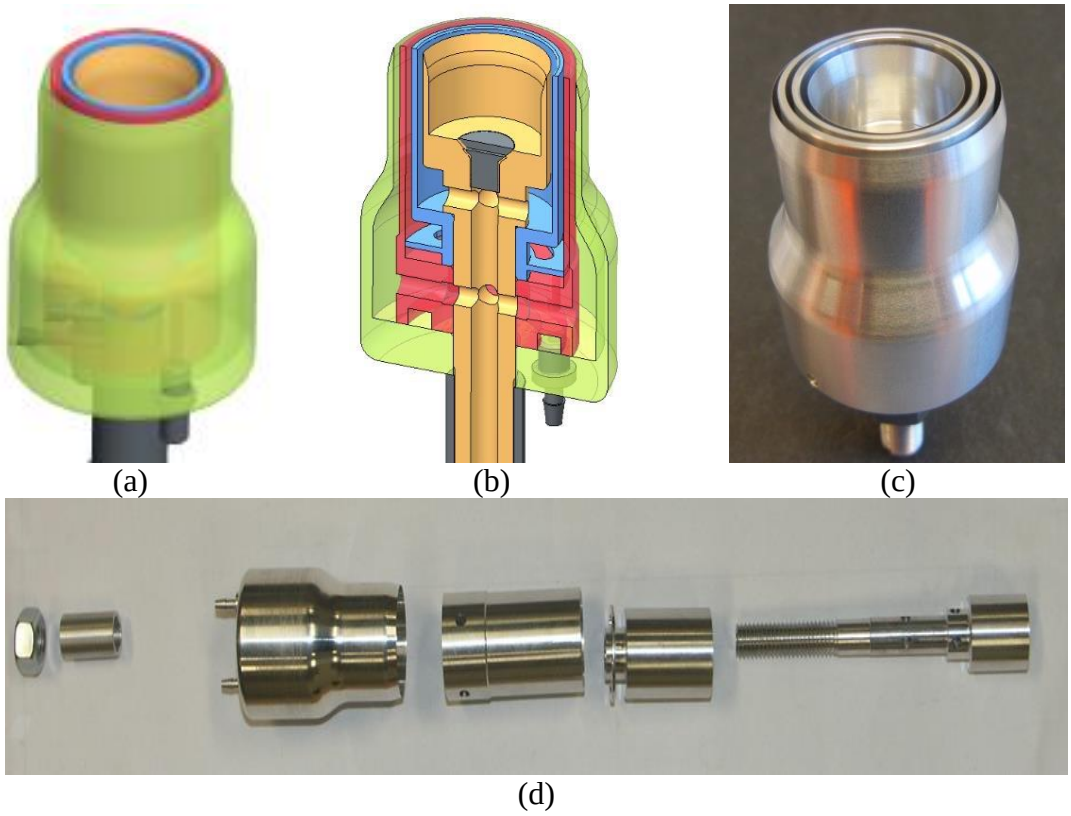

(a) (b) (c)

(d)

Figure 65 *(a) The model of cylindrical coaxial spinning electrode, (b) the model of cylindrical coaxial spinning electrode with show of the special system of feeding chambers to ensure the creation of the homogeneous polymeric two-layer, (c, d) The cylindrical coaxial spinning electrode of the second generation (Valtera, 2014).*

The experiments were carried out in Spinner 1 (Nanoprogres) with controlled atmospheric conditions; temperature was 23±2°C and relative humidity was 32±2 %. Spinning electrode was clamped in holder and connected to the tubes with core and shell polymer solutions of PVA. The special dosing tubes system for homogeneous creation of the polymeric two-layer is shown in Figure 66. The spinning electrode was connected to the HV source (Spellman Sl100) and positively charged. This one was located 130 - 200 mm below the negatively charged collector from stainless steel with thickness 2 mm and size 160 mm x 355 mm (width x depth). The Spunbond nonwoven was placed under the collector and unwounded with constant velocity 0,05 mm/s throughout electrospinning process. Polymer solutions were supplied into the chambers of spinning electrode using the syringe pumps (NEMESYS, Cetoni, GE.) and fed at a rate of 10 - 30 ml/h (core) and of 30 - 80 ml/h (shell).

Figure 66 *The cylindrical coaxial spinning electrode of the second generation with the special feeding system for creation of the homogeneous polymeric two-layer (Valtera, 2014)*

Coaxial electrospinning started with achieving the critical voltage Uc +28/-28 kV. It was found that the optimal voltage Uopt for start of electrospinning of PVA was +33/-30 kV and +30/-28 kV for optimal coaxial electrospinning process. The optimal distance *L* between electrodes was 130 mm for electrospinning of PVA. Electrospinning ran uniformly across the all surface of the spinning polymer solution. The optimal feed rate v_f was 60 ml/h for the shell solution and 25 ml/h for the core solution. This higher feed rate was equal to the high productivity of the cylindrical coaxial spinning electrode. It was founded that lower value HV was used to the optimal coaxial electrospinning in comparison with the original concept of the spinning electrode. The optimal parameters of the tested polymer solutions are listed in Table 13.

Figure 67 shows the formation of the Taylor cones on the polymeric two-layer and start of the coaxial electrospinning realized using cylindrical coaxial spinning electrode of the second generation. The images show homogeneous polymeric two-layer without its slumping and the large number of Taylor cones.

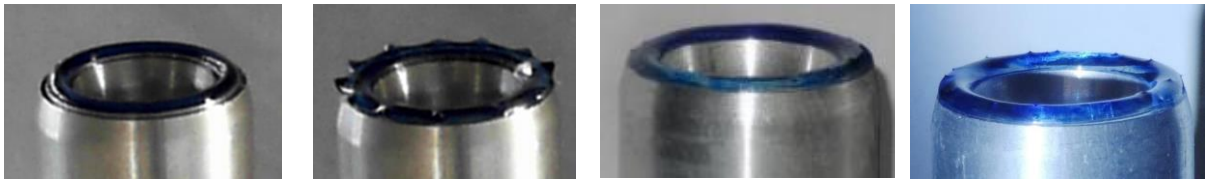

(a) (b) (c) (d)

Figure 67 *The formation of the Taylor cones on the polymeric two-layer and start of the coaxial electrospinning realized using cylindrical coaxial spinning electrode.*

Table 13 *Process parameters of tested polymer solutions using cylindrical coaxial spinning electrode of the 2nd generation (DC electrospinning)*

The shell solution	The core solution	L[(a)] [mm]	U_c[(b)] [kV]	U_{opt}[(c)] [kV]	v_s[(d)] [ml/hr]	v_c[(e)] [ml/hr]	f_r[(f)]
12% PVA	4% PVA + Prussian Blue	130	+28/-28	+30/-30	80	40	2:1
12% PVA	4% PVA	160	+28/-28	+30/-30	30	10	3:1
12% PVA	5% PVB + Prussian Blue	160	+30/-30	+37/-35	45	15	3:1
14% PCL	4% PCL	125	+20/-20	+24/-20	60	20	3:1
10% PCL	5% PVA	190	+30/-30	+33/-33	65	15	4:1
10% PVB	5% PVB	150	+28/-28	+33/-33	50	30	2:1
10% PVB	5% PVB	150	+28/-28	+33/-33	50	40	2:1
15% PUR	5% PVB	130	+30/-30	+33/-33	50	10	5:1

(a) L is the distance between electrodes
(b) U_c is the critical value of the voltage
(c) U_{opt} is the optimal value of the voltage
(d) v_s is the feed rate of the shell polymer solution
(e) v_c is the feed rate of the core polymer solution
(f) f_r is the feeding ratio

The electrospinning started with achieving of the critical value of the HV, see (Table 13). The large number of polymer jets on the entire surface of the polymeric two-layer was observed throughout coaxial electrospinning. The coaxial electrospinning process realized using this new spinning electrode of the second generation is shown in Figure 68.

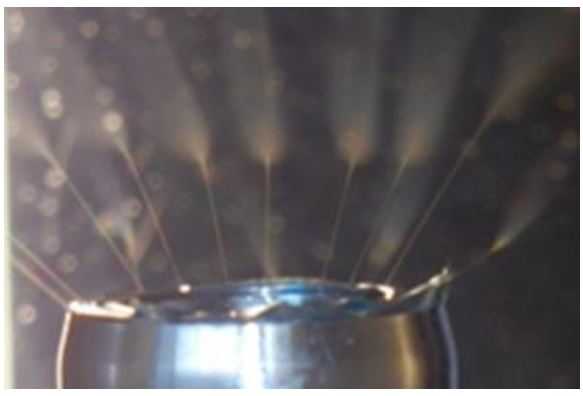

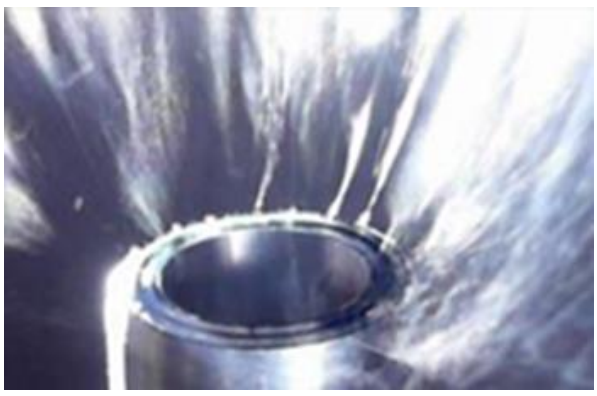

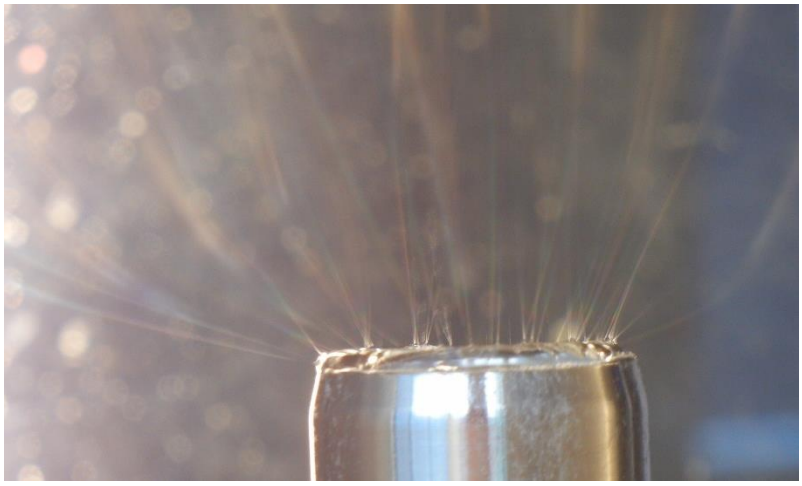

Figure 68 *Needleless coaxial electrospinning realized using cylindrical coaxial spinning electrode of the second generation.*

In the next step, AC technology was used for testing of this new needleless coaxial spinning electrode. PVB and PUR were used as tested polymer solutions. The spinning electrode was clamped in the spinning electrode holder and connected to the HV source and to the special dosing tubes system as is shown in Figure 69. Polymer solutions were supplied into the chambers of spinning electrode using the peristaltic pumps (New Era Pump Systems, Inc. NY) and fed at a rate of 30 - 130 ml/h (core) and of 50 - 320 ml/h (shell). There is much higher feed rate in case of AC electrospinning technology compared to the DC technology. The optimal parameters of the tested polymer solutions are listed in Table 14.

(a) (b)

Figure 69 *AC coaxial electrospinning realized using the cylindrical coaxial spinning electrode (Vysloužilová, 2014)*

Table 14 *Process parameters of tested polymer solutions using cylindrical coaxial spinning electrode of the second generation (AC electrospinning)*

The shell solution	The core solution	L [a] [mm]	U_c [b]	U_{opt} [c]	v_s [d] [ml/hr]	v_c [e] [ml/hr]	f_r [f]
10% PVB	5% PVB	150	60 %	70 %	300	120	2:1
10% PVB	5% PVB	150	70 %	90 %	300	120	2:1
15% PUR	5% PVB	130	maximal	-	300	120	2:1

[a] L is the distance between electrodes
[b] U_c is the critical value of the voltage
[c] U_{opt} is the optimal value of the voltage
[d] v_s is the feed rate of the shell polymer solution
[e] v_c is the feed rate of the core polymer solution
[f] f_r is the feeding ratio

It was founded that PVA electrospinning realized using AC is impossible. This polymer solution is not suitable for this technology. The cylindrical coaxial spinning electrode is not suitable for AC electrospinning of PUR as demonstrated experiments. PVB

seems to be ideal polymer solution for experiments with this new needleless coaxial spinning electrode realized using AC technology.

The cylindrical coaxial spinning electrode with a smooth, nearly constant surface curvature of its orifice allows running electrospinning without loss of energy caused by spark discharges from sharp edges. This new concept of the spinning electrode allows the minimal polymer waste consisting in elimination of polymer solution slumping. This electrode is suitable for DC and AC electrospinning due to modified orifice and smaller average. The productivity of this spinning electrode was investigated and compared to the other kinds of the coaxial spinning electrodes developed within this work, project SGS 21012 and cluster Nanoprogres. Table 15 shows parameters of coaxial electrospinning realized using different kinds of coaxial spinning electrodes with focus on number of polymer jets *n*, productivity *P* and diameter d of core-shell nanofibers.

Table 15 *Process parameters and productivity of the developed coaxial spinning-electrodes*

Coaxial spinning electrode	**L[(a)] [mm]**	**U_c[(b)] [kV]**	**U_{opt}[(c)] [kV]**	**v_c[(d)] [ml/h]**	**v_s[(e)] [ml/h]**	**n[(f)]**	**P[(g)] [g/h]**	**d[(h)] [nm]**
Needle spinner	130	36	40	2.5	4.8	1	0.64±0.03	330±60
Conductive pool spinner	130	34	36	-		6±3	0.82±0.99	290±62
Nonconductive pool spinner	130	30	34	-		10±5	0.9±0.96	280±50
Weir spinner (50 mm)	130	40	48	8	12	40±8	2.67±0.99	270±60
Weir spinner (100 mm)	140	66	60	15	35	50±10	3.45±0.83	270±52
Cylindrical spinner (95 mm)	190	56	66	6	25	50±10	2.18±0.66	280±97
Cleft electrode	150	60	65	3	9	20±8	2.67±0.99	270±60

[(a)] L is the distance between electrodes
[(b)] U_c is the critical value of the voltage
[(c)] U_{opt} is the optimal value of the voltage
[(d)] v_c is the feed rate of the core polymer solution
[(e)] v_s is the feed rate of the shell polymer solution
[(f)] n is the number of polymer jets
[(g)] P is the productivity of the spinning electrode
[(h)] d is the average value of fiber diameters

Core-shell nanofibers with incorporated liposomes

Cylindrical coaxial needleless spinning electrode was used for electrospinning of liposomes with encapsulated substances for their protection from the outside environment. These experiments were done within Andrea Míčková (2nd Faculty of Medicine, Charles University in Prague). Unilamellar liposomes were prepared from soybean-derived L-α-phosphatidylcholine or L-α-phosphatidylcholine from egg yolk (PC; Avanti Polar Lipids, Inc.) using the extrusion method (Mayer 1986, Mickova 2015). The dry lipid films were resuspending in 1ml of TBS.

PCL was dissolved in chloroform/ethanol (ratio 9:1) and the solution at concentration of 10 % (w/v) was prepared as the shell. PVA was dissolved in distilled water and the solution at concentration of 5 % (w/v) with FITC Dextran (25 mg/mL; 10,000 MW; purchased from Sigma Aldrich) or with liposomes containing encapsulated FITC Dextran (25 mg/mL) was prepared as the core.

The cylindrical coaxial spinning electrode was used for these experiments, see in (Figure 65). This was connected to a HV source (Glassman, series FC) and positively charged. The collector with thickness 2 mm and size 160 mm x 355 mm (width x depth) was located at the distance 190 mm above spinning electrode. Polymeric solutions were transferred into plastic syringes, empowered by a syringe pump and dosed at a rate of 6 ml/h (core solution) and of 45 ml/h (shell solution). Voltage +35/-33 kV was used. The electrospinning was carried out at ambient temperature 23 ± 0,4 °C and at a relative humidity 55 ± 0,5 %. The analysis of the produced core-shell nanofibrous layers with incorporated liposomes is described in detail in chapter 3.7.5.

3.6 Electrospinning of hyaluronic acid and carboxymethyl cellulose

Coaxial electrospinning is technology suitable for incorporation of the active agent and biopolymers into core-shell nanofibers. This one allows the creation of the special systems such as materials for drug delivery, cosmetic and food industry. Hyaluronic acid (HA) and carboxymethyl cellulose (CMC) were electrospun by coaxial electrospinning to achieve core-shell nanofibers for medical use. Initial experiments were done with CMC. This polymer was selected as a model material of hyaluronic acid, because this is easily available and cheaper than HA. Its chemical structure is similar to HA.

In the first step, blend of CMC (Kelco, USA) and PEO (Mw = 400.000, Sigma Aldrich, UK) was prepared as the core polymer solution for coaxial needle electrospinning. The CMC solution with concentration of 1 and 3 % (w/v) was prepared and mixed with the PEO solution with concentration of 3 % (w/v). The solution of PVA (Sloviol, Chemicke zavody Novaky, SK) with concentration of 12 % (w/v) was prepared as the shell material. Crosslinking agent glyoxal (3 % (w/v) of dry matter of PVA) and phosphoric acid (4 % (w/v) of dry matter of PVA) were added to the PVA solution. The distilled water was used as the solvent of all three solutions. In the next step, CMC itself was used as the core solution in order to maximize the concentration of CMC in the nanofibrous layer. CMC polymer solutions at concentration of 1 and 2 % (w/v) were prepared and used as core solutions.

The Spinner 1 (Nanoprogres) was used for the coaxial electrospinning of CMC/PVA. In the first step, blend of CMC/PEO was used as the core material. PEO was added to the CMC in order to better spinnability of this polymer solution and decrease of its viscosity. The needle coaxial spinning electrode was connected to a HV source (Spellman Sl100) and positively charged. The electrode was located 160 mm below the negatively charged collector from stainless steel with size 160 mm x 355 mm (width x depth). The Spunbond nonwoven was placed under the collector for nanofiber deposition. This nonwoven was unwound with constant velocity v throughout electrospinning process. The experiments were carried out in a chamber with controlled atmospheric conditions; temperature was 22±2 °C and RH was 33±3 %. Process parameters of the coaxial electrospinning of the blend of CMC in the core are listed in Table 16.

Based on the successful electrospinning of the blend of CMC/PEO as the core, the next experiments with the CMC solution at concentration of 1 and 2 % (w/v) in the core were done. Process parameters of the coaxial electrospinning of the CMC in the core are listed in Table 17.

The coaxial electrospinning run very well; the uniform nanofibrous layers were created. Following the successful model electrospinning of the CMC, the HA and its sodium salt were used as the core solutions of the core-shell nanofibers in the next experiments.

Table 16 *Process parameters of the coaxial electrospinning of the PVA (shell) with incorporated blend of CMC/PEO (core)*

Shell solution	**Core solution**	**U[(a)] [kV]**	**v_c[(b)] [ml/h]**	**v_s[(c)] [ml/h]**	**L_0[(d)] [mm]**	**v_z[(e)] [mm/s]**	**v_u[(f)] [mm/s]**	**L[(g)] [mm]**
12 % PVA	1% CMC/ 3%PEO	±22	1	3	±50	10	0,1	160
12 % PVA	1% CMC/ 3%PEO	±22	0,8	2	±50	10	0,1	160
12 % PVA	1% CMC/ 3%PEO	±22	0,5	1,8	±50	10	0,1	160
12 % PVA	3% CMC/ 3%PEO	±22	0,3	1	±100	10	0,1	160
12 % PVA	3% CMC/ 3%PEO	±22	0,6	1	±100	10	0,1	160
12 % PVA	3% CMC/ 3%PEO	±22	0,6	1	±100	15	0,1	160

[(a)] U is the voltage
[(b)] v_c is the feed rate of the core polymer solutions
[(c)] v_s is the feed rate of the shell polymer solutions
[(d)] L_0 is the limit of the spinning electrode from zero possition
[(e)] v_z is the feed rate of the spinning electrode in z-axis
[(f)] v_u is the speed of unwinding of Spunbond nonwoven
[(g)] L is the distance between electrodes

Table 17 *Process parameters of the coaxial electrospinning of the PVA (shell) with incorporated CMC (core)*

Shell solution	**Core solution**	**U[(a)] [kV]**	**v_c[(b)] [ml/h]**	**v_s[(c)] [ml/h]**	**L_0[(d)] [mm]**	**v_z[(e)] [mm/s]**	**v_u[(f)] [mm/s]**	**L[(g)] [mm]**
12 % PVA	1% CMC	±22	0,5	1,8	±50	10	0,1	160
12 % PVA	1% CMC	±22	0,4	1,3	±50	10	0,1	160
12 % PVA	2% CMC	±22	0,5	2	±50	10	0,1	160
12 % PVA	2% CMC	±22	0,3	1,2	±50	10	0,1	160

[(a)] U is the voltage
[(b)] v_c is the feed rate of the core polymer solutions
[(c)] v_s is the feed rate of the shell polymer solutions
[(d)] L_0 is the limit of the spinning electrode from zero possition
[(e)] v_z is the feed rate of the spinning electrode in z-axis
[(f)] v_u is the speed of unwinding of Spunbond nonwoven
[(g)] L is the distance between electrodes

Sodium hyaluronate ‘Hyalgan’ was obtained from Fidia Farmaceutici (Italy) as the solution with natrii hyaluronas at concentration of 1 and 2 % (w/v). This solution was used as the core material. In the first step, blends of the Hyalgan and 3 % (w/v) PEO in ratio 1:1 and 2:1 were prepared. In the next step, Hyalgan itself was used as the core solution. The PVA at concentration of 12 % (w/v) dissolved in the distilled water and PCL (Mn = 45.000, Sigma Aldrich, UK) at concentration of 14 and 16 % (w/v) dissolved in chloroform/ethanol (9:1) were used as the shell solutions.

The needle coaxial spinning electrode placed in air conditioning chamber was used for initial experiments. This electrode was connected to the HV source (SI100, Spellman) and positively charged. The electrode was located 110-150 mm below the grounded disc collector with average 180mm. The applied HV ranged between 20 - 25 kV. Polymer solutions were supplied into 10 ml plastic syringes with a syringe pump (KDS-100-CE, KD Scientific Inc.) and fed at a constant rate of 0.2ml/h (core) and of 0.6ml/h (shell).The electrospinning was done at ambient temperature 20°C and at a relative humidity 50 %. Core-shell nanofibers were collected on the Spunbond fabric located under the collector (Vysloužilová, 2011).

In the next step, the coaxial electrospinning was realized in the Spinner 1 (Nanoprogres) using POM coaxial needle spinning electrode. Initial experiments were done with PVA as the shell material. Based on the experiments with CMC were used the same parameters for coaxial electrospinning of Hyalgan. These parameters were modified to obtain of the optimal homogeneous nanofibrous layer with maximal concentration of Hyalgan. In the next step, PCL was used as the shell solution. The experiments were carried out in the chamber with controlled atmospheric conditions; temperature was 21±1 °C and RH was 35±4 % for electrospinning of PVA, 35 – 52 % for electrospinning of PCL. It was founded, higher RH was better was electrospinning of PCL. Process parameters of the coaxial electrospinning of the Hyalgan in the core are listed in Tables 18 - 20.

Table 18 *Process parameters of the coaxial electrospinning of 12 %(w/v) PVA (shell) with incorporated 1 % (w/v) Hyalgan (core)*

Experiment	**U[(a)] [kV]**	**v_c[(b)] [ml/h]**	**v_s[(c)] [ml/h]**	**L_0[(d)] [mm]**	**v_z[(e)] [mm/s]**	**v_u[(f)] [mm/s]**	**L[(g)] [mm]**
1	(+)22/(-) 22	0,3	1,3	±50	10	0,1	160
2	(+)23/(-) 23	0,3	1,3	±50	10	0,1	160
3	(+)22/(-) 18	1,3	3	±70	20	0,1	140
4	(+)22/(-) 21	1	2,3	±70	20	0,1	120
5	(+)21/(-) 21	0,8	2,3	±70	20	0,1	130
6	(+)21/(-) 21	0,8	2,3	±70	20	0,1	130

[(a)] U is the voltage
[(b)] v_c is the feed rate of the core polymer solutions
[(c)] v_s is the feed rate of the shell polymer solutions
[(d)] L_0 is the limit of the spinning electrode from zero possition
[(e)] v_z is the feed rate of the spinning electrode in z-axis
[(f)] v_u is the speed of unwinding of Spunbond nonwoven
[(g)] L is the distance between electrodes

Table 19 *Process parameters of the coaxial electrospinning of 14 % (w/v) PCL (shell) with incorporated 1 % (w/v) Hyalgan (core)*

Experiment	**U[(a)] [kV]**	**v_c[(b)] [ml/h]**	**v_s[(c)] [ml/h]**	**L_0[(d)] [mm]**	**v_z[(e)] [mm/s]**	**v_u[(f)] [mm/s]**	**L[(g)] [mm]**
1	(+)21/(-)21	2,3	10	±70	20	0,1	160
2	(+)21/(-)21	2,5	10	±70	20	0,1	170
3	(+)20/(-)20	3,3	10,1	±70	30	0,1	170
4	(+)20/(-)18	3,3	10,3	±70	30	0,1	180
5	(+)18/(-)18	3	11	±70	30	0,1	190
6	(+)18/(-)18	2,3	11	±70	30	0,1	190

[(a)] U is the voltage
[(b)] v_c is the feed rate of the core polymer solutions
[(c)] v_s is the feed rate of the shell polymer solutions
[(d)] L_0 is the limit of the spinning electrode from zero possition
[(e)] v_z is the feed rate of the spinning electrode in z-axis
[(f)] v_u is the speed of unwinding of Spunbond nonwoven
[(g)] L is the distance between electrodes

Table 20 *Process parameters of the coaxial electrospinning of 16 % (w/v) PCL (shell) with incorporated 1 % (w/v) Hyalgan (core)*

Experiment	**U[(a)] [kV]**	**v_c[(b)] [ml/h]**	**v_s[(c)] [ml/h]**	**L_0[(d)] [mm]**	**v_z[(e)] [mm/s]**	**v_u[(f)] [mm/s]**	**L[(g)] [mm]**
1	(+)18/(-)18	2,3	11	±70	30	0,1	190
2	(+)18/(-)18	3,3	13	±70	30	0,1	190
3	(+)18/(-)18	3	14,6	±70	30	0,1	190
4	(+)18/(-)18	2,3	15	±70	30	0,1	190
5	(+)18/(-)18	2,3	15,3	±70	30	0,1	190

[(a)] U is the voltage
[(b)] v_c is the feed rate of the core polymer solutions
[(c)] v_s is the feed rate of the shell polymer solutions
[(d)] L_0 is the limit of the spinning electrode from zero possition
[(e)] v_z is the feed rate of the spinning electrode in z-axis
[(f)] v_u is the speed of unwinding of Spunbond nonwoven
[(g)] L is the distance between electrodes

In the next step, the sodium hyaluronate in the powder form extracted from a rooster combs (Sigma Aldrich, UK) and technical HA (500 – 750 kDa, Contipro, CZ) were used for next experiments. These materials were selected to obtain of coaxial nanofibrous systems with the maximal concentration of HA. The solutions of HA (Sigma Aldrich, UK) at concentration of 2 and 3 % (w/v) and the solutions of HA (Contipro, CZ) at concentration of 1 % (w/v) were prepared dissolved in distilled water as used as core solutions. The solution of PCL at concentration of 14 % (w/v) was prepared by dissolving in chloroform/ethanol (9:1) and used as the shell.

Coaxial electrospinning was realized in the Spinner 1 (Nanoprogres) using POM coaxial needle spinning electrode. The process of electrospinning was optimized to obtain the homogeneous nanofibrous layer with the maximal concentration of the incorporated HA in core-shell nanofibers. The experiments were carried out in a chamber with controlled atmospheric conditions; temperature was 22 ± 1 °C and RH was 31 ± 1 %. There were problem with coaxial electrospinning of HA at concentration of 3 % (w/v). The viscosity of this core solution was higher than viscosity of the shell solution and the shell jet cannot pulls up the core solution. The optimal process parameters were founded during experiments. The ideal feed rate for the creation of the optimal bi-component droplet and continuously coaxial electrospinning was 0,5 ml/h (core) and 5,7 ml/h (shell). The distance between electrodes was 140 mm and the optimal HV was + 15 kV (spinning electrode) and – 8 kV (collector). The

Spunbond nonwoven was placed under the collector. This nonwoven was unwound with constant velocity 0,1 mm/s throughout electrospinning process. The velocity of the spinning electrode in z-axis was 10 mm/s and limit from the zero position was ±70 mm. Homogeneous nanofibrous layers of core-shell nanofibers with incorporated HA were obtained. It was founded, coaxial electrospinning of HA is possible.

The morphology of produced nanofibrous layers was observed using scanning electron microscopy (SEM, Tescan, CZ). The SEM images from this analysis are shown in Figure 70. Images show produced nanofibrous structures by coaxial needle electrospinning. There are some ball defects between nanofibers, in case of PCL/HA, see in Figure 70 b, c. These ball defects tend to be observed in case of PCL. They are problems of the PCL polymer solution itself consisting of system chloroform and ethanol. These defects not cause problems with biocompatibility of this nanofibrous layer.

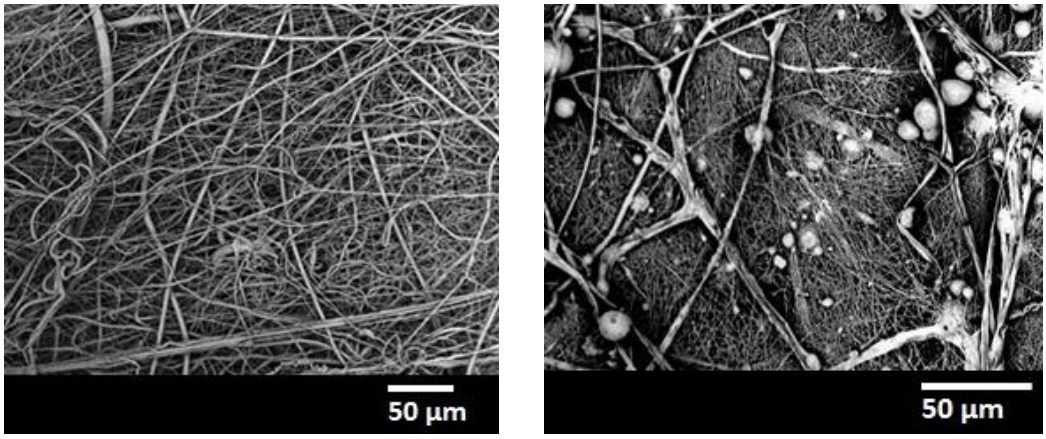

(a) (b)

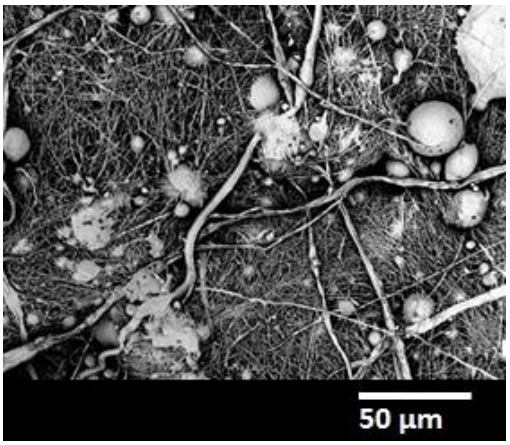

(c)

Figure 70 *SEM image of coaxial nanofibers with incorporated HA: (a) PVA/HA nanofibers (b) 14 % (w/v) PCL/HA, (c) 16 % (w/v) PCL/HA.*

It was verified, electrospinning of HA is possible using coaxial electrospinning. HA was used as the core part of the core-shell nanofibers and nanofibrous layers were produced. These layers are suitable for example for use in medicine, cosmetic or food industry.

3.7 Visualization of coaxial electrospinning process

Detailed examination of the electrospinning process from the primary instabilities on the surface of the polymer solution to the production of nanofibers is necessary to understand the behavior of electrospinning polymer solutions in the electric field. This chapter deals with visualization of the coaxial electrospinning process and identification of its critical conditions. The formation and position of the Taylor cones, the investigation of the critical value of the characteristic wavelength λ and the polymeric jets are main objectives of this chapter. An occurrence of corona discharges generated by the highly charged polymeric jets roots was also examined within this work using the Corona Camera (Vyslouzilova, 2015).

The choice of appropriate setting of the electrospinning process and optimal parameters with their control throughout electrospinning process is necessary to production of quality uniform nanofibrous layers required properties. The maximum electric charge density should be concentrated on the surface of the electrospun polymer solution, while its distribution should be homogeneous. Uneven distribution of polymeric jets and uncontrolled deposition of nanofibers on the collector is a consequence of the inhomogeneous distribution of electric charge. A density of the polymeric jets (the distance between the neighbouring polymeric jets) on the surface of the polymer layer is an important aspect of electrospinning process. This density corresponds to the characteristic wavelength λ. The detail investigation of wavelength λ focusing on its critically value λc, plays key role for determination of the electric field strength Ec. This is value when the electrospinning process is initiated, first Taylor cones are observed and nanofibers begin to be formed (Lukas, 2008; Vyslouzilova, 2015).

A web camera Microsoft LifeCam Studio with a 1080p sensor and the camera Nikon Coolpix S8100 (Nikon, Jap.) were used for general view over the electrospinning process, observation of the polymer droplet/layer creation at the spinning electrode orifice and state of electrospinning. The electrospinning realized using needle coaxial spinning electrode, the weir spinner and the cleft electrode is shown in Figure 71. The figure 72 shows the formation

of polymeric two-layer at the orifice of the cylindrical coaxial spinning electrode of the second generation and DC and AC electrospinning realized by this one.

(a) (b) (c)

Figure 71 *The electrospinning recorded by the web camera and the camera Nikon Coolpix S8100: (a) the needle coaxial electrospinning, (b) the needleless electrospinning realized using the weir spinner and (c) the cleft electrode with the polymer solution slumping (Vysloužilová, 2015).*

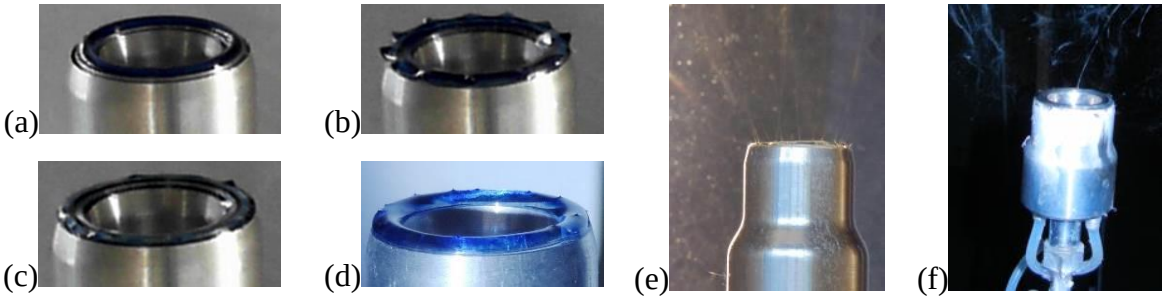

(a) (b) (c) (d) (e) (f)

Figure 72 *The record of needleless electrospinning realized by cylindrical coaxial spinning electrode: (a) the core polymer layer formation, (b) the emerging instability on the polymer layer before reaching value of Ec, (c) Taylor cones, (d, e) DC electrospinning, (f) AC electrospinning (Vysloužilová, 2015).*

The formation of bi-component Taylor cone during needle coaxial electrospinning was observed by optical microscope within Clemson University, NC, USA. Process was recorded by a camera (Dalsa - Falcon-14M100, Stemmer). The emerging instability on the surface polymeric droplet was observed after switch of HV source. The Taylor cone originated from the mechanism of the "fastest forming instability," i.e., of the fastest growing capillary wave as is shown in Figure 73. Taylor cone created from the shell polymer solution (the transparent part of the bi-component droplet in Figure 73) pulled up the core solution (the dark part of the bi-component droplet in Figure 73) and both materials were drawn and elongated together by electric forces to produced core-shell nanofibers (Vysloužilová, 2015).

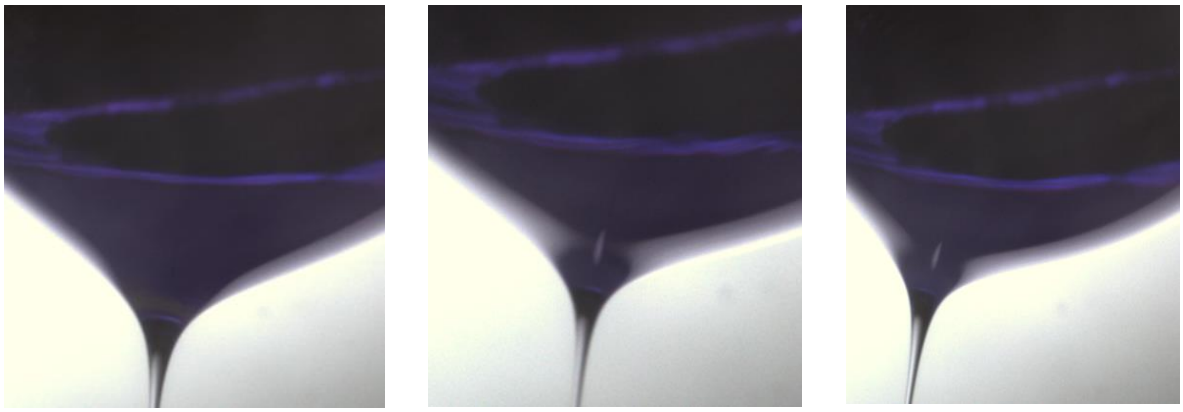

Figure 73 *The bi-component polymeric droplet during coaxial electrospinning process recorded by the camera Dalsa - Falcon-14M100, Stemmer (Clemson, NC, USA): The shell Taylor cone (the light transparent part of the bi-component droplet) pulls up the core solution (the dark part of the bi-component droplet), (Vyslouzilova, 2015).*

In the next step, non-coaxial electrospinning process was investigated as is shown in Figure 74. Different images of coaxial and non-coaxial electrospinning process show difference between coaxial and standard variant of electrospinning.

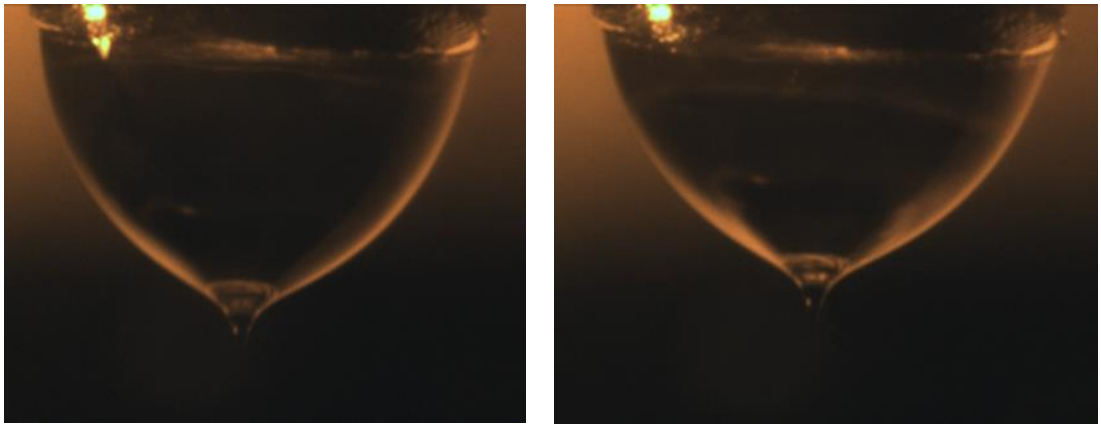

Figure 74 *Non-coaxial electrospinning process without the core solution recorded by the camera Dalsa - Falcon-14M100, Stemmer (Clemson, NC, USA): The different displaying of coaxial and non-coaxial polymer droplet is caused by different light during experiments. This was necessary to clear observed of the core solution inside the shell one in case of coaxial variant of electrospinning (Vysloužilová, 2015).*

The formation of the polymer bi-component droplet at the orifice of the needle coaxial spinning electrode and the layer/two-layer, respectively in case of needleless coaxial electrospinning and their uniformity were investigated in the next step. The HD camera Panasonic HC-W850 with 120 fps (Panasonic, UK) and the high speed camera iSPEED 3 with up to 150 000 fps (Olympus, USA) were used for these observing. The emerging

instabilities, the formation of Taylor cones and polymeric jets as well as their shape, number, stability, density (characteristic wavelength λ) and their behavior throughout electrospinning process were investigated. The detail of the polymeric jets observed during needle and needleless coaxial electrospinning is shown in Figure 75. The detail of bi-component roots of polymeric jets composed of the shell polymer solution pulls up the core one are shown in Figure 75 a, d. Polymer jets in alignment were observed in case of the cleft spinning electrode (Figure 75b).

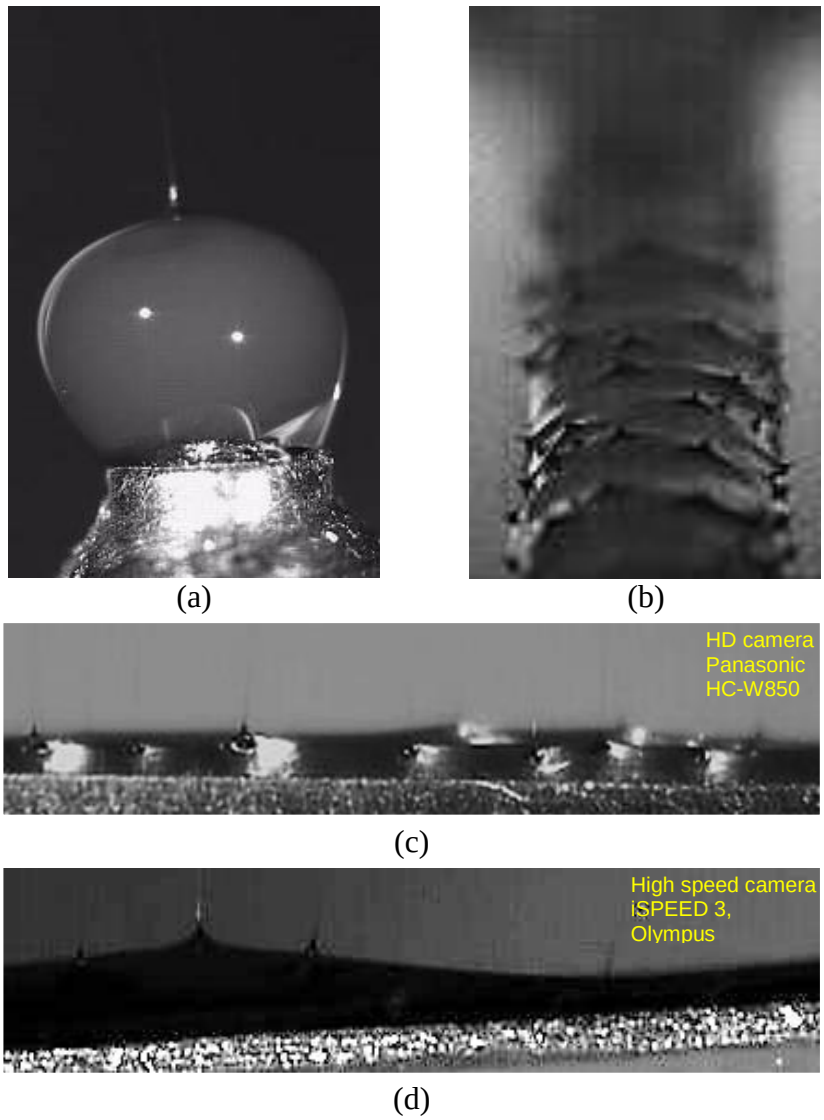

Figure 75 *The detail of polymer jets during electrospinning realized by (a) the coaxial needle spinning electrode, (b) the cleft electrode, (c, d) the weir spinner of the 2nd generation (Valtera 2014)*

The UV Corona camera CoroCam 1 (Uvirco Technologies, SA) was used for investigation of the distribution of the Taylor cones and polymeric jets (characteristic

wavelength λ) as well as for observation of corona discharges occurrence as can be seen in Figure 55 (Chapter 3.5.5) (Vysloužilová, 2015). Characteristic wavelength λ and its critical value could be identified and behavior of polymeric jets throughout electrospinning process could be observed as is shown in Figure 76. This method can also detected an unsuitably chosen dosage of polymer solutions (low speed), resulting in uncovering the surface of the spinning electrode and the emergence of spark discharges.

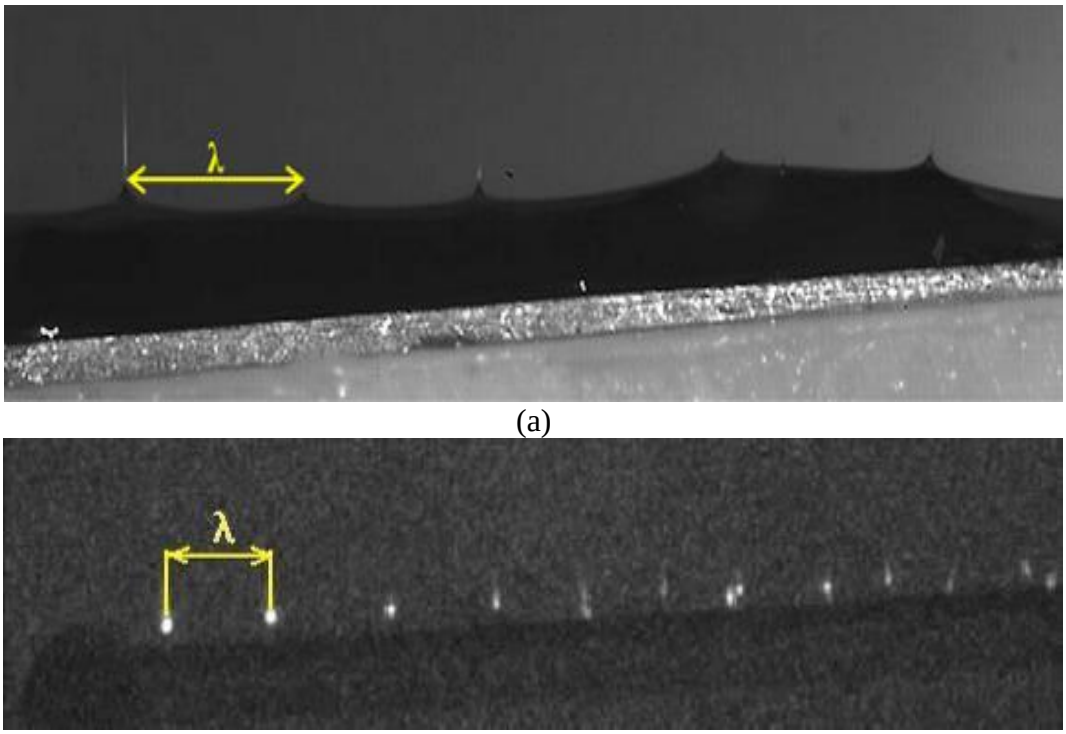

(a)

(b)

Figure 76 *The characteristic wavelength λ in case of needleless electrospinning recorded by (a) the high speed camera and (b) the UV camera (Vyslouzilova, 2015)*

These visualization methods can be used for the assessment of individual needle and needleless electrospinning processes. The formation of the optimal polymeric droplet/layer respectively can be observed and the feed rate of polymer solutions can be changed based on the obtained knowledge from these experiments. The productivity of spinning electrodes by means of the number of Taylor cones/polymer jets respectively can be investigation. In order to prevent undesirable corona discharges on the spinning electrodes, it is beneficial to observe the electrospinning using the UV camera and set appropriate process parameters to obtain the maximal productivity of spinning electrodes and homogeneous quality of nanofibrous layer.

3.8 Analysis of core-shell structure

Polymer nanofibers are very fine fibers and an analysis of the core-shell structure is not easy. The cut of micro fibrous layer and the observation of a cross-section on using microscope is a relatively simple matter for the cross-section analysis. This method does not easily apply in case of polymer nanofibers. These very fine fibers tend to pull inwards the structure and this is hard to find the cross-section of nanofibers, see in (Figure 77).

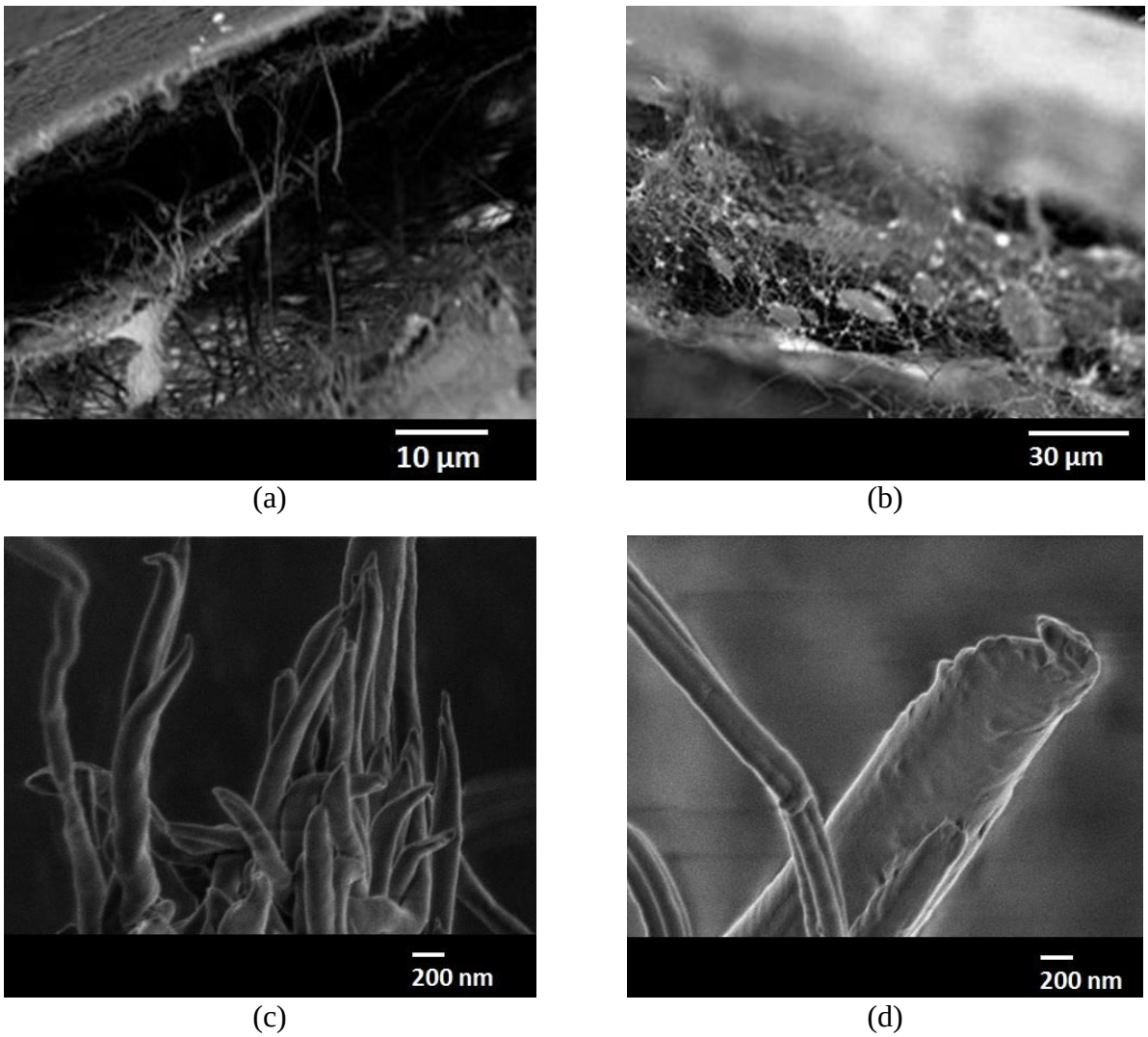

(a) (b)

(c) (d)

Figure 77 *The cross-sections of the core-shell nanofibers observed using SEM (FEI Phenom) with SE detector (a, b) (Vysloužilová 2013a) and with BSE detector (Zeiss) by Pavel Kejzlar, KMI, TUL (c, d).*

Transmission electron microscopy (TEM), confocal laser scanning microscopy or cutting by an ion beam are commonly used methods to analysis of core-shell structure. The problem is these methods are difficult, expensive and not readily available. Only some

centers and universities are equipped with these special equipment. Difficult availability of these methods causes longer time to obtain of results and evaluation of experiments. Different methods of cutting of produced nanofibrous layers, analyzes realized using SEM, TEM, optical and fluorescent microscopy, Fourier transform infrared spectroscopy (FTIR), Raman spectroscopy and method of phase contrast were used for proof of core-shell structure in this work.

3.8.1 Cutting of nanofibers

There are several methods to obtain a cross-section of nanofibrous layer. The simplest one is a mechanical cutting realized by sharp knife, razor or scissors, see in (Figure 78 and 79). The condition of very sharp tool is essential. Otherwise, the deformation of fibers occurs and nanofiber cross-section cannot be observed. A fracture of nanofibers in liquid nitrogen is the next possibility to obtain the cross-section of nanofibers. The problem is in too cold ambience and also in case of water-soluble polymeric solutions as core or shell part of the core-shell nanofibers. Nanofibers are often deformed and analyze cannot be made. The ion beam is next possibility to obtain cutting nanofibers, see (Figure 80). The problem is in the unavailability of this method (just few institutions have this equipment and know how to make the cut of the nanofibers) and in too high price for this analyze. The ion beam cutting is not suitable method for each material. Destruction of nanofibers can be caused.

Different mechanism of cutting the nanofibrous structures made within this work are shown in Figure 78. There is seen that achievement of the clear cross-sections these very fine structures is not easy. Obtain the proof of core-shell structure realized by this method is very complicated.

In the next step, the core-shell nanofibrous yarn with incorporated Prussian blue in the core was produced, see (Chapter 3.4) to obtain more compact structure for easier cutting and SEM analysis. The result of this experiment is shown in Figure 79.

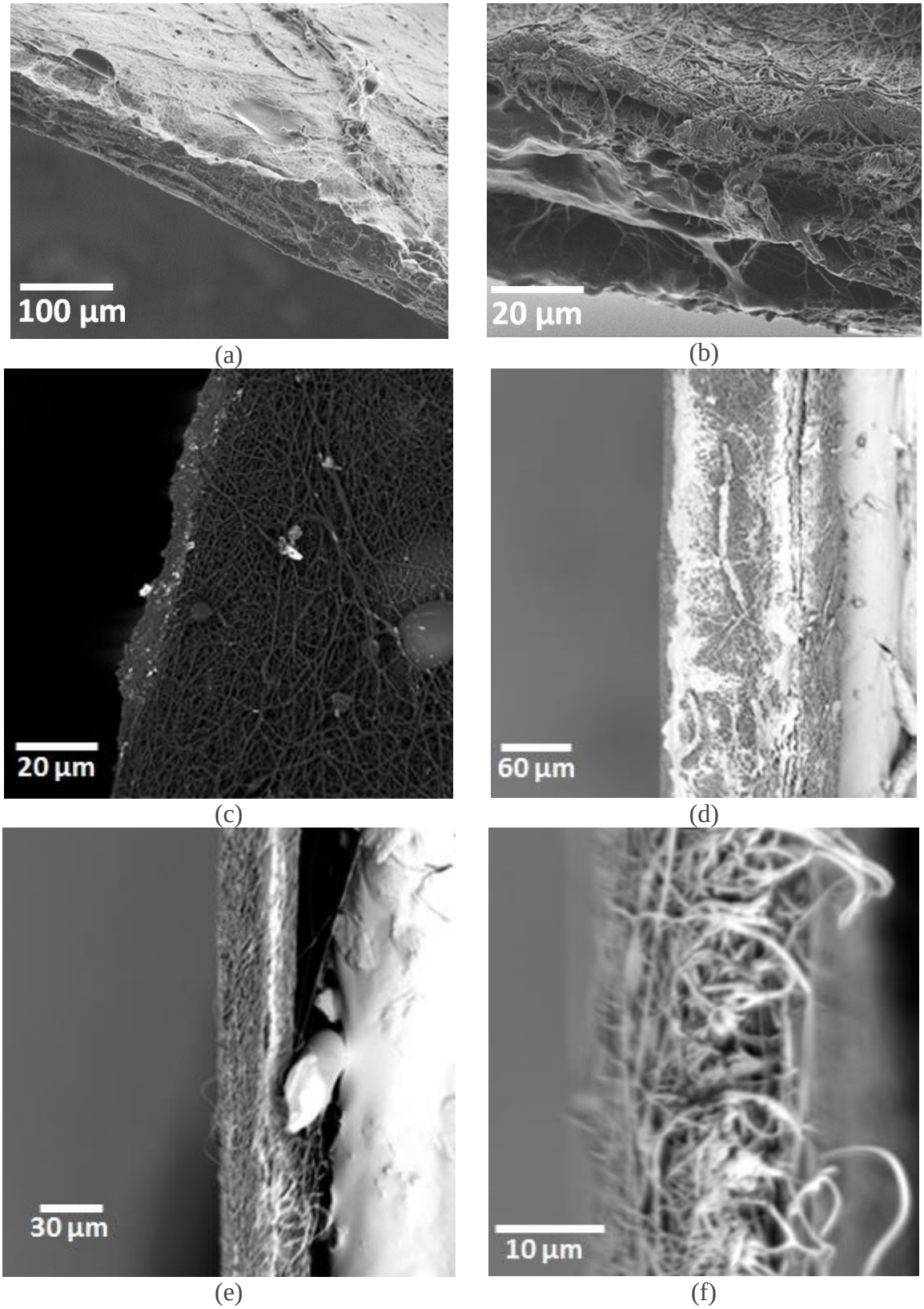

Figure 78 *The mechanical cross-section of nanofibrous layer observed by (a,b) SEM Zeiss, Germany and (c - f) SEM Phenom (G2, FEI).*

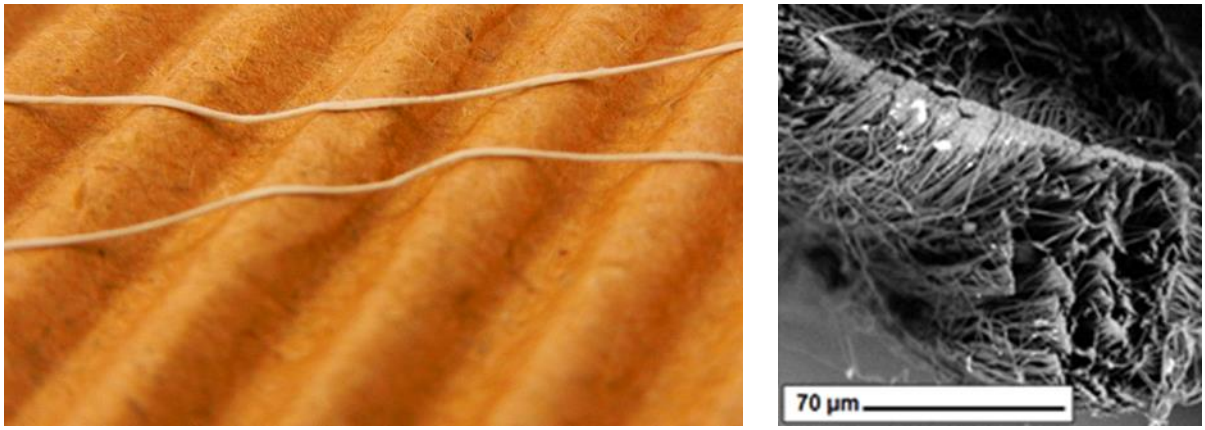

(a) (b)

Figure 79 *Nanofibrous yarn produced using rotation collector Sioux: (a) produced nanofibrous yarns, (b) the mechanical cross-section of nanofibrous yarn observed SEM Phenom (G2, FEI).*

The method of ion beam cutting, see in (Figure 80) and cryogenic mill using CryoMill (Retsch, Germany), see in (Figure 81) were used for analysis of CMC incorporated in core-part nanofibers as their core part. These methods allow observation of core-shell nanofibers. However, finding of the cross-section of nanofiber with clear core-shell structure in case of cryogenic mill is not easy, because there are many cross-sections with deformed structure, as can be seen in Figure 81.

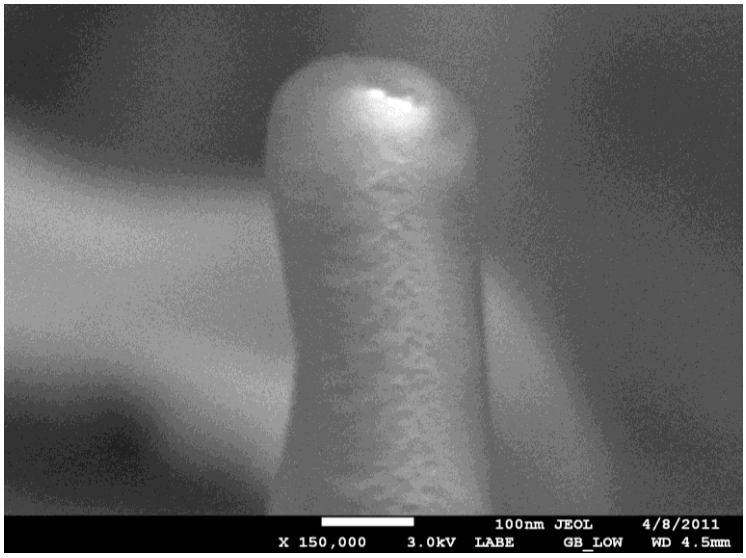

Figure 80 *The ion beam cut of core-shell nanofiber PCL (shell) - CMC/PEO (core) observed by Jeol (Germany). The core part has white color and the shell one has grey color.*

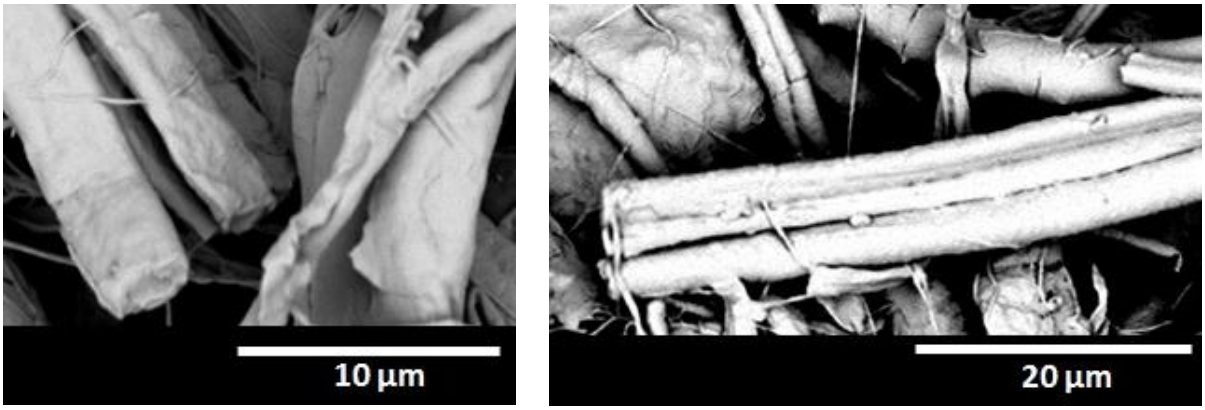

Figure 81 *Core-shell nanofibers PVA (shell) - CMC/PEO (core) analyzed by cryogenic mill by Retsch (Germany) and observed by SEM Phenom (FEI).*

3.8.2 Analysis by optical microscopy

Optical microscopy was used for analysis of incorporated vegetable oil into core-shell nanofibers as their core part realized using needleless pool spinning electrode. Optical microscopy uses visible light and a system of lenses to magnify images of the observed samples. This microscopy is suitable for analyzing of the micron and sub-micron samples. Due to the use of the visible light (wavelength λ = 360 - 750 nm), the observation of the nanofibers with fiber diameter below this value is impossible. There were produced sub-micron fibers with the average diameter of nanofibers 680 ± 50 nm and a magnification was 1000 x. This is reason, why the core-shell nanofibers with incorporated vegetable oil could be observed by the optical microscope as is shown in Figure 82.

The analysis was composed of two parts. First, the core-shell nanofibers were observed by the optical microscope. In the second part, this nanofibrous layer was placed at an angle of 45° under the optical microscope and this was left in this position for 48 hours. This experiment led to the verification of the incorporation of the vegetable oil into core-shell nanofibers and excluded its location on the surface of the nanofibers. In the last case, the beads with incorporated vegetable oil would slump down from nanofibers and the oil foil would be created. The result of this experiment is shown in Figure 82.

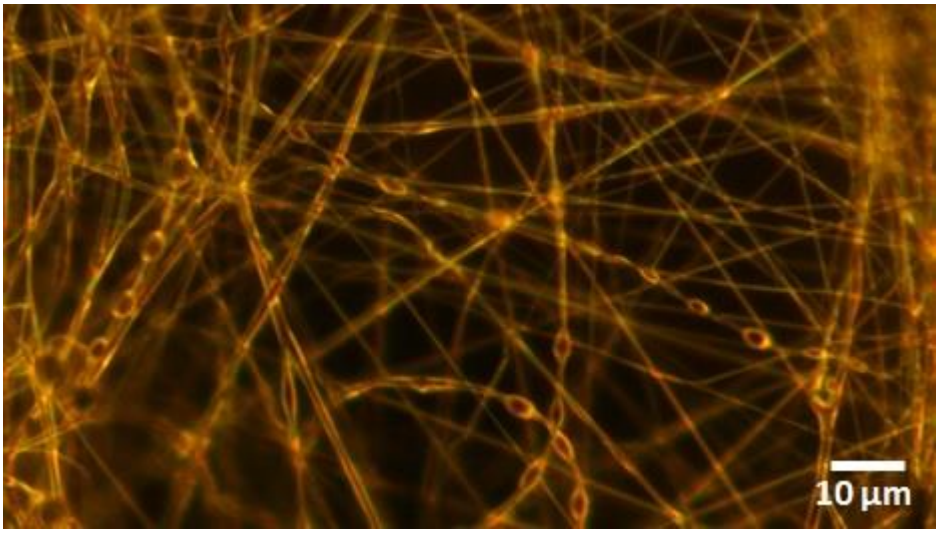

Figure 82 *Core-shell nanofibers with incorporated vegetable oil observed by optical microscopy after 48 hours.*

Beads with incorporated vegetable oil were on the same location without moving/slumping throughout time of experiment. This leads to the conclusion that oil was incorporated into the core and fixed by the shell and core-shell nanofibers were produced.

3.8.3 Analysis using Transmission electron microscopy

Transmission electron microscopy (TEM) is an analytical method allowing visualization and analysis of samples in area of "microworld" and "nanoworld". Transmission electron microscope is a type of electron microscope that based on passing of electrons through an ultra-fine sample. This technology uses a focused beam of electrons at 100 – 400 kV accelerating voltage illuminating an area of an electron transparent sample. This means thickness of sample of the order of 5 – 100 nm for 100 keV electrons. This dimension depends on the density and elemental composition of the sample and the resolution desired (Reimer, 2008), (AMMRF, 2013).

Transmission electron microscope composed of an electron gun, an anode, a system of condenser lenses, a specimen, system of objective lenses and a viewing screen. The electron beam produced by an electron gun (a cathode) and it passes through the anode. Tungsten, Lanthanum Hexaboride (LaB6) or Cerium Hexaboride (CeB6), they are commonly used cathodes. The electron beam focused by electromagnetic lenses and it's transmitted through the specimen that is in part transparent to electrons and in part scatters them out of beam. The image is magnified and focused by system of objective lenses. This system

composed of the objective lens, an intermediate lens and a projector lens. The objective lens is the highest performing lens of microscope and this is called "the heart of microscope". The Image is displayed on the viewing screen as a fluorescent screen, on a layer of photographic film or to be detected by a sensor.

Core-shell nanofibers of PVA (shell) and PVA with Prussian blue (core) were prepared for TEM analysis. Samples were observed by TEM Hitachi H7650 in The Electron Microscopy Center at the University of South Carolina, USA. Images show that nanofibers were produced by coaxial electrospinning technology, but fuzzy boundaries of nanofibrous "edges" are there. There are shown core-shell nanofibers of PVA (shell) and PVDF with incorporated magnetic nanoparticles (core), in Figure 83 d-f. Figures shown lines of core and shell part of nanofibers, but these nanofibrous "edges" are not focused.

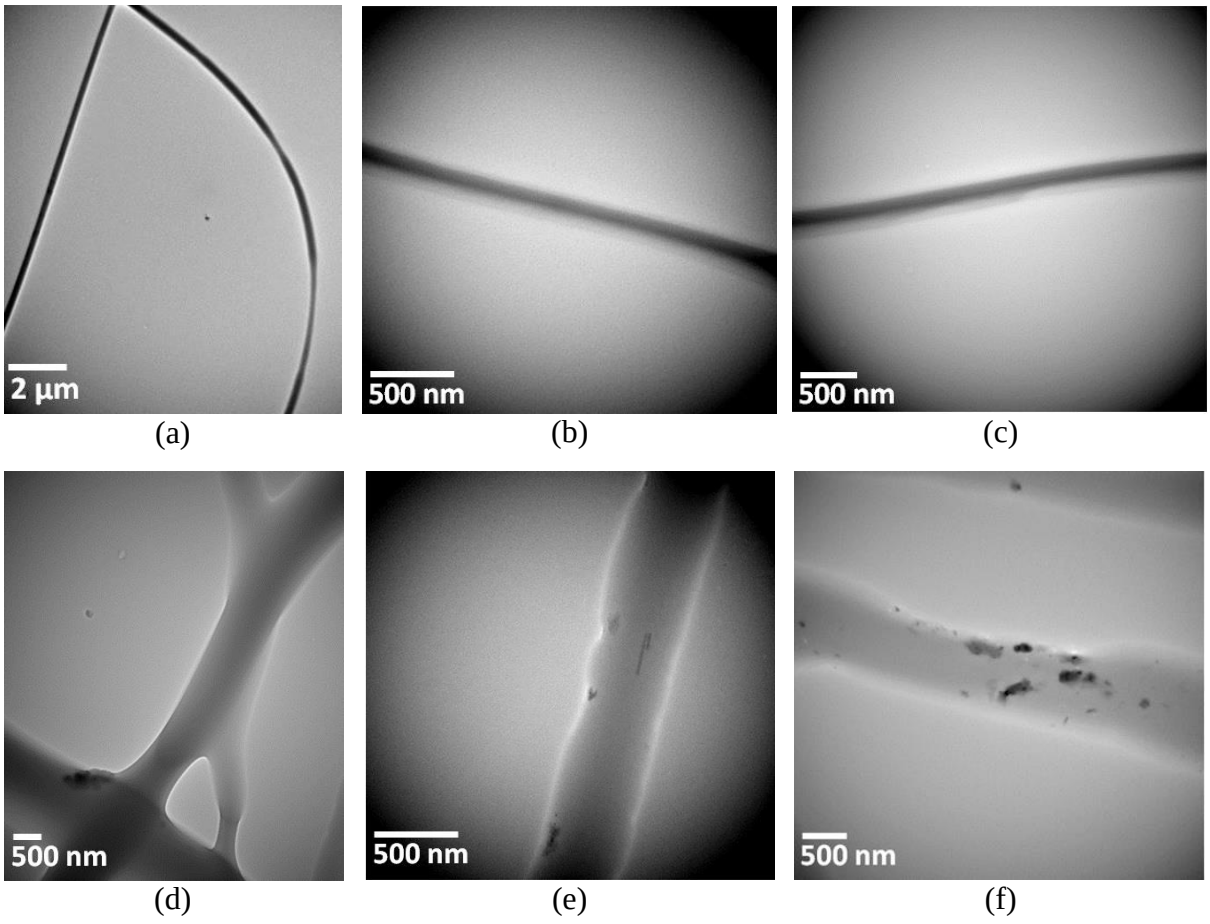

Figure 83 *TEM images of PVA/PVA core-shell nanofibers with incorporated Prussian blue (a – c) and PVA/PVDF core-shell nanofibers with incorporated magnetic nanoparticles (d – f).*

Images show magnetic nanoparticles in core-shell nanofibers and lines of core part in core-shell nanofibers, but the proof of core-shell structure is insufficient in this case, because this is not unambiguous. The problem of the analysis by transmission electron microscope is a difficult focusing of line between the core and the shell part of the transparent sample. It can be observed seeming core-shell structure in case of non-coaxial nanofibers.

A pitfall of TEM analyses of core-shell nanofibers is a difficult choice of the suitable investigated materials and demanding preparation of suitable specimens. Water-soluble polymeric materials are difficult to analysis for that reason the impossibility of observing the sharp boundary between core and shell material as can be seen in Figure 83 a-c.

3.8.4 Fourier transform infrared spectroscopy

Fourier transform infrared (FRIR) spectroscopy is the method to obtain an infrared spectrum of absorption or emission of substances. Infrared radiation is passed through the sample. Some of this radiation is absorbed by the sample and some of this is passed through the sample.

PVA solution at concentration of 12 % (w/v) was used as the shell. Disinfection was prepared as the core. Disinfection is the liquid that is un-spinnable using electrospinning process. Therefore this one was selected as the core. The needle coaxial spinning electrode was used for this experiment. This electrode was connected to the HV source (Spellman Sl100) and positively charged (23 kV). The collector located at the distance 130 mm above spinning electrode was connected to the HV source (Spellman Sl100) and negatively charged (20 kV). Polymer solutions were transferred into a 20 ml plastic syringe, empowered by a syringe pump (neMESYS, Cetoni) and dosed at a constant rate of 1,2 ml/h (core) and of 3,3 ml/h (shell). The electrospinning was carried out at ambient temperature 22±1°C and at a relative humidity 40±2%. Core-shell nanofibers were collected on the Spunbond nonwoven, located under the collector.

FT-IR analysis was used for characterization of core-shell structure of produced nanofibers. PVA powder, disinfection and core-shell nanofibers with incorporated disinfection in the core were analyzed. Results from this analysis are shown in Figure 84. Blue line indicates PVA, red line indicates disinfection and green line indicates core-shell nanofibers of PVA (shell) with incorporated disinfection (core).

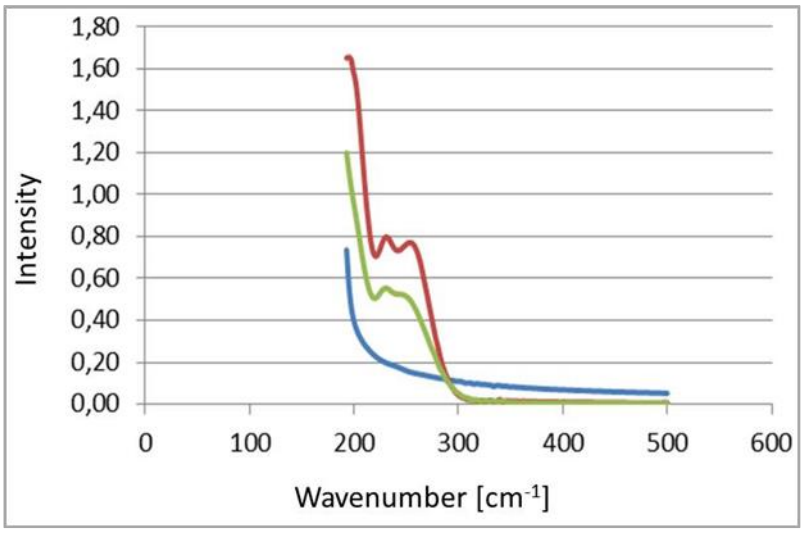

Figure 84 *FTIR spectroscopy of PVA (blue line), disinfection (red line) and core-shell nanofibers PVA/disinfection (green line).*

The course of individual curves in the graph shows a presence of the disinfection in core-shell nanofibers. The intensity of itself disinfection is higher than intensity of the disinfection incorporated into core-shell nanofibers enveloped by the PVA shell.

3.8.5 The phase contrast method

The phase contrast method is relatively simply analysis of core-shell structure of nanofibers. This one uses elements with higher atomic number incorporated in core part of core-shell nanofibers. Due to these elements, the core part appears significantly brighter than the shell one during observed by SEM. This indicates their presence in the core part of nanofibers. The contrast increases with increasing atomic weight of elements. Phase contrast method could be relatively easy, fast and inexpensive way to receive proof of core-shell structure of coaxial nanofibers, because expensive material as well as expensive analyses are not needed.

Polyvinyl alcohol (Sloviol R16,Chemicke zavody Novaky, SK) was used for this experiment. A solution of 12 % (w/v) PVA dissolved in distilled water was prepared as the shell. The solution of 4 % (w/v) PVA dissolved in the Prussian blue was used as the core. The Prussian blue $[Fe_4[Fe(CN)_6]_3]$ is a dark blue pigment containing iron. This was used for a better observation of coaxial electrospinning process and to achieve phase contrast during SEM analysis (Vysloužilová 2013).

The needle coaxial spinning electrode was used for this experiment. This was connected to the HV source (Spellman Sl100) and positively charged (22 kV). The collector

located at the distance 130 mm above spinning electrode was connected to the HV source (Spellman Sl100) and negatively charged (15 kV). A nonwoven Spunbond (Pegas, CZ) for collecting the nanofibers was located under collector.

Polymeric solutions were transferred into a 20 ml plastic syringe, empowered by a syringe pump (neMESYS, Cetoni) and dosed at a constant rate of 1.5 ml/h (core) and of 3 ml/h (shell). The electrospinning was carried out at ambient temperature 21°C and at a relative humidity 40%. Core-shell nanofibers were collected on the Spunbond nonwoven, located on the collector.

The morphology of produced nanofibrous layers was observed using SEM by Phenom (FEI) and Zeiss (Germany). The phase contrast method was used for detection of core-shell structure of produced nanofibrous layers. SEM images of these samples are shown in Figure 85 and 86. There are obvious brightly illuminated areas in core-shell nanofibers. This is the core material with the Prussian blue containing iron (element with higher atomic number).

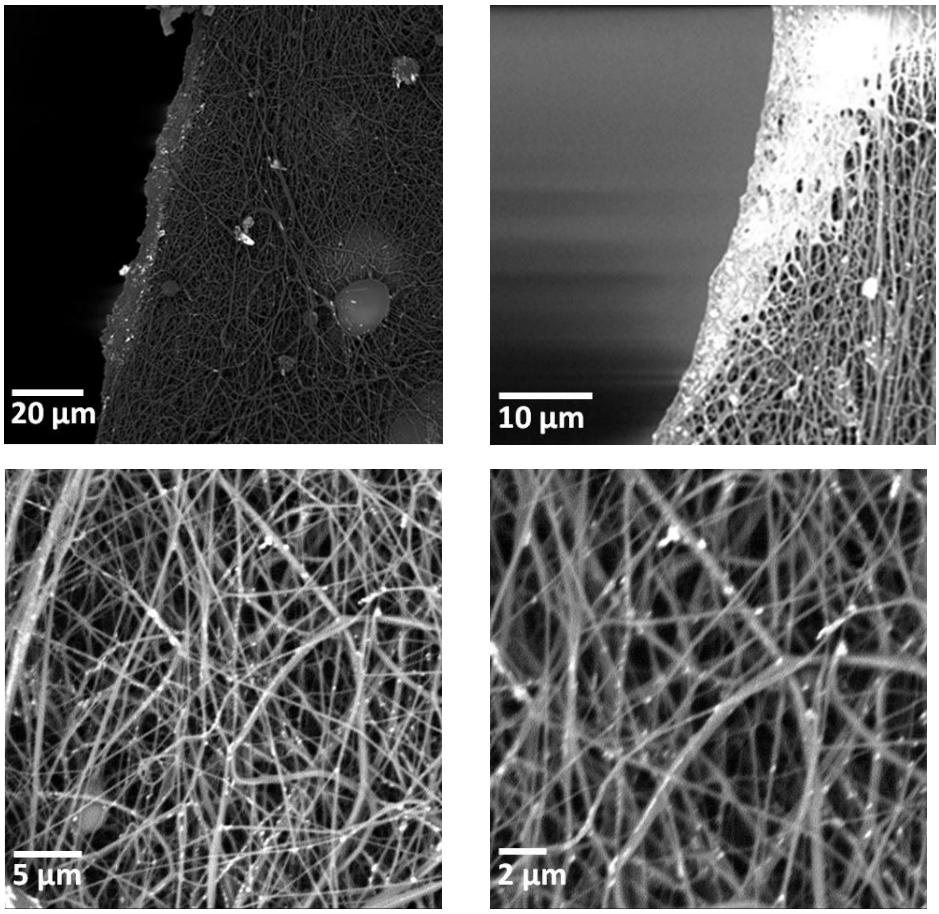

Figure 85 *SEM images of the core-shell nanofibrous structures with incorporated Prussian Blue produced by cylindrical coaxial spinning electrode (Phenom, FEI)*

As can be seen in Figure 85 and 86, there is problem in quality image display of core-shell nanofibers. Generally, analyzed nanofibrous layer is coated by a thin gold or carbon layer before the SEM analysis. This leads to increase of conductivity and receiving quality image without undesirable interference and defocusing. This coating is not possible in case of phase contrast method. This layer has resulted elimination of the phase contrast and the proof of the presence of elements with higher atomic number in the core is not possible. Investigation of this incorporated material realized by phase contrast method is possible just without coating nanofibrous layer. Phase contrast can be observed and proof of core-shell structure can be done but images do not have good quality

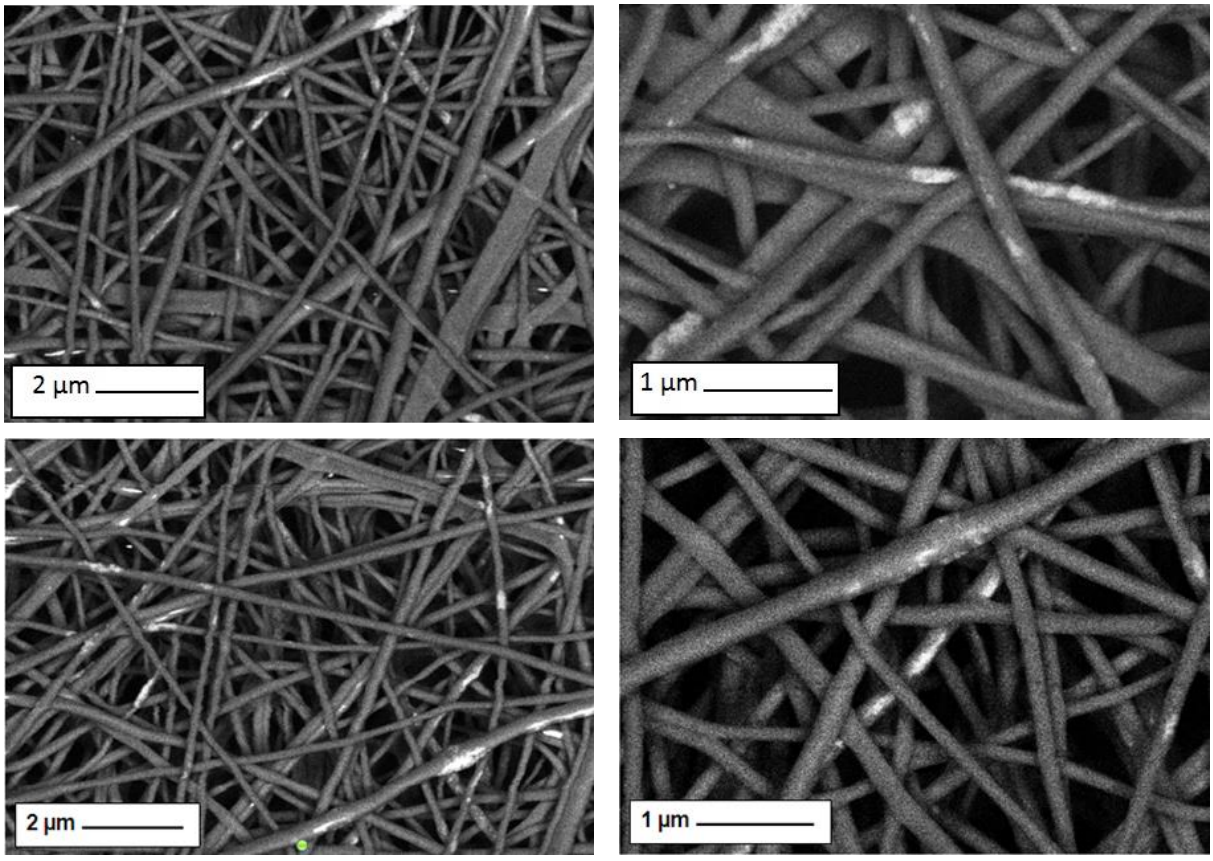

Figure 86 *SEM images of the core-shell nanofibrous structures with incorporated Prussian Blue observed by Pavel Kejzlar, KMT, FS, TUL(Zeiss, GE)*

The new method to proof of the coaxial structure of core-shell nanofibers was designed and verified in this work. Bi-component nanofibers with core-shell structure were produced by the needle coaxial electrospinning and analyzed by the SEM. Due to the use of elements with higher atomic number in core material (Prussian blue), the core-shell structure could be detected. An advantage of the phase contrast method is a low price and easy and relatively fast analysis (Vysloužilová 2013).

3.8.6 Fluorescence microscopy

Method of optical fluorescent microscopy and confocal laser scanning microscopy were used as next possibilities leads to the proof of core-shell structure of produced nanofibers in this work. Optical fluorescent microscopy was used for detected of iron and magnetic nanoparticles incorporated in core part of core-shell nanofibers. Confocal laser scanning microscopy was used for analysis of core-shell structure using fluorescent agents.

Optical fluorescent microscopy

This method was selected for investigation of iron and magnetic nanoparticles incorporated in core part of core-shell nanofibers. The produced nanofibrous layer were analyzed using Optical fluorescent microscopy, see in (Figure 87 and 88). Images shown illuminated nanoparticles of iron (Figure 87) and magnetic nanoparticles (Figure 88) incorporated in core part of the core-shell nanofibers.

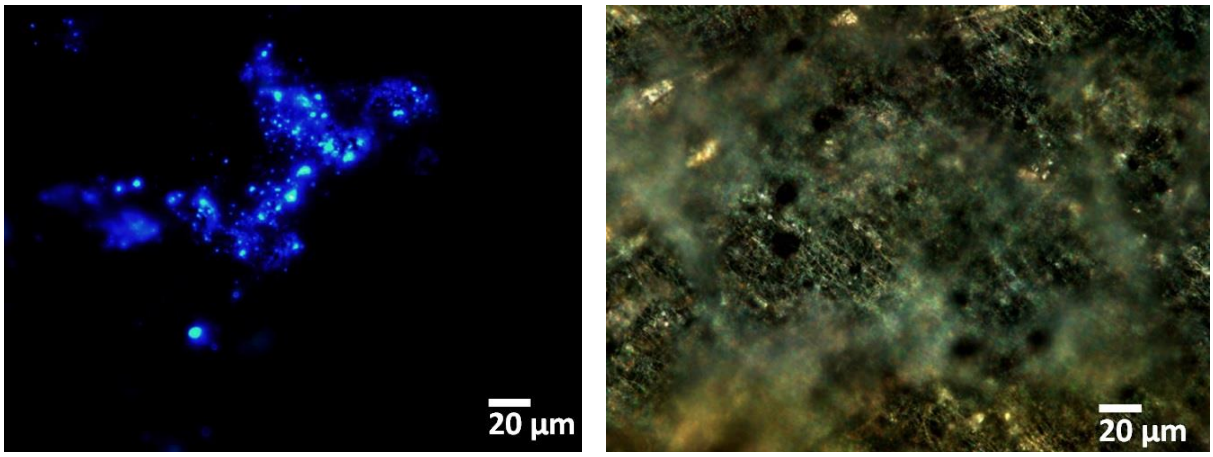

(a) (b)

Figure 87 *Core-shell nanofibers with incorporated nanoparticles of iron: (a) illuminated iron nanoparticles in core-shell nanofibers in UV mode, (b) image of fibrous structure in mode of daylight (project KONTAKT ME 10145)*

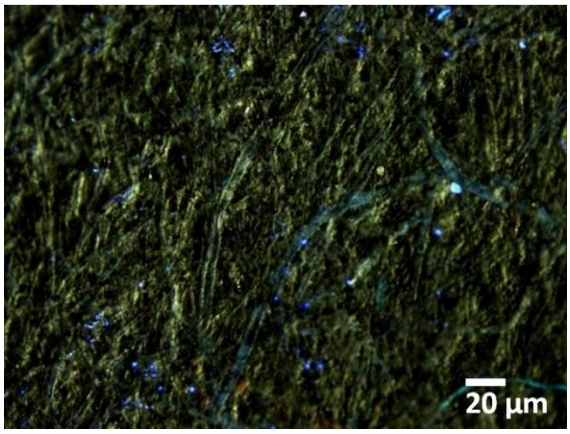

(a)

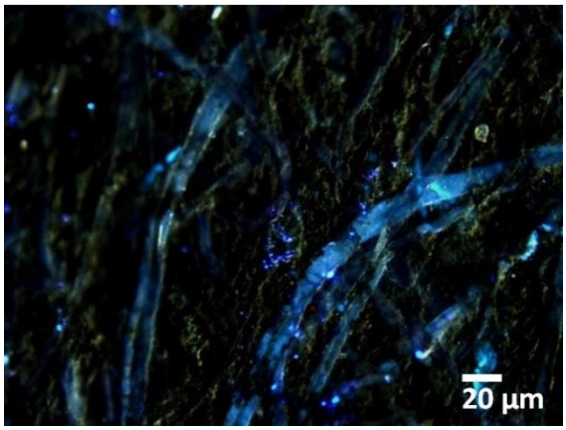

(b)

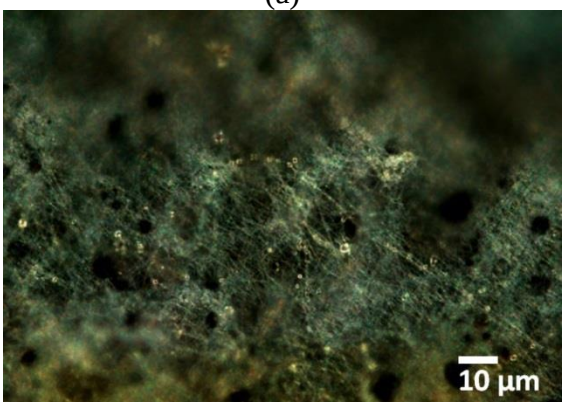

(c)

Figure 88 *Core-shell nanofibers with incorporated magnetic nanoparticles: (a) illuminated magnetic nanoparticles in core-shell nanofibers (combination of the daylight and UV mode), (b) image of fibrous structure in UV mode, (c) image of fibrous structure in daylight mode (project KONTAKT ME 10145)*

Confocal laser scanning microscopy

Confocal laser scanning microscopy was used for investigation of core-shell structure using fluorescent substances. In the first step, fluorochrome Rhodamine B was added to the core solution and FITC Dextran to the shell one. Rhodamine B excites at wavelength 540 nm and emits at 625 nm with red color signal. Excitation maximum of fluorophore FITC Dextran is 490 nm and the emission maximum is 520 nm. FITC Dextran emits with green color signal. In the next experiment, carried out in collaboration with Matej Buzgo (2nd Faculty of Medicine, Charles University in Prague), the core solution was prepared with a protein conjugated with phycoerythrin and Alexa Fluor 700. Phycoerythrin absorbs blue light (420–700 nm) and with combination of the red-absorbing dye Alexa Fluor 700, a red shift in the emission spectrum occurs as a result of Förster resonance energy transfer. These properties of the selected fluorophores allowed single-wavelength excitation of both fluorophores (i.e., excitation at 488 nm for both FITC-dextran and IgG-PE-AF700) but difference between the emission spectra of FITC-dextran and IgG-PE-AF700.

PVA (Sloviol R16,Chemicke zavody Novaky, SK) was used for these experiments. The solution of 12% (w/v) PVA dissolved in distilled water was prepared as the shell and mixed with FITC-dextran (2 mg/ml, MW 10000, Sigma Aldrich, UK). The solution of 5% (w/v) PVA dissolved in distilled water was prepared as the core and mixed with Rhodamine B (2mg/ml, 479,01 Sigma Aldrich, UK) and with the protein conjugated with phycoerythrin and Alexa Fluor 700 in the second experiment. The red food pigment was added to facilitate better observation of the electrospinning process.

The needle and needleless coaxial spinning electrodes (weir spinner of the second generation) were used for these experiments. The coaxial spinning electrode was connected to the HV source (Spellman Sl100) and positively charged (23 kV in case of needle and 30 kV in case of needleless coaxial spinning electrode). The disc collector with diameter of 150 mm located at the distance 130 mm above spinning electrode was connected to the HV source (Spellman Sl100) and negatively charged (20 kV in case of needle and 30 kV in case of needleless coaxial spinning electrode). A nonwoven Spunbond (Pegas, CZ) for collecting the nanofibers was located under collector. Polymeric solutions were transferred into a 20 ml plastic syringe and empowered by a syringe pumps (KDS-100-CE, KD Scientific Inc.). The feed rate for the core polymer was 2.5 ml/h (needle spinning electrode), 8 ml/h (weir spinner) and the feed rate for the shell polymer was 4 ml/h (needle spinning electrode) and 12 ml/h (weir spinner). Electrospinning process was performed at room temperature 21°C and at 45% humidity. Core-shell nanofibers were collected on the Spunbond nonwoven, located on the collector.

Analyzes of the core-shell structure of produced nanofibers were realized using a Zeiss LSM 5 DUO confocal laser scanning microscope. Figure 89 shows results from the needle coaxial electrospinning without phycoerythrin and Alexa Fluor 700. Figure 90 shows results from the needle coaxial electrospinning with phycoerythrin and Alexa Fluor 700 incorporated in the core (FITC-dextran has λ_{ex} = 488 nm, λ_{em} = 520 nm; IgG-PE-AF700 has λ_{ex} = 488 nm, λ_{em} = 780 nm).

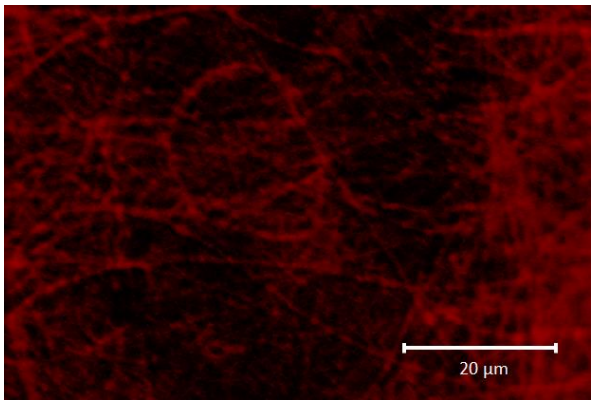

(a)

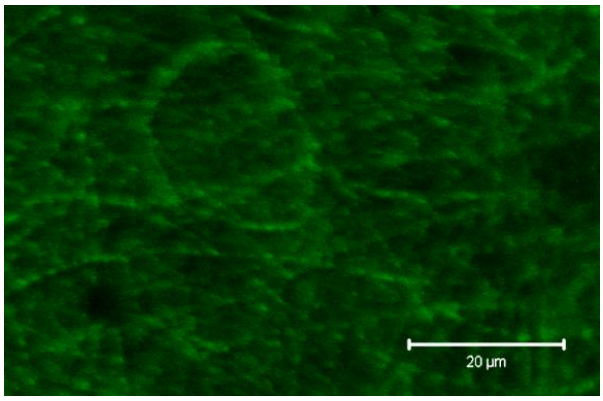

(b)

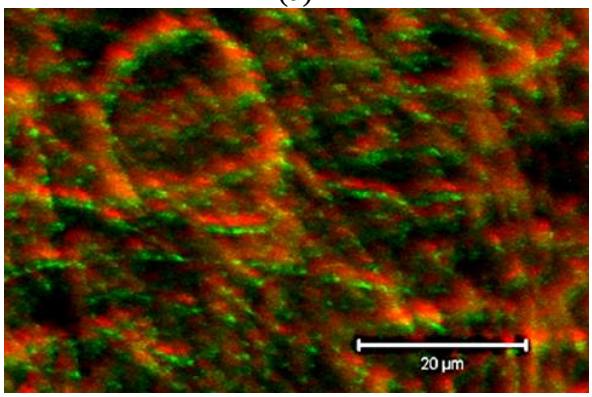

(c)

Figure 89 *Core-shell nanofibers with incorporated FITC-dextran in the shell (green signal) and Rhodamine B (red signal) in the core observed using confocal fluorescent microscopy Zeiss LSM 5 DUO: (a) the core with Rhodamine B, (b) the shell with FITC-dextran, (c) the observation realized with two lasers to analysis of core-shell structure.*

A movement of the core and shell signal (green and red color in the Figure 89c, respectively) is evident when observing core-shell nanofibers without IgG-PE-AF700. Two lasers in at the same time are used to detection of both signals (core and shell one). There is the movement of these signals and it is impossible to say, if structure of core-shell or side-side was achieved. This movement has been removed binding IgG-PE-AF700 on the Rhodamine B in core as is shown in Figure 90. Figure 90c shows the combination of both lasers at the same time during analysis using confocal fluorescent microscopy. There is not any movement of signals and core-shell structure of nanofibers can be observed.

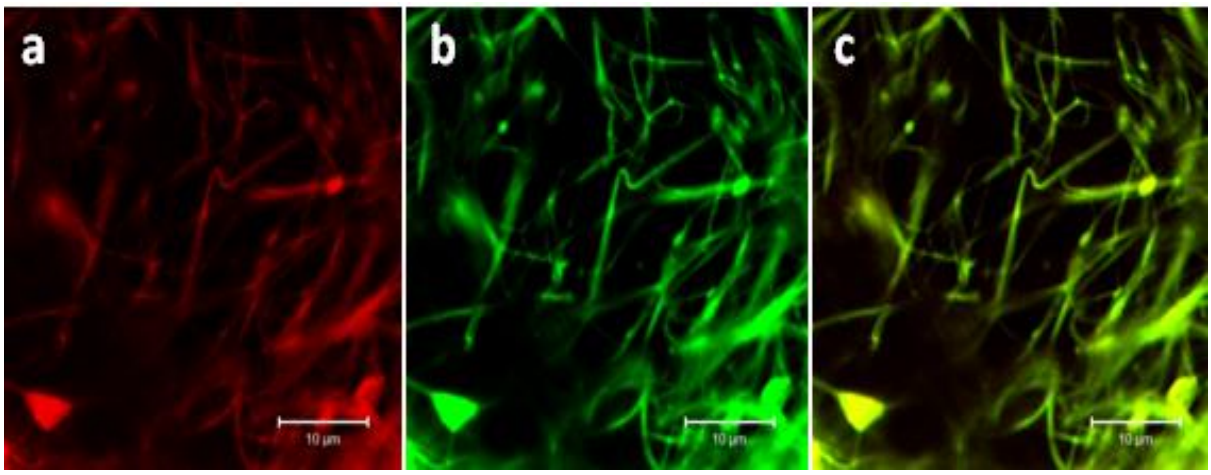

Figure 90 *Core-shell nanofibers with incorporated FITC-dextran in the shell (green signal) and Rhodamine B with IgG-PE-AF700 (red signal) in the core observed using confocal fluorescent microscopy Zeiss LSM 5 DUO: (a) the core, (b) the shell, (c) observing realized with two lasers to analysis of core-shell structure. Collaboration with Matej Buzgo (2nd Faculty of Medicine, Charles University in Prague)*

The proof of core-shell structure of nanofibers was supported by the new method of analysis - observation of the signals from the core and shell part of nanofibers using two lasers of the confocal fluorescent microscopy. Due to IgG-PE-AF700 incorporated into the core, the shift of the emission spectra of Rhodamine B was achieved and both of these signals (red and green one) could be observed at the same time.

The fluorescent analysis was supplemented by the investigation of signal intensity profiles of fluorophores of the core-shell nanofibers. This analysis was done within Matej Buzgo (2nd Faculty of Medicine, Charles University in Prague) and Jiří Kula (The Department of Textiles Evaluation, Technical University at Liberec). The micrograph shows the signal of the shell-incorporated fluorophore (FITC-dextran, green signal) and the signal of the core-incorporated fluorophore (IgG-PE-AF700, red signal), as well as the combination of both signals from core-shell nanofiber. There is recorded a tracking of imaginary nanofiber cross-section from one side of the nanofiber to the other, see in (Figure 91). The signal intensity of the IgG-PE-AF700 in the core is lower than FITC-dextran in the shell. The energy loss during resonance transfer, its lower quantum yield, and signal loss is caused by crossing through the boundary between the core and the shell part of the core-shell nanofiber. The signal intensity profile of the core-shell nanofiber (Figure 91a) shows that the signals are increasing near the periphery of the nanofiber and peaked in the central part of the nanofiber. The signal from the core (red line) has a delayed increase in the fluorescence intensity

compared to the shell one (green line). The full width at half-maximum (FWHM) was determined for both the core and the shell intensity profiles to characterization of the peaks. The ratio of the shell FWHM to the core FWHM of the core-shell nanofibers produced by the needle spinning electrode was 1.64 ± 0.35 and 1.35 ± 0.13 in case of the weir spinner of the second generation, see in (Figure 91b). This means, the shell part is thicker than the core one and this leads to the next proof of the core-shell morphology of the examined nanofibers. These results indicate that the both the needle and needleless coaxial spinning electrodes enables the production of the nanofibers with the core-shell structure.

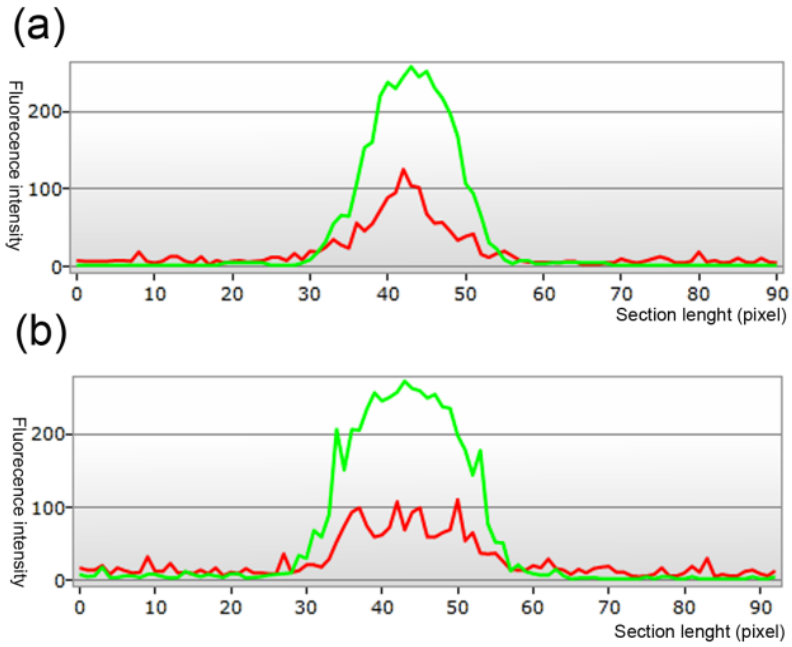

Figure 91 *Signal intensity profiles of fluorophores for core-shell nanofibers realized by (a) the needle coaxial spinning electrode and (b) the weir spinner of the second generation. Fluorescence intensity profiles of FITC-dextran incorporated in the shell (green line) and IgG-PE-AF700 incorporated in the core (red line). Collaboration with Jiří Kula and Matej Buzgo.*

Analysis of core-shell nanofibers with incorporated liposomes

Confocal laser scanning microscopy was also used to proof the core-shell structure of nanofibers with liposomes. Necessity of the aqueous medium is disadvantage for these substances. Experiments incorporating the liposomes into the aqueous core were done. Protection of the liposomes against ambient environment was managed by the PCL shell.

FITC-dextran was encapsulated into liposomes and these were electrospun as the core part of the core-shell nanofibers using needleless coaxial electrospinning. Cylindrical coaxial spinning electrode of the 2nd generation was used for this experiment. These two materials were prepared during this experiment: Core-shell nanofibers of PCL (shell) and PVA with FITC-Dextran (core) were formed in the first stage. Second, core-shell nanofibers of PCL (shell) and PVA with encapsulated FITC-Dextran in liposomes (core) were formed. Material and process parameters are listed in the Chapter 3.5.8. Figure 92a shows core-shell nanofibers of PCL/PVA with incorporated FITC-Dextran in the core. Green signal of the FITC-Dextran can be observed across the length of fibers. Liposomes with incorporated FITC-Dextran are shown in Figure 92b. In this case can be observed significant change due to fluorophore encapsulated in liposomes. This also means that the liposomes in the core were not damaged and the fluorophore remained safely incorporated inside of the liposomes.

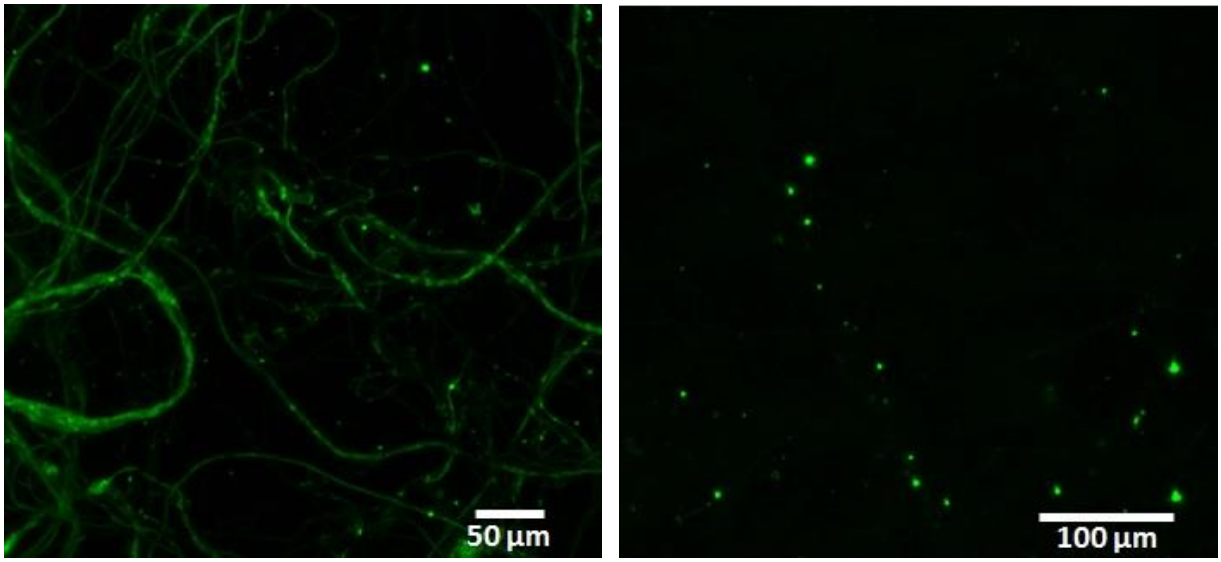

(a) (b)

Figure 92 *Core-shell nanofibers of PCL/PVA with FITC-Dextran (a) and core-shell nanofibers of PCL/PVA with FITC-Dextran incorporated in liposomes (b). Collaboration with Andrea Míčková (2nd Faculty of Medicine, Charles University in Prague).*

Analysis of core-shell nanofibers PVA/PVB

Combination of confocal laser scanning microscopy and scanning electron microscopy (SEM) was used for observation of produced core-shell nanofibrous structures PVA/PVB.

Core-shell nanofibers of PVA (shell) and PVB (core) were used for this experiment. Water soluble PVA solution at concentration of 12 % (w/v) was dissolved in distilled water.

PVB at concentration of 5 % (w/v) was dissolved in ethanol. Fluorophore FITC-Dextran was added to the core solution.

Core-shell nanofibers were produced by the coaxial needle spinning electrode. This electrode was connected to the HV source (Spellman Sl150) and positively charged. The electrode was located 120 mm below the negatively charged disc collector with the diameter of 120 mm connected to the HV source (Spellman Sl150). The Spunbond nonwoven was placed under the collector for core-shell nanofibers deposition. Polymer solutions were fed to the needle spinning electrode using the dosing pumps Nemesys 14.1 (Cetoni, DE). The feeding rate of the core and shell material was 0,3 ml /h (core) and 2,1 ml/h (shell). The applied voltage was ± 22 kV. The experiments were carried out in the chamber with controlled atmospheric conditions; temperature was 21 ± 0,5 °C and RH was 30 ± 1,5 %.

This layer was analyzed by the SEM (Vega 3, Tescan) and confocal scanning laser microscopy, see in (Figure 93). The beads of the PVB with FITC-Dextran incorporated in PVA can be seen in these images. Green signal of this fluorophore can be observed across the length of fibers (Figure 93 c, d) and in the beads of PVB (Figure 93 d).

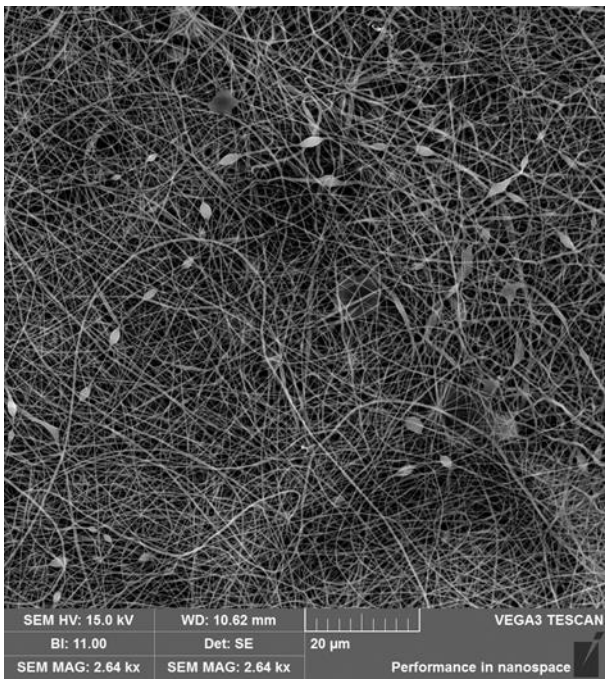

(a)

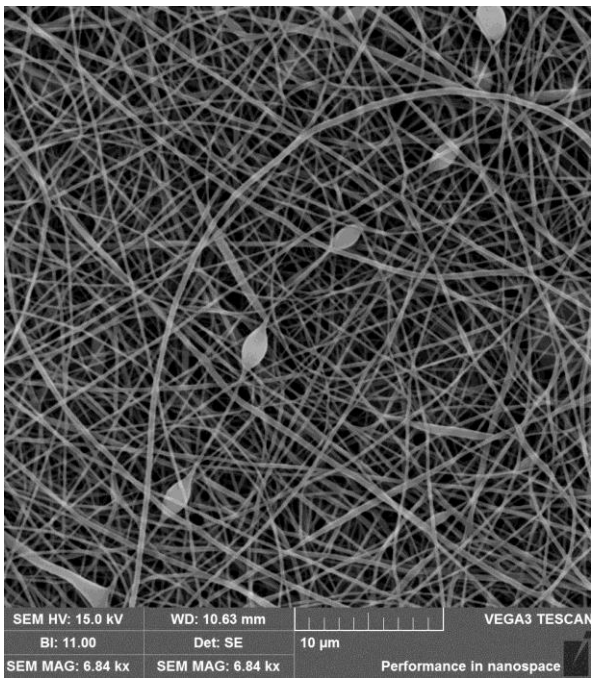

(b)

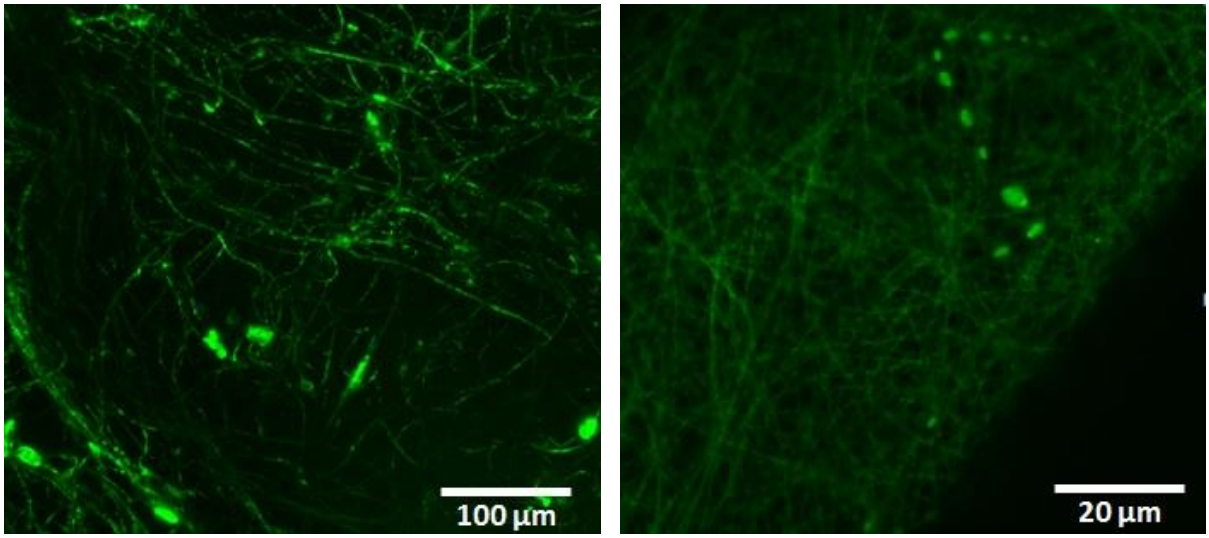

(c) (d)

Figure 93 *Core-shell nanofibers of PVA/PVB with FITC-Dextran observed by SEM (a, b) and by confocal laser scanning microscope (c, d). Collaboration with Matej Buzgo and Andrea Míčková (2nd Faculty of Medicine, Charles University in Prague)*

Many different analysis leads to proof the core-shell structure of core-shell nanofibers were done within this work. This is not easy to provide a clear proof of core-shell structure in case of very fine fibers. Therefore, different ways allowing achievement this proof of core-shell structure of nanofibers or combination of these methods were designed and investigated within this work.

4 Summary

Technology of coaxial electrospinning was investigated in this work. Different kinds of needle and needleless coaxial spinning electrodes were designed, developed and tested. This work focused on the development of sophisticated spinning coaxial electrodes from different construction materials and various shape for the purpose of the finding of the optimal spinning electrodes for a wide range of electrospun materials. Duraluminium, Teflon, PP, POM and HDPE TIVAR 1000 were selected as possible construction materials of needle coaxial spinning electrodes. Needle spinning electrodes from these materials were designed and their functionality was verified. In the next step, optimal design of spinning electrodes focusing on the shape of their orifice was investigated and designed within this work. Coaxial needle spinning electrodes allowing the electrospinning of polymer solutions with water-based solvents as well as volatile solvents and various chemical-based liquids and biomedical liquids were developed and tested.

Needleless coaxial electrospinning electrodes were developed and tested in the next part of this work to increase the productivity of core-shell nanofibers. The needleless coaxial electrospinning is a relatively new technology for production of core-shell nanofibers from a free surface of polymeric two-layer. This method was developed at Technical University of Liberec and patented in 2009 (Pokorný). The developing of this needleless spinning electrode took place in conjunction with this work. The apparatus called the Weir spinner and the cylindrical coaxial spinning electrode were designed, developed, investigated and tested within this work. The main advantage of the cylindrical construction of the last one coaxial spinning electrode is electrospinning process without a loss of electric energy caused by spark discharges. Another its advantage is a reduction of polymer solution slumping from this spinning electrode.

Experiments with needleless electrospinning lead to determination of the characteristic wavelength λ. This one is a distance between neighboring polymeric jets during needleless electrospinning. Electrospinning process starts with a certain critical value of electric field strength E_c and critical value of the characteristic wavelength λ_c. These parameters were examined during electrospinning process and their effect on the process was investigated in detail.

Dispersion laws for a free surface of non-viscous and viscous liquids were derived during this work. They allow a determination of a relaxation time of electrospinning. This is

time of Taylor cone formation after HV switching. Dispersion relations were verified with experiment of electrospinning of PVA solutions with concentration from 5 – 15 % (w/v). The dependence of the time delay T on the electrospinning number Γ was found.

The analysis of the core-shell structure of nanofibers was investigated with this work. This analysis is not easy. Transmission electron microscopy (TEM), confocal laser scanning microscopy or cutting by an ion beam are commonly used methods. The problem is that these methods are both difficult and expensive. Only some centers and universities have these special equipments. This thesis described the special new method leads to easy detection of core-shell nanofibrous structure. The phase contrast method allows proving the core-shell structure using elements with higher atomic number in the core part of core-shell nanofibers. Scanning electron microscopy (SEM) was used for this investigation. Brightly illuminated areas of core with these heavy elements can be observed in comparison with grey areas without these heavy elements. The advantage of the phase contrast method is a low price and easy and relatively fast analysis. Other different analysis leads to proof the core-shell structure of produced core-shell nanofibers were done within this work. TEM analysis, FT-IR analysis, fluorescent analysis and special method combining the last one with investigation of the signal intensity profiles of fluorophores in core and shell part of the nanofibers were used and verified.

5 List of papers published by the author

5.1 Publications

Valtera J., Vysloužilová L., Komárek, J., Skřivánek, J., Žabka, P., Beran J., Lukáš D., Protrusion of the Rod Electrode in the Electrospinning Process, Journal of Nanotechnology (2015), Article ID 301636, doi:10.1155/2015/301636

Vysloužilová L., Valtera J., Pejchar K., Beran J., Lukáš D., Design of coaxial needleless electrospinning electrode with respect to the distribution of electric field, Applied Mechanics and Materials, Vol. 693 (2014), pp 394-399, ISSN: 1660-9336, doi:10.4028

Lukáš D., Raab M., Vysloužilová L., Košťáková E., Mikeš P., Fyzika polymerů, Technická univerzita v Liberci (2013), ISBN 978-80-7494-029-3

Vysloužilová L., Seidl M., Hrůza J., Bobek J., Lukas D. and Lenfeld P., Nanofibrous filters for respirators, Applied Mechanics and Materials Journal, (2014), ISSN:1660-9336

Rampichová M., Chvojka J., Buzgo M., Prosecká E., Mikeš P., Vysloužilová L., Tvrdík L., Kochová P., Gregor T., Lukáš D., Amler E., Elastic three-dimensional poly (ε-caprolactone) nanofibre scaffold enhances migration, proliferation and osteogenic differentiation of mesenchymal stem cells, Cell Proliferation, Vol. 46, Issue 1, (2013), pp 23–37

Prosecká, E., Buzgo, M., Rampichová, M., Kocourek, T., Kochová, P., Vysloužilová, L., Tvrdík, D., Jelínek, M., Lukáš, D. and Amler, E., Thin-Layer Hydroxyapatite Deposition on a Nanofiber Surface Stimulates Mesenchymal Stem Cell Proliferation and Their Differentiation into Osteoblasts, Journal of Biomedicine and Biotechnology, Article ID 428503, (2012), doi:10.1155/2012/428503

Vysloužilová L., Váša P., Soukupová J., Pokorný P., Chvojka J., Pejchar K., Žabka P., Lukáš D., Beran J., Předávací dokument ke spineru 1, Nanoprogres – The Czech-based nanotechnology cluster, Technická Univerzita v Liberci, Liberec (2012), Czech Republic

5.2 Contribution in conference proceeding

Valtera, J., Bilek, M., Vyslouzilova, L., Komarek, J., Skrivanek, J., Soukupova, J., Zabka, P., Lukas, D., Beran, J., Wire Spinner for Coaxial Electrospinning, In: Nanocon 2015, October, 14 - 16. 2015, Brno, Czech Republic

L. Vysloužilová, J. Valtera, M. Bílek, J. Soukupová, J. Komárek, P. Žabka, J. Skřivánek, J. Beran and D. Lukáš, Visualization of electrospinning process, In: NART 2015, August 31 - September 2, Liberec, Czech Republic

Vysloužilová L., Pejchar K., Valtera J., Pokorný P., Beran J., Lukáš D., Cylindrical Coaxial Spinning Electrode for Needleless Coaxial Electrospinning, In: The Fiber Society Spring 2014, Technical Conference Fibers for Progress, (2014), Liberec, Czech Republic

Vysloužilová L., Pejchar K., Pokorný P., Lukáš D., Increase the Productivity of Coaxial Electrospinning, In: The Fiber Society, (2013), Clemson, South Carolina, USA

Pejchar K., Vysloužilová L., Beran J., Lukáš D., Bílek M., Pokorný P., The Slit Needleless Electrode for the Electrospinning, In: Nanocon 2013, October 16. – 18., 2013, Brno, Czech Republic, ISBN 978-80-87294-44-4

Vysloužilová L., Bajáková J., Grégr J., Pejchar K., Lukáš D., Phase Contrast Method for Demonstrating of Coaxial Structure of Core/Shell Nanofibers, In: Nanocon 2013, Brno, Czech Republic, ISBN 978-80-87294-44-4

Vysloužilová L., Mohrová J., Lukáš D., Coaxial electrospinning of biopolymers for humen use, In: Strutex, 19th International Conference, 3. – 4. 12. 2012, Liberec, Česká Republika

Vysloužilová L., Buzgo M., Mohrová J., Pokorný P., Bílek M., Pejchar K., and Lukáš D., Productivity Enhancement of core/shell nanofiber, In: Nanocon 2012, Brno, October 23 – 25, 2012, pp. 42, Ostrava, Czech Republic, ISBN 978-80-98294-32-1

Vysloužilová L., Zařízení pro koaxiální elektrostatické zvlákňování, In: Workshop pro doktorandy Fakulty strojní a Fakulty textilní Technické univerzity v Liberci, Světlanka, 17. – 20. 9. 2012, pp. 135–139, Technická univerzita v Liberci, 2012, Česká Republika, ISBN 978-80-7372-891-5

Kejzlar, P., Vysloužilová, L., Voleský, L., Andršová, Z., and Kroisová, D., Bionics: Egg shell. In: PANMS 2012 Conference Proceedings. Hejnice, 2012. P. 55-58. ISBN 978-80-7372-890-8

Vysloužilová L., Mohrová J., Lukáš D., Electrospinning of biopolymers, In: Strutex, (2011), Liberec, Czech Republic, ISBN 978-80-7372-786-4

Vysloužilová L., Mohrová, J., Chvojka J., Hégrová B., Mikeš P. and Lukáš D., Production of Bicomponent Nanofibers with incorporation Particles, In: Nanocon2011, Ostrava, Czech Republic, ISBN: 978-80-87294-27-7

L. Vysloužilová, Jehlové a bez-jehlové koaxiální elektrostatické zvlákňování, In: Workshop pro doktorandy Fakulty strojní a Fakulty textilní Technické univerzity v Liberci, str. 136-140, Rokytnice, 19,-22, září. 2011, Technická univerzita v Liberci, ISBN 978-80-7372-765-9

Vysloužilová L., Mohrová J., Mikeš P., Amler E. and Lukáš D., Electrospinning of hyaluronic acid, In: FiberMed11, Tampere, Finland (2011)

Pokorny, P., Mikes, P., Vyslouzilova, L., Hazuchova, A., Lukas, D.: Relaxation Time of Electrospinning, in Proceedings of the International Conference of the Czech Society of

Biomechanics, Human Biomechanics 2010, Sychrov, Czech Republic, October 4-6, 2010, Number Publication: 55-090-10, ISBN 978-80-7372-648-5

Vysloužilová L., Vodseďálková K., Pokorný P., Lukáš D. and Buzgo M., Needleless co-axial electrospinning, In: Nanofibers for the 3rd Millennium, North Carolina (2010), USA

L. Vysloužilová, Bezjehlové koaxiální elektrostatické zvlákňování, In: Workshop pro doktorandy Fakulty strojní a Fakulty textilní Technické Univerzity v Liberci, str. 114-118, Rokytnice, 20.-23.září 2010, ISBN 978-80-7372-642-3

5.3 Patents

Technická univerzita v Liberci, Liberec, CZ. Způsob vytváření funkční nanovlákenné vrstvy a zařízení k provádění způsobu. Původce: Pokorný P, Lukáš D, Mikeš P, Vysloužilová L, Chvojka J, Hégrová B, Lukáš R, Amler E, Buzgo M, Louda P. Patent č. 302901. Datum publikace patentu 11.01.2012. Úřad průmyslového vlastnictví

6 References

BANGHAM, A. D., STANDISH, M. M., WATKINS, J. C. Diffusion of univalent ions across the lamellae of swollen phospholipids. *J Mol Biol, 13(1).* 1965. pp. 238-252.

BARTON, A. F. M. CRC *Handbook of Solubility Parameters and Other Cohesion Parameters,* 2nd ed. CRC Press LLC. Florida. USA. ISBN 0-8493-0176-9. 2000.

BAZILEVSKI, A., YARIN, A. L., MEGARIDIS, C. M. Co-electrospinnig of core-shell fibres using a single-nozzle technique. *Langmuir, 23.* 2007. pp. 2311-2314.

BORDES, C., FRÉVILLE, V., RUFFIN, E., MAROTE, P., GAUVRIT, J. Y., BRIANCON, S., LANTÉRI, P. Determination of poly(ε-caprolactone) solubility parameters: Application to solvent substitution in a microencapsulation process. International Journal of Pharmaceutics 383. 2010. pp. 236-243.

BORNAT, A. *Production of electrostatically spun products.* U.S. Patent 4689186 A. 1987.

BOYS, C. V. On the production, properties, and some suggested uses of the finest threads. *Proceedings of the Physical Society of London.* 1887.

4SPIN. *Contipro a.s.* [online]. ©2015 Available at: *http://www.4spin.info/.*[Accessed 20 June 2016].

COOLEY, J. F. *Apparatus for electrically dispersing fluids.* Patent 692,631. 1902.

DING, B., KIMURA, E., SATO, T., FUJITA, S., SHIRATORI, S. Fabrication of blend biodegradable nanofibrous nonwoven mats via multi-jet electrospinning. *Polymer, 45.* 2004. pp. 1895-1902.

DOSHI, J., RENEKER, D. H. Electrospinning process and applications of electrospun fibres. *J. Electrostat, 35.* 1995. pp. 151-160.

DROR, Y., SALALHA, W., AVRAHAMI, R., ZUSSMAN, E., YARIN, A. L., DERSCH, R., GREINER, A., WENDORF, J.H. Comparison of Cylinder and Disk Nozzles. *Journal of Applied PolymerScience, 114.* 2009. pp. 3524-3530.

DUCHACEK, V. Polymery: Výroba, vlastnosti, zpracování, použití, VŠCHT Praha (3. vyd.), ISBN 978-80-7080-788-0. 2011.

DUMAS, R. K., RANDY, K., LI, Ch-P., ROSCHIN, I. V., SCHULLER, I. K., LIU, K. Magnetic Fingerprints of sub-100 nm Fe Nanodots. *Physical review B, 75, (13).* 2007.

DZENIS, Y. Spinning continous fibers for nanotechnology. *Science 304.* 2004. pp. 1917-1919.

KENAWY, E. R., BOWLIN, G. L., MANSFIELD, K., LAYMAN, J. SIMPSON, D. G., SANDERS, E. H., WNEK, G. E. Release of tetracycline hydrochloride from electrospun poly(ethylene-co-vinylacetate), poly(lactic acid), and a blend. *Journal of Controlled Release 81.* 2002. pp. 57-64.

ELECTROSPINTECH. ElectrospinTech. Electrospinning setup providers. [online]. ©2012 Available at: http://electrospintech.com/espin-supplier.html#.V2hP-PmLTIW [Accessed 25 June 2015].

ELMARCO. Elmarco.com. [online]. ©2004 Available at: http://www.elmarco.com/photogallery/ [Accessed 10 December 2015].

FILATOV, Y. N. *Electrospinning of Fibrous Materials [in Russian]*. s. l.: Neft' i Gas Publishing House. 1977.

FLORY, J. P. Thermodynamics of High Polymer Solutions, *J. Chem. Phys. 9.* 1941. pp. 660 – 661.

FORMHALS, A. *Process and apparatus for preparing artificial threads. U. S. Patent No. 1 975 504* 1934.

FORWARD, K. M., FLORES, A., RUTLEDGE, G. C. Production of core/shell fibers by electrospinning from a free surface. *Chemical Engineering Science.* 2013. pp. 250-259.

FRENKEL, J. *Kinetic Theory of Liquids.* New York. Dover Publications. 1955.

GREINER, A., WENDORFF, J. H. Electrospinning: A fascinating method for the preparation of ultrathin fibers. *Angewandte Chemie International Edition, 46*. 2007. pp. 5670– 5703.

GUGGENHEIM, E. A. *Mixtures*. Clarendon Press. Oxford. 1952.

JIN, H.-J., FRIDRIKH, S. V., RUTLEDGE, G. C., KAPLAN, D. L. Electrospinning Bombyx mori Silk with Poly(ethylene oxide). *Biomacromolecules 3 (6).* 2002, pp. 1233-1239.

HAITAO, N., TONG, L. XUNGAI, W. Needleless Electrospinning. I.A. Comparison of Cylinder and Disk Nozzles. *Journal of Applied PolymerScience, 114.* 2009. pp. 3524-3530.

HILDEBRAND J. H. and SCOTT, R. L. *Solubility of Nonelectrolytes*. 3rd ed. Reinhold Publishing Corp. New York. 1950.

MI Ústav fyziky a materiálového inženýrství. Hodnocení rozpustnosti polymerů. [online]. ©2009 Available at: //ufmi.ft.utb.cz/texty/fyzika_pol/FP1_lab_01.pdf [Accessed 10 August 2012].

HUANG, Z-M., ZHANG, Y-Z., KOTAKI, M., RAMAKRISHNA, S. A review on polymer nanofibers by electrospinning and their application in nanocomposites. *Composites science and technology*. 2003, pp. 2223-2253.

HUGGINS M. L. The thermodynamic properties of liquids, including solutions. I. Intermolecular energies in monotonic liquids and their mixtures. *J. Phys. Chem. 74 (2),* 1940. pp. 371 - 378.

HUGGINS M. L. Solutions of Long Chain Compounds. *J. Chem. Pays. 9, 440*. 1941.

CHAN, K. H. K., KOTAKI, M. Fabrication and morphology control of poly(methyl methacrylate) hollow structures via coaxial electrospinning. *Applied Polymer Science, 111.* 2009. pp. 408 – 416.

CHETRI, P., DASS, N. N., SARMA, N. S., Development of a catalyst for solution of poly(vinyl alcohol) in non-aqueous medium. *Chinese Journal of Polymer Science Vl. 26, No. 4*. 2008. pp. 399 – 404.

IHS, Inc. Chemical Economics Handbook. [online]. ©2016 Available at: https://www.ihs.com/products/polyvinyl-butyral-chemical-economics-handbook.html [Accessed 12 Marc 2016].

JI, Y., GHOSH, K., SHU, X. Z., LI, B., SOKOLOV, J. C., PRESTWICH, G. D., CLARK, R. A. F., RAFAILOVICH, M. H. Electrospun three-dimensional hyaluronic acid nanofibrous scaffolds. *Biomaterials, 27.* 2006. pp. 3782-3792.

JIANG, G., QIN, X. An improved free surface electrospinning for high throughput manufacturing of core-shell nanofibers. *Material Letters.* 2014. pp. 259-262.

JIANG, H., WANG, L., ZHU, K. Coaxial electrospinning for encapsulation and controlled release of fragile water-soluble bioactive agents. *Journal of Controlled Release, 143.* 2014. pp. 296–303.

JIRSAK, O., SANETRNIK, F., LUKAS, D., KOTEK, V., MARTINOVA, L., CHALOUPEK, J. *A method of Nanofibres production from a polymer solution using electrostatic spinning and a device for carrying out the method.* Patent WO2005024101. 2005.

KLEIN, S., KUHN, J., AVRAHAMI, R., TARRE, S., BELIAVSKI, M., GREEN, M., ZUSSMAN, E. Encapsulation of Bacterial Cells in Electrospun Microtubes. *Biomacromolecules, 10.* 2009. pp. 1751-1756.

KORNEV, K. G., TSAI, CH-CH., LUKAS, D., MIKES, P. Flexible fiber-based micro and nanofluidics for probing liquids. Patent US 9383292 B1. 2012.

KUMAR, M. N. V. R. A review of chitin and chitosan applications. *React. Funct. Polym. 46.* 2000. pp. 1 – 27.

KURBAN, Z., LOVELL, A., BENNINGTON, S. M., JENKINS, D. W. K., RYAN, K. R., JONES, M. O., SKIPPER, N. T., DAVID, W. I. F. A Solution Selection Model for Coaxial Electrospinning and Its Application to Nanostructured Hydrogen Storage Materials. *J. Phys. Chem. C, 114.* 2010, pp. 21201–21213.

LAPČÍK, L., Jr., LAPČÍK, L. Hyaluronan: Preparation, Structure, Properties, and Applications. *Chemical reviews, 98.* 1998. pp. 2663 - 2681.

LARMOR, J. On the Influence of Electrification on Ripples. *Proceedings of the Cambridge Philosophical Society. Mathematical and physical sciences 7.* 1890. pp. 69-72.

LAURENT, T. C., LAURENT, U. G., FRASER, J. E. Functions of hyaluronan. *Rheum Dis. 54.* 1995. pp. 429-432.

LI, D., XIA, Y. Direct Fabrication of Composite and Ceramic Hollow Nanofibers by Electrospinning. *Nano Letters, 4.* 2004. pp. 933-938.

LIAO, I. C., CHEW, S. Y., LEONG, K. W. Aligned core-shell nanofibers delivering bioactive proteins. *Nanomedicine (Lond), 1(4).* 2006. pp. 465-71.

LIU, N., CHEN, X-G., PARK, H-J. Effect of MW and concentration of chitosan on antibacterial activity of Escherichia coli, *Carbohydrate Polymers, 64, 1.* 2006. pp. 60 -65.

LODISH, H., BERK, A., MATSUDAIRA, P., KAISER, CH. A., KRIEGER, M., SCOTT, M., ZIPURSKY, S. L., DARNELL, J. *Molecular Cell Biology.* New York. W.H. Freeman and Company. 2004. ISBN 0-7167-4366-3.

LUKAS, D., SARKAR, A., MARTINOVA, L., VODSEDALKOVA, K., LUBASOVA, D., CHALOUPEK, J., POKORNY, P., MIKES, P., CHVOJKA, J., KOMAREK, M. Physical principles of electrospinning (electrospinning as a nano-scale technology of the twenty-first century). *Textile Progress, 41. No. 2.* 2009. pp. 1-83.

LUKAS, D., SARKAR, A., POKORNY, P., Self-organization of jets in electrospinning from free liquid surface: A generalized approach, *Journal of Applied Physics, 113, No. 8*. 2008, 084309 1-7.

MA, Z., KOTAKI, M., RAMAKRISHNA, S. Electrospun cellulose nanofiber as affinity membrane. *Journal of membrane science, 265, 115.* 2005, pp. 115-123.

MACDIARMID, A.G., Jones, W.E. Jr., NORRIS, I.D., GAO, J., JOHNSON, A. T. Jr., PINTO, N.J., HONE, J., HAN, B., KO, F. K., OKUZAKI, H., LLAGUNO, M. Electrostatically-generated nanofibers of electronic polymers. *Synthetic Metals 119.* 2001, pp. 27-30.

Macromolecular Physics, KMF. [online]. ©2011 Available at: *http://kmf.troja.mff.cuni.cz/vyzkum/index.php?id=klubko_globule* [Accessed 11 August 2015].

MARK, J. E., *Polymer data Handbook*, Oxford University Press, Inc. 1999.

MEISSNER, B., ZILVAR, V., Fyzika polymerů, Struktura a vlastnosti polymerních materiálů, Bratislava, SNTL, Nakladatelství technické literatury Alfa, 1987

MICKOVA, A, BUZGO, M, BENADA, O, RAMPICHOVA, M, FISAR, Z, FILOVA, E, TESAROVA, M, LUKAS, D, AMLER, E. Core/shell nanofibers with embedded liposomes as a drug delivery system. *Biomacromolecules 13(4).* 2012. pp. 952-62.

MÍČKOVÁ, A., Biodegradable *Nanofibers for Tissue Engineering and Controlled Drug Delivery*, PhD Thesis, Charles University in Prague, 2015.

MILLER-CHOU, B.A., KOENIG, J.L., A review of polymer dissolution, *Prog. Polym. Sci. 28*, 2003, pp. 1223-1270.

MOGHE, A. K., GUPTA, B. S. Co-axial Electrospinning for Nanofiber Structures: Preparation and Applications. *Polymer Reviews, 48.* 2008, pp. 353-377.

MORTON, W. J. *Method of dispersing fluids.* Patent US705691 A 1902.

MYSCOPE. Office for Learning and Teaching. [online]. © 2013 Available at: http://www.ammrf.org.au/myscope/tem/background/. [Accessed 5 June 2015].

NO, H. K., PARK, N. Y., LEE, S. H., MEYERS, S. P. Antibacterial activity of chitosan oligomers with different molecular weights, *Int J Food Microbiol. 74(1-2)*, pp. 65-72, 2002.

PALLAV. Solubility and Polarity Chart. [online]. © 2013 Available at: http://www.pallavchemicals.com/miscibility_and_polarity_chart.html. [Accessed 17 July 2016].

PEJCHAR, K. Výzkum a vývoj zařízení pro výrobu nanovláken. Výzkumná zpráva. ISRN TUL – KTS/TZ/PZ - - 14/13/CZ - - CZ + SGS. Technická univerzita v Liberci. 2013.

PILLAI, C. K. S., PAUL, W., SHARMA, P. Chitin and chitosan polymers: Chemistry, solubility and fiber formation, *Progress in Polymer Science, 34, (7).* 2009. pp. 641 – 678.

POKORNY, P., KOSTAKOVA, E., SANETRNIK, F., MIKES, P., CHVOJKA, J., KALOUS, T., BILEK, M., PEJCHAR, K., VALTERA, J., LUKAS, D. Effective AC needleless and collector less electrospinning for yarn production. *Phys Chem Chem Phys, 16 (48).* 2014, pp. 26816-26822.

POKORNÝ, P. *Fontanovy spinner*. Patent PV 2009-425 Czech Republic. 2009.

POKORNY P., MIKES P. and LUKAS D. Electrospinning jets as X-ray sources at atmospheric conditions. *Epl-Europhys Lett.* 92(4). 2010. doi: 10.1209/0295-5075/92/47002

RAMAKRISHNA, S., FUJIHARA, K., TEO, W-E., LIM, T-CH., MA, Z. An Introduction to Electrospinning and Nanofibers, World Scientific Publishing Co. Pte. Ltd., Singapore, ISBN: 978-981-256-415-2. 2005.

REIMER, L., KOHL, H. *Transmission Electron Microscopy: Physics of Image Formation*. Münster, Germany. Springer, 2008. ISBN: 978-0-387-40093-8.

REZNIK, S. N., YARIN, A. L., ZUSSMAN, E., BERCOVICI, L. Evolution of a compound droplet attached to a core-shell nozzle under the action of a strong electric field. *Phys. Fluids, 18 (6).* 2006.

ROBESON, L.M., *Polymer Blends*, Ohio, USA, Hansen Gardner Publications, Inc, 2007. ISBN-13: 978-1569904084.

SILL, T. J., RECUM, H. A. Electrospinning: Applications in drug delivery and tissue engineering. *Biomaterials, 29.* 2008. pp. 1989-2006.

SONG, T., ZHANG, Y.Z., ZHOU, T.J. Fabrication of magnetic composite nanofibers of poly(e-caprolactone) with FePt nanoparticles by coaxial electrospinning. *Journal of Magnetism and Magnetic Materials 303.* 2006. pp. e286-e289.

SU, Y., SU, Q., LIU, W., JIN, G., MO, X., RAMAKRISHNA, S. Dual-drug encapsulation and release from core-shell nanofibers. *J Biomater Sci. Polym. Ed. 23(7).* 2012. pp. 867-871.

SUN, Z., ZUSSMAN, E., YARIN, A.L., WENDORFF, J.H., GREINER, A. Compound Core-Shell Polymer Nanofibers by Co-Electrospinning. *Adv. Mater., 15.* 2003, pp. 1929.

TAYLOR, G. Disintegration of Water Drops in an Electric Field. *Proceeding of the Royal Society of London A., Mathematical, Physical & Engineering Sciences,280.* 1964. pp. 383-397.

TONKS, L. A Theory of Liquid Surface Rupture by a Uniform Electric Field. *Phys.Rev. 48. 562.* 1935.

TUCKER, N., STANGER, J.J., STAIGER, M.P., RAZZAQ, H., HOFMAN, K. The History of the Science and Technology of Electrospinning from 1600 to 1995. *Journal of Engineered Fibers and Fabrics.* 2012. pp. 63-73.

UTRACKI, L. A., FAVIS, B. D. Polymer Alloys and Blends, Handbook of Polymer Science and Technology, Vol. 4, Composites and specialty applications, Cheremisionoff, N. P., CRC Press, New York, USA. 1989. ISBN: 0-8247-8021-3.

VALTERA, J. Výzkum a vývoj zařízení pro výrobu nanovláken, Výzkumná zpráva. ISRN TUL – KTS/TZ/PZ - - 2014/05/CZ - - CZ + SGS, Technická univerzita v Liberci. 2014.

VAVŘÍKOVÁ, E., VINŠOVÁ, J. Chitosan a jeho farmaceutické aplikace, *Chem. listy 103.* 2009. pp. 56 – 65.

VODSEĎÁLKOVÁ, K. 2010. *Koaxiální elektrostatické zvlákňování.* Disertační práce. Technická Univerzita v Liberci, 2010.

VYSLOUŽILOVÁ, L., MOHROVÁ, J., LUKÁŠ, D. Electrospinning of biopolymers. In: Strutex 2011. Liberec. Czech Republic. 2011. ISBN: 978-80-7372-786-4.

VYSLOUŽILOVÁ, L., BUZGO, M., MOHROVÁ, J., POKORNÝ, P., BÍLEK, M., PEJCHAR, K., LUKÁŠ, D. Productivity Enhancement of core/shell nanofibers. In: *Nanocon2012.* Ostrava. Czech Republic. 2012. ISBN 978-80-98294-32-1.

VYSLOUŽILOVÁ. L., MOHROVÁ, J., CHVOJKA, J., HÉGROVÁ, B., MIKEŠ, P., LUKÁŠ, D. Production of Bi-component Nanofibers with incorporated Particles. In: *Nanocon2011*. Ostrava Czech Republic. 2011. ISBN: 978-80-87294-27-7.

VYSLOUŽILOVÁ, L., VODSEĎÁLKOVÁ, K., POKORNÝ, P., LUKÁŠ, D., BUZGO, M. Needleless co-axial electrospinning. In: *Nanofibers for the 3rd Millenium. North Carolina. USA.* 2010.

VYSLOUŽILOVÁ, L., BAJÁKOVÁ, J., GRÉGR, J., PEJCHAR, K., LUKÁŠ, D. Phase Contrast Method for Demonstrating of Coaxial Structure of Core/Shell Nanofibers. In: *Nanocon2013*, OSTRAVA. Czech Republic. 2013. ISBN 978-80-87294-44-4.

VYSLOUŽILOVÁ, L., PEJCHAR, K., VALTERA, J., POKORNÝ, P., BERAN, J., LUKAS, D. Cylindrical coaxial spinning electrode for needleless coaxial electrospinning. In: *The Spring Fiber Society 2014*, Technical Conference Fibers for Progress, Liberec, Czech Republic, 2014.

VYSLOUŽILOVÁ, L., VALTERA, J., BÍLEK, M., SOUKUPOVÁ, J., KOMÁREK, J., ŽABKA, P., SKŘIVÁNEK, J., BERAN, J., LUKÁŠ, D., Visualization of electrospinning process. In: *NART2015*, International conference. Liberec. Czech Republic. 2015.

YAN, X., PHAM, Q., MARINI, J., MULLIGAN, R., SHARMA, U., BRENNER, M., RUTLEDGE, G., FREYMAN, T. High-Throughput Needleless Electrospinning of Core-Sheath Fibers, *The Fiber Society, Rediscovering Fibers in the 21st Century*. Boston. Massachusetts. USA. 2012.

YARIN, A.L., ZUSSMAN, E. Upward needleless electrospinning of multiple nanofibers. *Polymer, Vol. 45*. 2004. pp. 2977-2980.

ZELENY, J. The electrical discharge from liquid points, and a hydrostatic method of measuring the electric intensity at their surface. *Phys. Rev. 3*. 1914. pp. 69–91.

ZHANG, Y., HUANG, Z-M., XU, X., LIM, CH. T., RAMAKRISHNA, S. Preparation of Core-Shell Structured PCL-r-Gelatin Bi-Component Nanofibers by Coaxial Electrospinning. *Chemical Matters, 16*. 2004. pp 3406 – 3409.